ANALYSIS OF POP-UP RINGS FOR THE FABRICATION OF GIANT MEMS HEMISPHERIC SHELL RESONATORS

by

Calvin Jones

A thesis

Submitted to the Faculty of Purdue University

In Partial Fulfillment of the Requirements for the degree of

Master of Science in Electrical and Computer Engineering

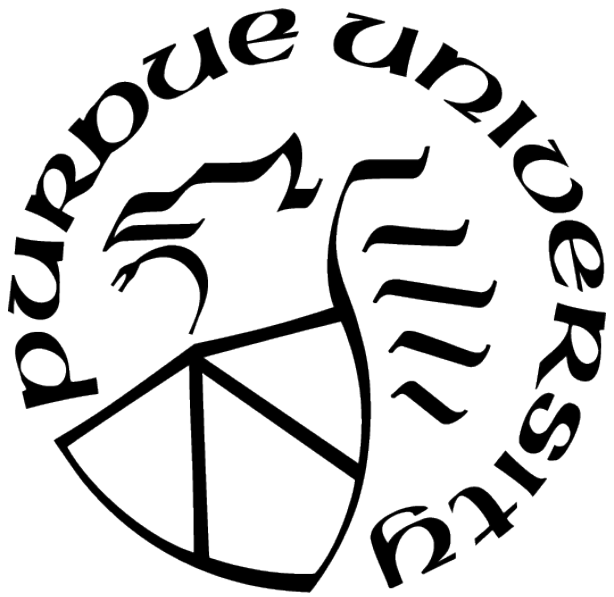

Electrical and Computer Engineering

West Lafayette, Indiana

December 2020

THE PURDUE UNIVERSITY GRADUATE SCHOOL
STATEMENT OF COMMITTEE APPROVAL

Dr. Sunil Bhave, Chair

School of Electrical and Computer Engineering

Dr. Dana Weinstein

School of Electrical and Computer Engineering

Dr. Mahdi Hosseini

School of Electrical and Computer Engineering

Approved by:

Dr. Dimitrios Peroulis

ACKNOWLEDGMENTS

I would like to acknowledge Purdue University's Graduate School and Electrical and Computer Engineering Department. Specifically the OxideMEMS group under Dr. Sunil Bhave in the MEMS Microelectronics and Nanotecnology division within the Birck Nanotechnology Center. Also, thanks to Birck facilities and staff for the access and training that allowed the research to be conducted. Finally, a special acknowledgement to Dr. Mert Torunbalci for being the mentor on this project and setting up the designs that allowed for the start of the research.

TABLE OF CONTENTS

LIST OF TABLES

LIST OF FIGURES

Figure Page

Figure Page

Figure Page

Figure Page

LIST OF SYMBOLS

μ	micro
s	seconds
min	minutes

ABBREVIATIONS

HRG	hemispherical resonator gyroscope
HSR	hemispherical shell resonator
Q	quality factor
SCS	Single Crystal Silicon
SEM	Scanning Electron Microscope

NOMENCLATURE

HNA	1-Hydroflouric Acid-4-Nitric Acid-1-Acetic Acid
XeF_2	Xenon Diflouride
Si_3N_4	Silicon Nitride

GLOSSARY

COMSOL	Element analysis, solver and multiphysics simulation software
RIE	Reactive-ion etching used in microfabrication dry etches
in-plane acceleration	Force from acceleration that causes bending that is in-plane of the structure
out-of-plane acceleration	Force from acceleration that is applied perpendicular to the structure causing bending outside of its original plane
isotropic etch	A wet etch that maintains a uniform etch rate in all directions, in this case to create a symmetric hemispherical structure.

ABSTRACT

Fabrication of hemispherical structures for application in hemispherical resonator gyroscopes (HRG) is an integral part of modern sensing systems, especially in relation to space navigation. First, it is important for these structures to be as symmetric as possible in order to accurately track both in-plane and out-of-plane acceleration that occurs in fast moving satellites and space crafts. Next, they need to be larger for easier application in current mm scale systems and to maintain a lower noise floor and high quality factor. The work in this paper introduces a methodology for the analyzation of the micromachining process for larger symmetric hemispherical shell resonators (HSR). This is in order to increase their size while maintaining symmetry through isotropic etching using HNA and the pop-up ring mask design. The implementation of the pop-up ring mask allows for symmetric etching of <111> silicon and larger MEMS structures at a low cost while giving more design control to the user in comparison to alternative designs such as the pinhole. The investigation of how hemispheric structures are affected based on the adjustment of the pop-up ring design serves to both create larger symmetric HSRs and create a better model for future designs and applications. During this investigation, a range of design tests were done to create the hemispherical resonator molds in order to gauge the effectiveness of the pop-up ring changes. These results were then used to develop a method for achieving the desired larger symmetric HSRs.

1. INTRODUCTION

The hemispherical resonator gyroscope (HRG) is a popular option for sensing applications in space, land and water due to its high sensitivity and known reliability over a long period of time. The concept that led to the HRG was originally derived in 1890 by a physicist named G.H Bryan.[3] Bryan discovered that by rotating a vibrating wineglass that the vibrations occurred at a rate proportional to the rate of rotation.[3] This occurrence laid the foundation for basic gyroscope properties and is known as Bryan's effect. Experiments were done by slowly rotating isotropic discs, cylinders and spheres while simultaneously vibrating them to come up with the differential equations that would explain Bryan's effect.[3] These experimental discoveries were then later brought into practical use in 1965 because of the work done by Dr. Alfred Emslie.[1] Dr. Emslie worked at the time as a contractor for Alfred D. Little company researching the rotation sensitivity of symmetrical shells undergoing flexural vibrations.[1] During his research Dr. Emslie reviewed and compiled the work of Bryan. Based on his discoveries utilizing Bryan's original work in 1890, Dr. Ivan Simon and Dr. Lynch, who also worked at the same company, performed research that led to the first HRG sensing device.[1] Specifically, Dr. Ivan Simon did experiments to test the magnitude of Bryan's effect using vibrating metal rings and then Dr. Lynch designed the first theoretical model for vibrating hemispherical shells.[1] These experiments laid the groundwork for the HRG.

From this initial model the first experimental HRG was created. They were designed with two different methods, the first utilizing a wine glass model with a stem on the outside, Figure 1.1a, and the second being based on a mushroom model, Figure 1.1b, with the stem located inside the hemispherical shell.[1] The wine glass gyroscope design proved to be more successful, with the mushroom design failing because of its high susceptibility to its environment.[1] Then even though the wine glass design proved to work better under normal conditions, its downfall came about due to the gyroscope's large sensitivity to temperature.[1] The project was then abandoned until in 1975 NAVAIR funded an HRG group led by Tim Hanley.[1] Hanley decided to use fused quartz for the HRG fabrication because

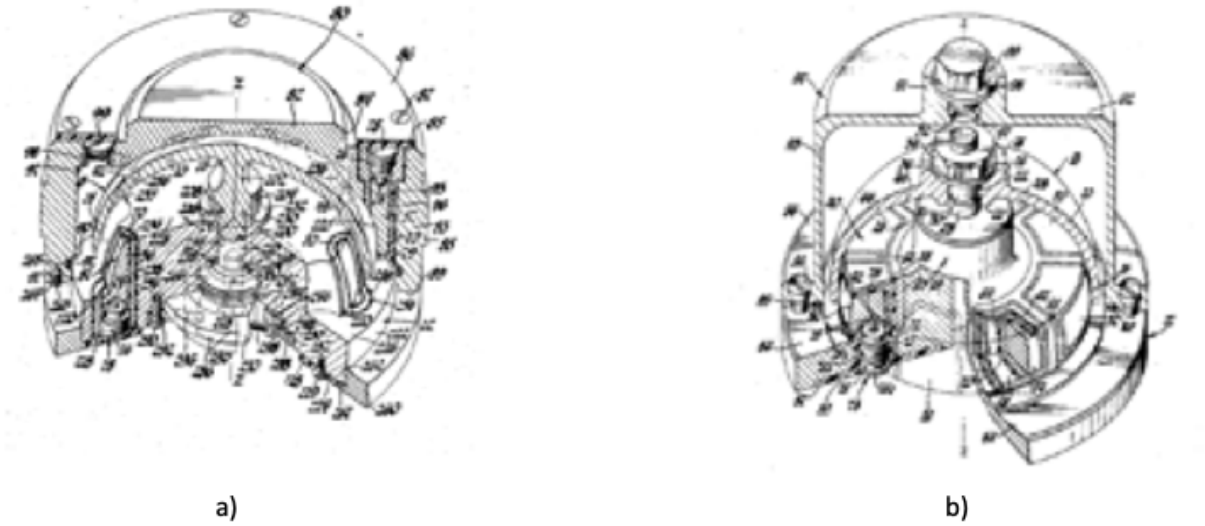

Figure 1.1. Diagrams from Northrop Grumman showing first HRG designs a) Wineglass resonator b) Mushroom resonator[1]

of its low internal damping.[1] This decision led to the high performance that made HRGs so popular. With the use of fused quartz, by the early 1980s Hanley's group was able to reach quality factors of over 10 million.[1] The subsequent testing that occurred led to the continued growth in popularity of the HRG and spurred on more research in the area. Not too much later in 1988 Zhuravlev and Klimov used spherically symmetric, isotropic, structures that could rotate in three dimensions in order to study Bryan's effect further in respect to gyroscope sensing.[3] From these experiments it was found that Bryan's effect is dependent upon its vibration mode.[3] This led to the discovery of the Bryan effect's many navigation sensing applications as well as its possible application in environmental dynamics.[3] These discoveries and initial models led to the motivation for the optimization of the HRG model. With the progress made in HRG fabrication and research, Northrop Grumman was eventually able to make the best macro HRG that has proven to be reliable in many aircraft and space applications. Even with the progress made by industry leaders such as Northrop Grumman, the production of these products were costly and as a result limited research and optimization capabilities.

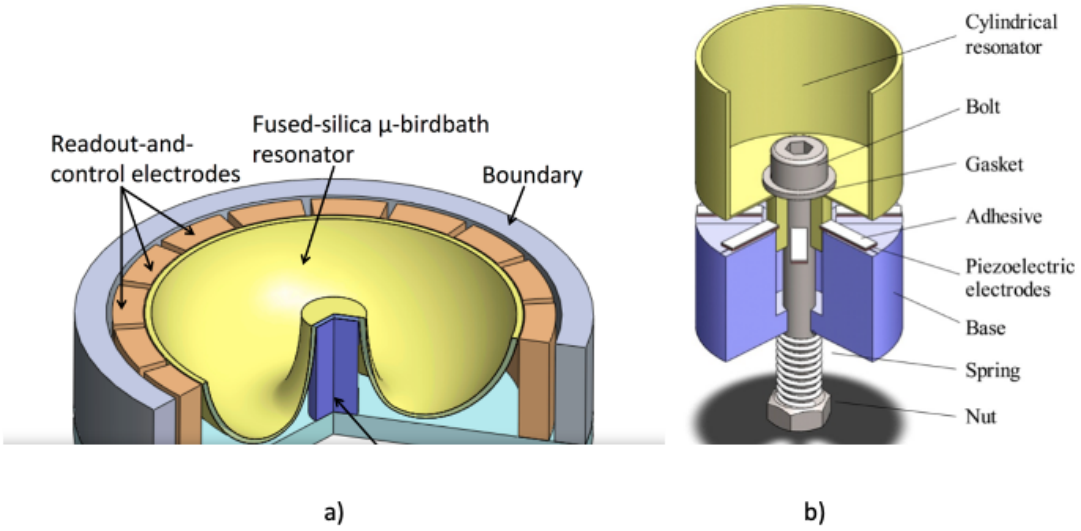

Figure 1.2. Popular non-symmetric HRG designs a) birdbath[8] b) cylinder[9]

With the success of the fused quartz HRG came the challenge of cost and size. The costs limited production to few companies and led to many trying to find other cost-efficient methods.[4] Also, the size of the HRG was based on the aircraft system needs of the 1990's and therefore did not have variability to smaller systems. From these challenges came about the production of micro hemispheric shell resonators (HSR). With the increase in popularity of microelectronic structure fabrication, the opportunity to make a more compact, symmetric 3D wineglass structure at a lower cost became a motivation in hemispheric resonator research. Methods such as glassblowing, blow molding, and deposition of structural thin films became the focus for trying to create these HSR structures.[6] From the various methods used, it became evident that the desired 3D resonator shape should have the anchor far away from the main point of vibration so that a high quality factor(Q) and small mode frequency split could be reached.[4] This led to the creation of variations of this design such as the "birdbath", "bubbles", "cylinders", and "pierced shell" resonators that all served to maintain a high Q, and small mode frequency split at the micro size, Figure 1.2.[4] These resonators allowed for sufficient operation because of these characteristics, but still faced the challenge of operating efficiently in more than one axis of acceleration. The lack of symmetry in these

fabricated structures led to sensitivity issues in either the x or z planes when simultaneous multi-plane acceleration occurred in things such as aircrafts or satellites.[4] This led to the resurgence of interest in a symmetric HSR which would be able to maintain insensitivity to x and z accelerations simultaneously during whole angle operation.[4]

In 2011 Dr. Laura Fegely of the OxideMEMS lab at Cornell University, investigated trying to make super symmetric 3D wineglass structures using isotropic etching on <111> and <100> single cystal silicon (SCS).[7] During these experiments the effectiveness of HNA and XeF_2 wet etches are compared along with the effects of varying mask pinhole sizes.[7] It was found that when comparing HNA and XeF_2, HNA proved to be the more effective isotropic wet etch because of its reduced surface roughness and constant out-of-plane radius.[7] In addition to this, etch windows were found to need to be larger than 10μm in order to prevent the Micro-HSR from becoming diffusion limited. With this information, mask pinholes of 20μm, 30μm, 40μm and 50μm were used in a test of 60 samples that were etched for 120s each.[7] The results showed that designs with larger pinholes had consistently higher etch rates and that the designs that were fabricated using <111> silicon wafers had a more desirable spherical shape.[7]

The findings of Dr. Fegely laid the foundation for the work that was then done by Dr. Mert Torunbalci with the OxideMEMS lab at Purdue University early in 2018. Their goal was to take the conclusions found during Dr. Fegely's trials and create acceleration insensitive HSR structures.[4] In these experiments, a HNA wet etch was used on <111> silicon wafers in order to experiment with the old methods used in Dr. Laura Fegely's test as well as try new alterations to the pinhole design.[4] During the initial trials, pinholes were used in a Si_3N_4 mask.[4] For the smaller pinholes there were similar finding to Dr. Fegely's experiments and the silicon molds became diffusion limited as seen in Figure 1.3a.[4] Then for the larger pinholes it was discovered that the final silicon molds had a poor aspect ratio that caused them to be shallow as shown in Figure 1.3b.[4] This led to the innovation of the pop-up rings in order to allow for deeper isotropic etching.[4] The pop-up rings have a center pinhole, silicon nitride rings, and etched gaps in a Si_3N_4 mask that allow for a deeper etch by

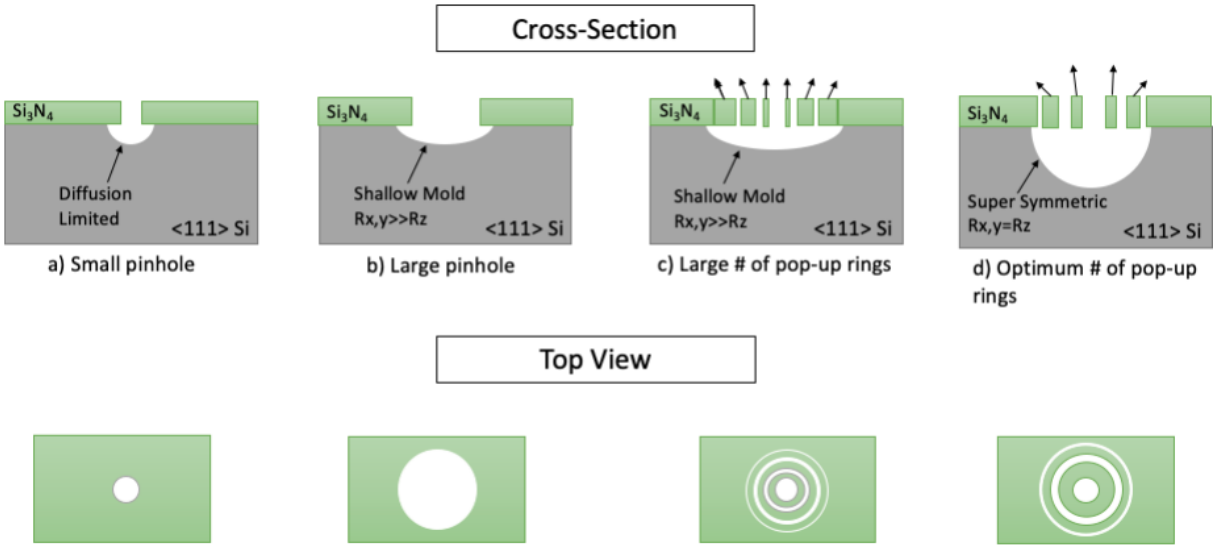

Figure 1.3. Cross-section drawing based on OxideMEMS 2018 paper of results from pop up rings and pinhole isotropic etches: a) 5um pinhole, b) 50um pinhole, c) large number of pop-up rings, d) optimum number of pop-up rings

forcing a larger amount of HNA in the center first until the subsequent rings pop off to allow for a more uniform and isotropic etch. The trials with the pop-up rings mainly varied the number of rings from two to five and targeted 100μm HSR molds.[4] Through these tests it was found that too many rings caused them to fly off too quickly leading to a shallow mold as can be seen in Figure 1.3c.[4] Eventually it was found that for 100μm devices two rings, two ring gaps and a pinhole, as seen in Figure 1.3d, created the most symmetric devices, shown in Figure 1.4.[4] After it was proven that these HSR devices could be fabricated, acceleration induced mechanical stress testing was done in COMSOL. A simulation created a plot of frequency shift versus x and z axis symmetry as shown in Figure 1.5.[4] The results show that a shallow device has great in-plane acceleration insensitivity, but bad out-of-plane and simultaneous in-plane and out-of-plane acceleration insensitivity. Then overly deep devices do great with out-of-plane acceleration insensitivity, but bad with in-plane and simultaneous in-plane and out-of-plane acceleration insensitivity. Finally, symmetric devices were found to have good in-plane and out-of-plane acceleration insensitivity as well as excellent simultaneous in-plane and out-of-plane insensitivity. These simulation results confirmed the importance of creating the symmetric structures as well as having design variability in order to shift the

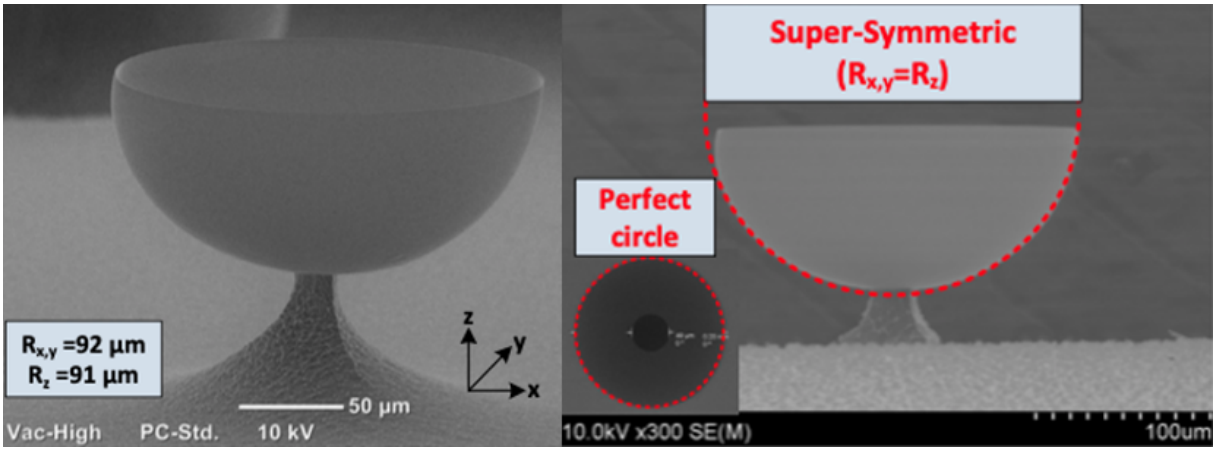

Figure 1.4. SEM image from the OxideMEMS 2018 paper of a super symmetric "100um device" using optimum pop-up rings

HSR characteristics based on the application. With these findings the next issue that then needed to be approached was scalability of these HSR devices using the pop-up rings method.

In this paper the pop-up ring design is investigated and utilized to improve upon the HSR by allowing for greater scalability of the devices. Fabrication trials are done with HSR silicon molds on a <111> silicon wafer using an isotropic HNA etch in order to make them larger while maintaining their smooth and symmetric characteristics. By attempting to increase the size of the structures, a wider spectrum of applications in MEMS gyroscope sensing becomes possible. Also, with an increase in size the anchor becomes farther away from the main point of vibration creating a high Q and small mode frequency split. An in-depth investigation into the characteristics of the pop-up rings is done in order to optimize the pop-up ring HSR as it is increased in size. These results are also compared to the older design methods such as the pinhole and the ideal 100μm HSR designs. The resulting optimized structures will allow for larger mm scale silicon HSR devices to maintain insensitivity to both in-plane and out-of-plane acceleration. They will also give greater design control to the HSR designer for future applications.

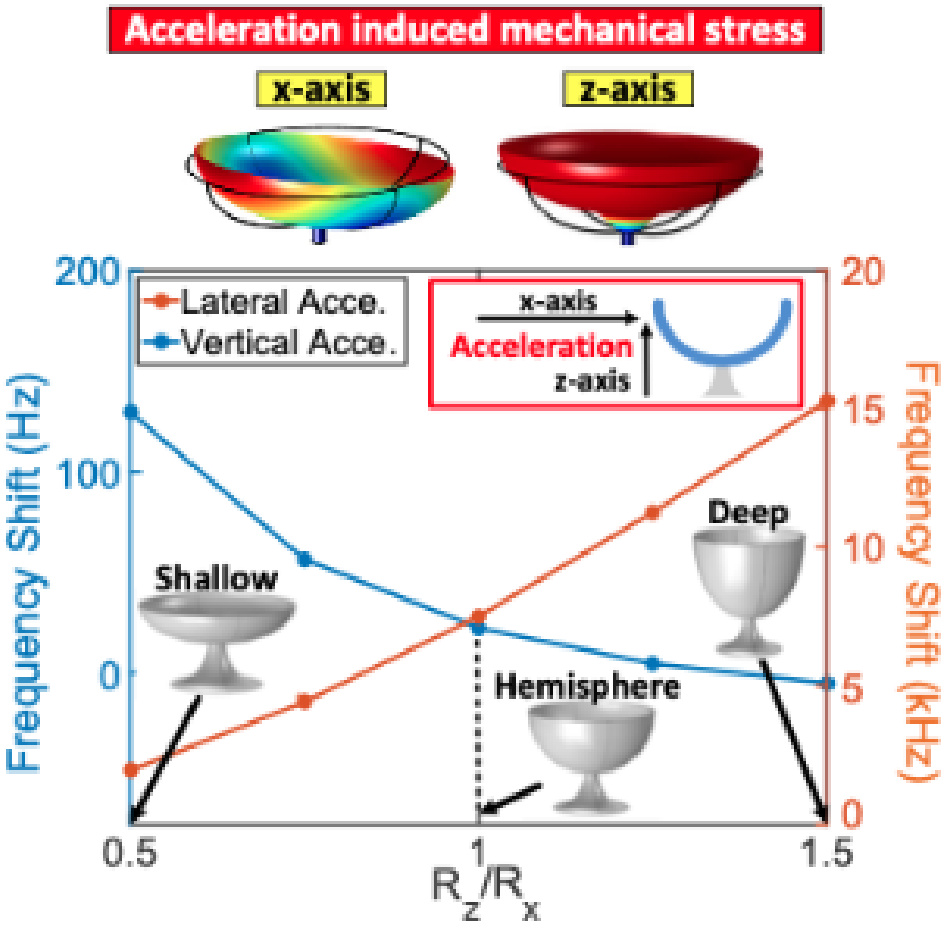

Figure 1.5. Image from OxideMEMs 2018 paper for COMSOL simulation results demonstrating frequency shift versus HSR symmetry[4]

2. EXPERIMENTAL SETUP

The testing of the affects of alterations of the pop-up rings on the HSR molds was done by varying pop-up ring mask designs, creating a Si_3N_4 mask, performing an isotropic etch with HNA and then measuring depth to test the symmetry and size of the structure. SEM pictures were also taken throughout the process to monitor the isotropy of the etch. For efficiency of the testing process, the fabrication done for these experiments only created the mold of the HSR structure rather than releasing the entire device. The process flow for this can be seen in the cross-sectional figures derived from the OxideMEMS 2018 HSR paper, as displayed in Figure 2.1.

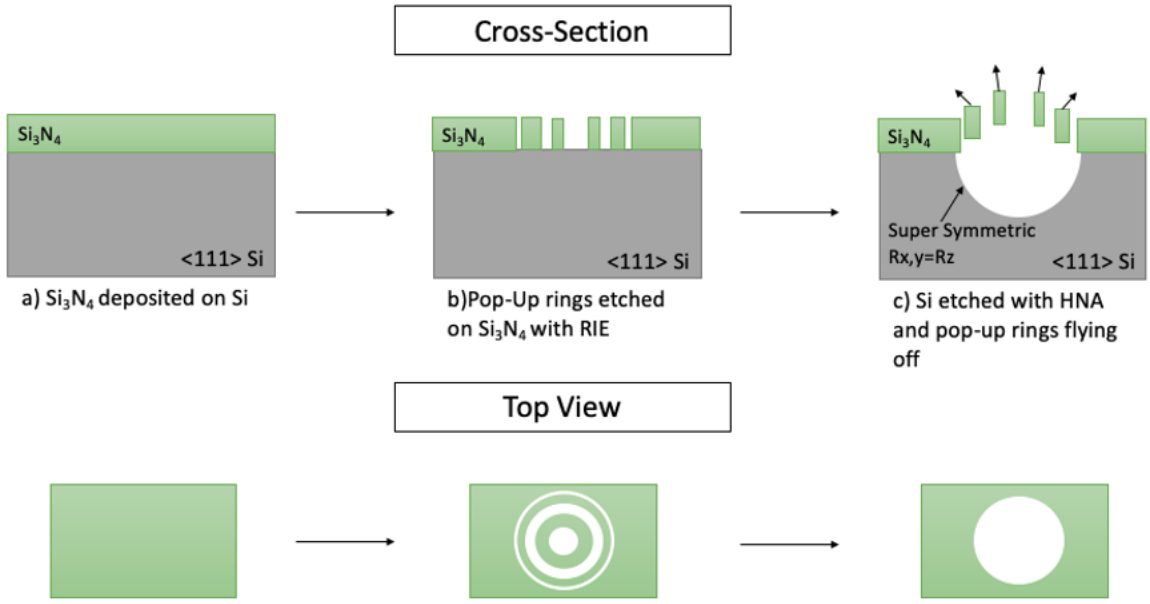

Figure 2.1. Cross-section of the HSR mold process flow: a) deposition of nitride on Si, b) dry etch used for creating the pop-rings, c) deep HNA isotropic etch to create the mold

The designs involved in these experiments used Si_3N_4 for the mask material on <111> silicon. Depositions of approximately 250nm, 400nm and 600nm were done using a LPCVD silicon nitride furnace in order to test isotropic wet etch depth limits in relation to silicon nitride thickness. Since only HSR molds are made for these trials, a single mask is used,

allowing for multiple designs to be tested without adding more complexity to the photolithography step. Also, due to the designs only needing a single mask, the Heidelberg Maskless Aligner is used to directly laser print the design. An RIE etch is then done to complete the mask fabrication. Once the mask is finished the wafer is diced into chips to allow for variations with etch times. The spherical mold is then etched using a 1:4:1 HNA isotropic etch. A combination of monitoring the undercut of the different design molds as well as measuring silicon nitride left after each wet etch period, allows for more accurate tracking of etch depths. Once a sufficient amount of silicon is etched to create a smooth and larger mold, the remaining silicon nitride is then stripped using hot phosphoric acid to prepare it for a depth measurement. Depth measurements are done on the silicon molds using the P-7 and Alpha Step surface profilometers. The resulting charts are then used to create a symmetry and size profile for the HSR molds. This process is done for different wafer mask designs adjusting the rings, gaps and pinhole each time for depth and symmetry improvement.

For comparison and analysis, pinhole and pop-up ring designs from both Dr. Laura Fegely's and Dr. Mert Torunbalci's HSR experiments were included in the fabrication trials. Up to 16 designs are able to be fabricated, allowing for designs with incremental changes to be fabricated and analyzed within the same batch. Each individual chip is designed with a rectangular strain relief, Figure 2.2a, in order to allow for a thicker nitride deposition while preventing surface cracks. Then each HSR design, Figure 2.2b, is sufficiently spaced apart in the center of the strain relief to give sufficient room for the etching of the mold. Based on the optimum pop-up ring design from Dr. Torunbalci and the OxideMEMS group, the pop-up rings were initially tested by proportionally increasing them up to 2.5 times the original size. From these results more designs were tested by methodically increasing and adjusting pinhole sizes, ring sizes, and gap sizes. The best of these designs are then modified in order to optimize size and symmetry of the HSR molds.

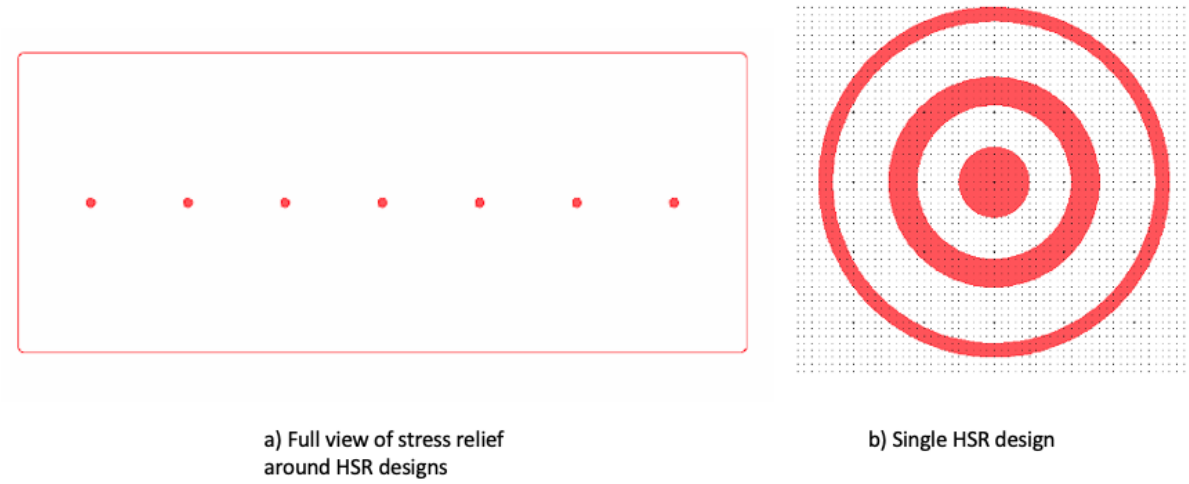

Figure 2.2. Topcell Layout for the Pop-Up Ring Designs

3. RESULTS

3.1 Initial Optimal Design Testing

Initially it was found that little was known about the properties of the pop-up rings due to few data points besides those pertaining to the 100μm HSRs. It was decided because of this, that initial experiments should spread across 16 designs that incrementally increased in size from the known 100μm devices, Figure 3.1a, by 10μm in order to target 250μm devices, Figure 3.1b.

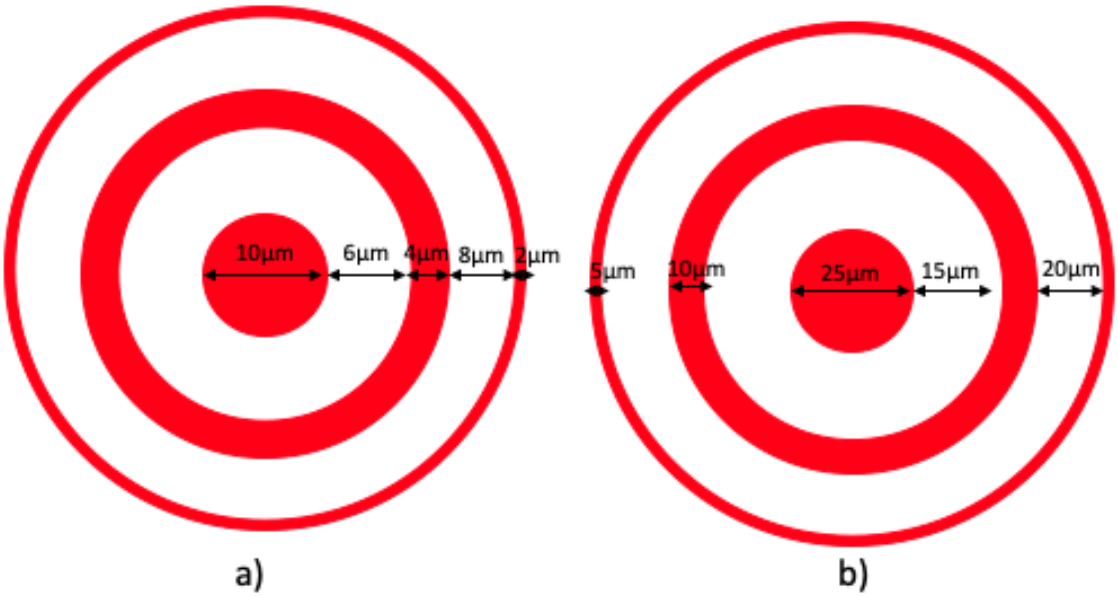

Figure 3.1. a) Optimized 100μm design from 2018 OxideMEMS trials. b) Proportionally increased design that targeted 250.

With the initial batch, the fabrication was done using a <100> SCS wafer and a silicon nitride mask that was 250nm thick. The first thing that was confirmed with this trial was that HNA etching done on <100> silicon creates a squarer profile rather than spherical as shown in Figure 3.2a. Next, the target undercut sizes were not able to be reached because the silicon nitride mask stripped prematurely during the wet etch, seen in Figure 3.3. Also, it was noticed that even before the chip was entirely stripped of silicon nitride, that the silicon nitride around the designs would begin to fail after more than 60min of etching, shown in

Figure 3.2b. The premature failing of the mask around the designs would lead to a lower yield of finished HSR molds.

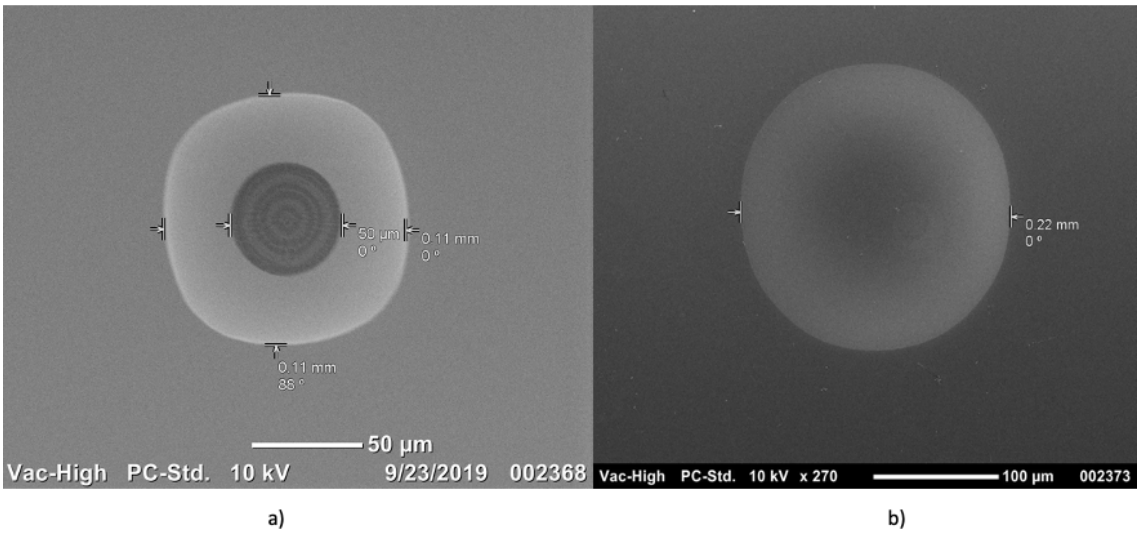

Figure 3.2. SEM images of "100μm" device undercut on <100> SCS: a) displaying a squarer mold profile, b) showing design when silicon nitride mask is stripped prematurely

Too thin of a mask did not allow for the initial trial to be completed and led to a thicker deposition being required before testing the initial designs again. The mask thickness was increased from 250nm to approximately 400nm to be able to reach approximately a 90min etch before the mask strips off. The wet etch for the initial trial was then able to reach 90min and the results for the first design trials were able to be found. Before the silicon nitride was stripped for depth and size profile analysis, an issue with the increasing of the silicon nitride rings could be seen in the SEM image displayed in Figures 3.4a. It is observed that when the rings become too large without a significant, non-proportional, increase in gap and pinhole sizes, the rings will no longer "pop" off as intended by the design. This lead to them sinking into the mold of the HSR and causing the etch not to go as deep as desired as shown in the depth measurement plot in Figure 3.4b.

The conclusion from the first design trial results was that the devices were seen to still be symmetric but did not increase in size substantially beyond 100μm. This led to the need

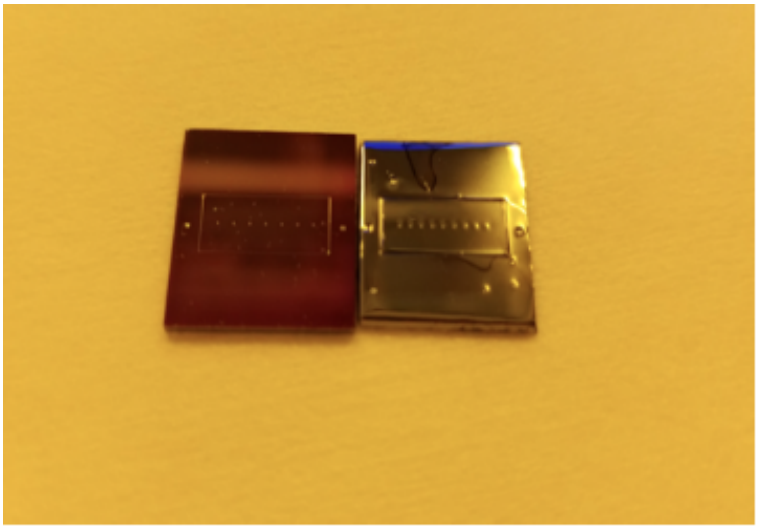

Figure 3.3. HSR design chips with silicon nitride(left) and stripped(right)

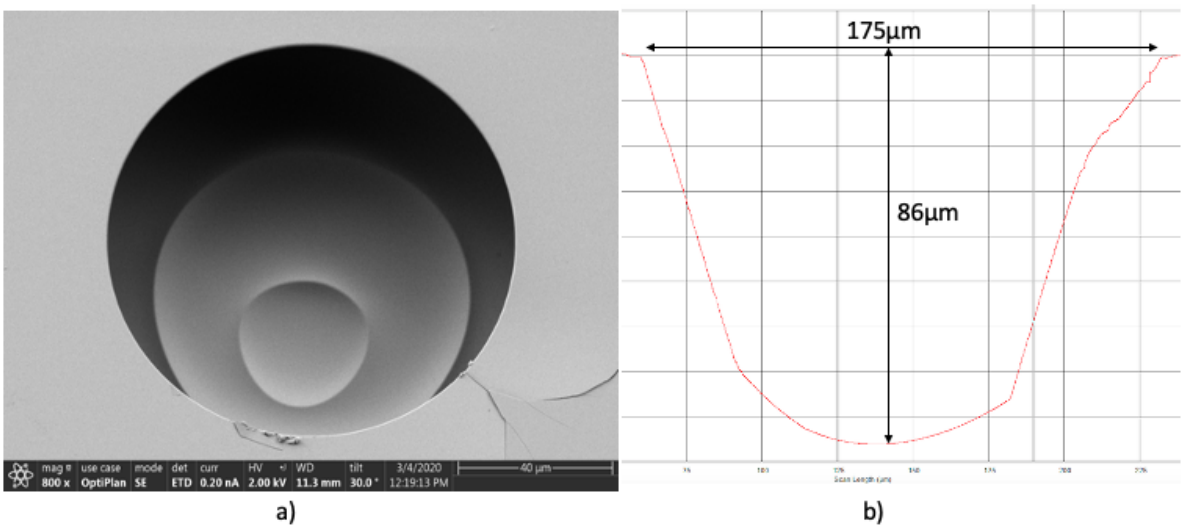

Figure 3.4. a)SEM image of collapsed pop-up rings in the HSR mold b) and resulting depth measurement

for the next round of experiments to start substantially increasing the pinhole and gap sizes to increase the etch depth within a reasonable 90 min etch period. Because of this, the next round of trials were done with the optimal ring and gap sizes being used with the pinhole increasing in 10μm increments up to 50μm, shown in figure 3.5a. Then within the same trial the alternative design increased both the pinhole and the first gap size by 10μm and 1μm steps respectively as seen in Figure 3.5b. With these next set of designs, a test could be

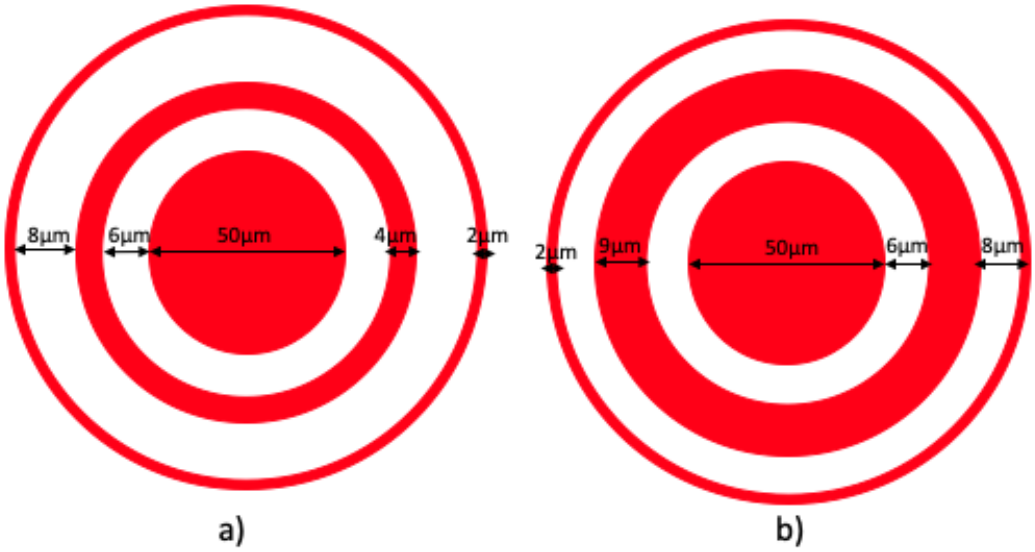

Figure 3.5. a) Largest design of increasing pinhole design with "optimal" rings and gaps based on the design in Figure 3.1a b)Largest design of increasing pinhole and first gap with the other gap and rings having "optimal" sizing from the 100um design in Figure 3.1a

done to see whether increasing the size of the center most pinhole, gap or both could force a deeper etch before the rings fly off and the final mold is created. Also for comparison, pinhole only designs from 10μm to 50μm, increasing in 10μm increments, were fabricated at the same time along with the optimum 100μm device design as a control.

3.2 Pinhole and Gap Analysis

From the results of the next round of design trials, a comparative analysis is done between the pinhole only, optimal pop-up rings with increasing pinhole, and optimal pop-up ring with increasing pinhole and first gap designs. The designs in this trial are etched until a majority of the silicon nitride mask is stripped, which is approximately 300nm of etching. It is decided that this is a proper stopping point for the wet etch due to the yield of each design dropping significantly after this point leading to poor analysis. The analysis is categorized by the pinhole sizes (10μm, 20μm, 30μm, 40μm, and 50μm) in order to see the differences between the three design types within the trial. A table of the findings, Table 3.1, is then

Table 3.1. Results from first set of designs in pinhole and gaps trial

Depth(μm)	**Radius(μm)**	**Depth to Radius Ratio(μm)**
	control(10μm pinhole)	
96	88	1.09
	pinhole only(10μm pinhole)	
48	38	1.26
	larger first gap(10μm pinhole)	
92	88	1.04
	ideal ring and gap(20μm pinhole)	
95	88	1.07
	pinhole only(20μm pinhole)	
60	50	1.2
	larger first gap(20μm pinhole)	
86	85	1.01
	ideal ring and gap(30μm pinhole)	
104	90	1.16
	pinhole only(30μm pinhole)	
60	50	1.2
	larger first gap(30μm pinhole)	
115	145	.79
	damaged(40μm pinhole)	
n/a	n/a	n/a
	pinhole only(40μm pinhole)	
68	60	1.13
	larger first gap(40μm pinhole)	
117	113	1.03
	ideal ring and gap(50μm pinhole)	
118	113	1.04
	pinhole only(50μm pinhole)	
79	75	1.05
	larger first gap(50μm pinhole)	
130	125	1.04

recorded to display the design type, depth, radius, and symmetry, based on the ratio of depth to radius.

The first designs to be analyzed are the designs with a 10μm pinhole as shown in figure 3.6. Based on the results displayed in Table 3.1, the control design held good symmetry after the 300nm etch but was limited to around 90μm in size. Similarly, the design in Figure 3.6c

where the first gap is increased, maintained its symmetry, but also was limited to around 90μm in size. The poorest result from these designs is shown to be the 10μm pinhole design that is diffusion limited and the least symmetric of the three. These results confirmed that the control continued to work well for designs 100μm and smaller, and that the small pinhole only design results in a diffusion limited mold that turned out to be the least symmetric. In addition to this, it is observed that the slight increase in the size of the first gap is not significant enough to greatly differ the results from the control design.

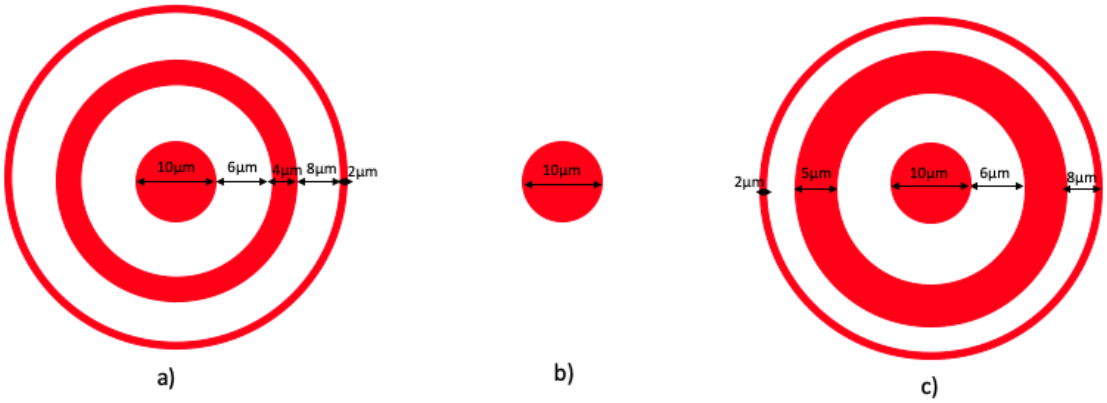

Figure 3.6. 10um pinhole designs a) optimum pop-up ring design from 100um devices, b) pinhole only design, and c) 10um pinhole with a larger first gap based on control design

Next, the 20μm pinhole designs are analyzed, shown in Figure 3.7. These designs proved to have similar results to the 10μm designs. The symmetry of the 20μm devices were made slightly better, an improvement of about .02 to .06, but the pop-up ring designs were still limited to less than 90μm in size and the pinhole was diffusion limited to about 60μm. Again, the increase of the first gap of the pop-up ring design, Figure 3.7c, was not substantial enough to differentiate it from the 100μm ring and gap design.

With the 30μm pinhole designs, Figure 3.8, the first noticeable increase in size is observed. The depth of the optimal ring and gap design reached slightly over 100μm in depth and maintained pretty good symmetry. The 30μm pinhole design with a larger first gap created the deepest etch, reaching a final depth of 115μm, but its symmetry though still okay,

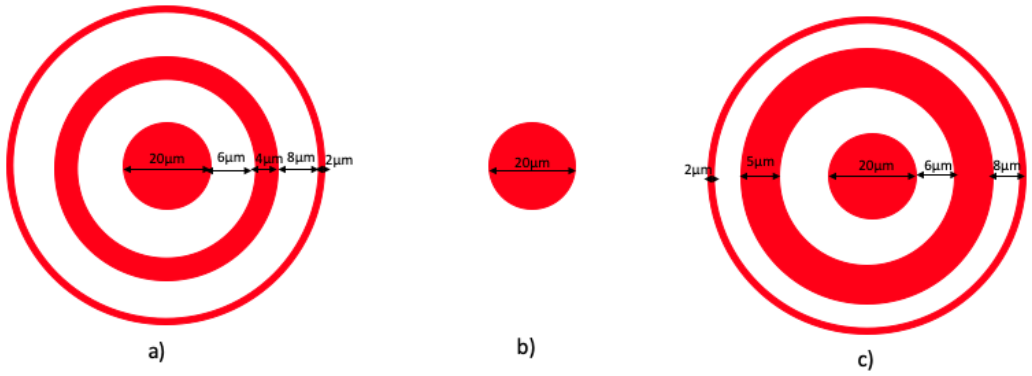

Figure 3.7. 20um pinhole designs a) optimum pop-up ring design from 100um devices, b) pinhole only design, and c) 20um pinhole with a larger first gap based on control design

declined to .79. In contrast to the pop-up ring designs, the pinhole only design did not improve in either size or symmetry and instead remained the same as the results from the 20μm pinhole only mold. With these results the trend of improvement in mold size, symmetry or both began to be recognized with the increase of pop-up ring size.

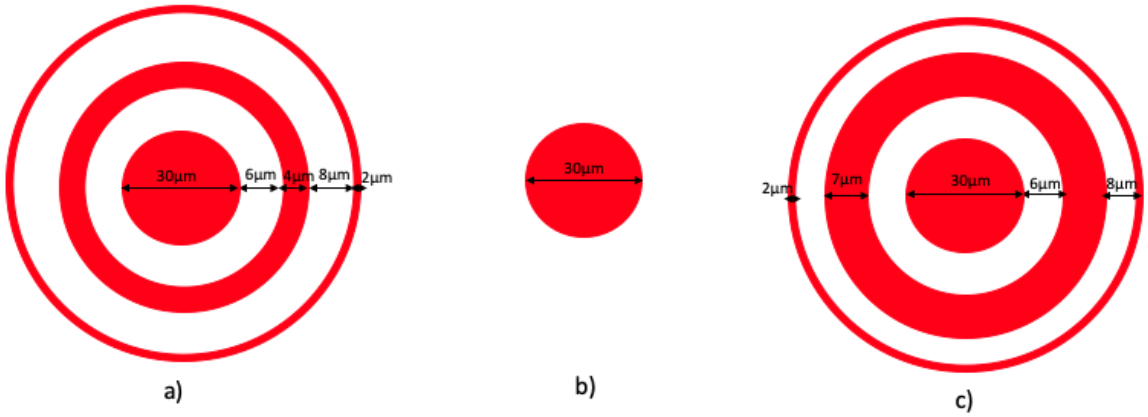

Figure 3.8. 30um pinhole designs a) optimum pop-up ring design from 100um devices, b) pinhole only design, and c) 30um pinhole with a larger first gap based on control design

The 40μm pinhole designs, Figure 3.9, continued the trend of improvement in the mold symmetry and size. The pop-up ring design with a larger inner ring gap slightly increased

its size to 117μm. In addition to this, the symmetry of the device improved significantly reaching a depth to radius ratio of 1.03. The pinhole only design, also improved in comparison from the other pinhole results, but still ran into the issue of being limited in size after a significant amount of etching. After approximately 80min of etching, the mold only reached 68μm in size. It is noted though that the pinhole only mold's symmetry did improve from the previous results reaching a depth to radius ratio of 1.13.

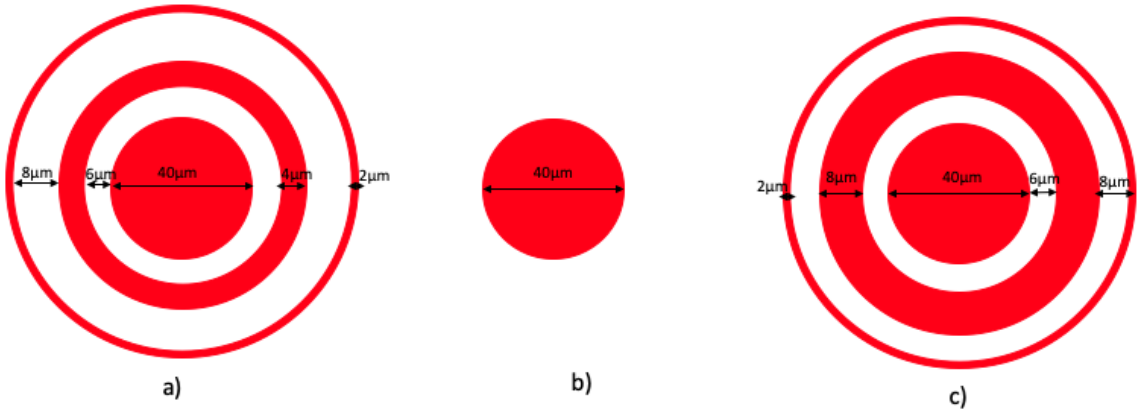

Figure 3.9. 40um pinhole designs a) optimum pop-up ring design from 100um devices, b) pinhole only design, and c) 40um pinhole with a larger first gap based on control design

Finally, the 50μm pinhole designs, Figure 3.10, showed the greatest improvement from the original 10μm designs. The 50μm pinhole design with ring and gap sizes from the optimal 100μm design improved in size to 118μm in depth, almost a 20% increase in size in comparison to the results from the related 10μm mold. In addition to the increase in mold size, the symmetry also improved to a depth to radius ratio of 1.04. Next, the 50μm design with a larger first gap noticeably improved in size and symmetry and resulted in the best HSR mold from the trial in terms of the balance of these two characteristics, as pointed out in Figure 3.11. The resulting mold size reached 130μm in depth, close to a 30% increase in size in comparison to the related 10μm mold. Then in addition to the size increase, the mold was able to maintain a good symmetry with a depth to radius ratio of 1.04. In comparison to the noticeable improvements of the pop-up ring designs, the pinhole only 50μm design also made

noticeable improvements in its size in comparison to its related 10μm design. Still it reached its limits at around 80μm at the end of this trial. The symmetry was also slightly worse than the final 50μm pop-up ring molds with a depth to radius ratio of 1.05. Although the best results from these trials did not display an extremely large increase in size, significant improvements were made in comparison to original 100μm designs. Also, the observations revealed information about the pop-up ring design that helped in moving to the next step of the experiments.

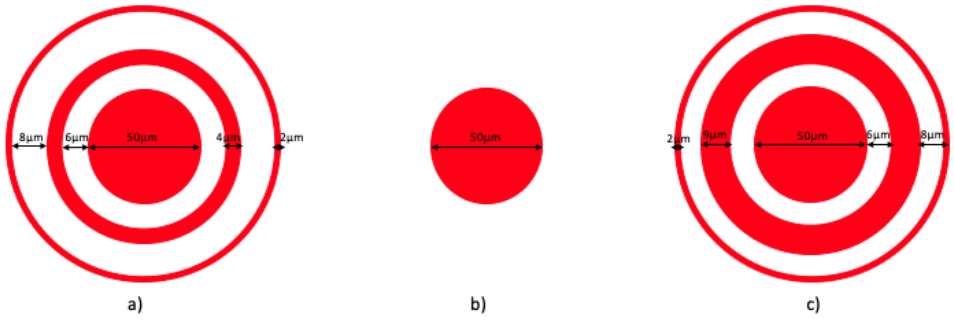

Figure 3.10. 50um pinhole designs a) optimum pop-up ring design from 100um devices, b) pinhole only design, and c) 50um pinhole with a larger first gap based on control design

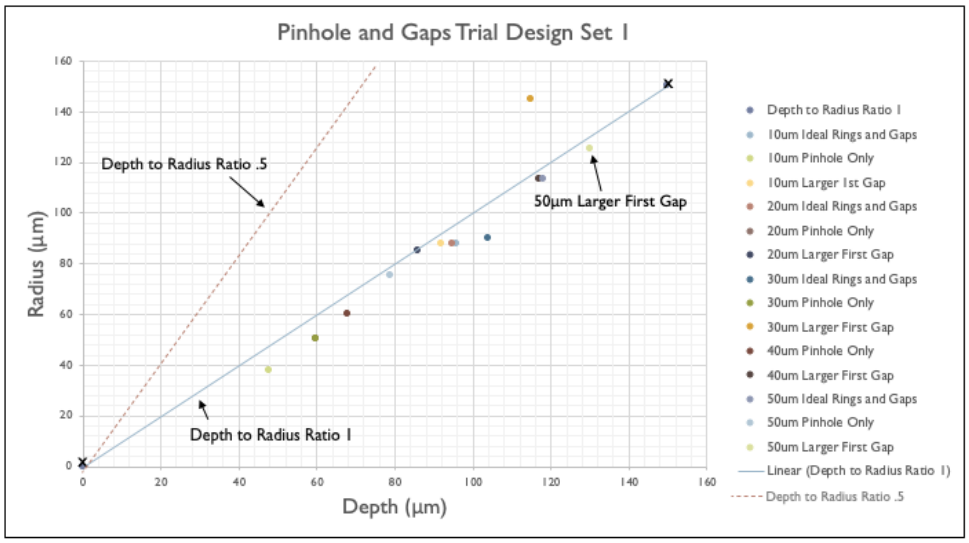

Figure 3.11. Plot of 1st set of pinhole and gaps trial results with largest 50μm design

The next pop-up up ring trial set out to expand upon the previous findings from the initial pinhole and ring gap experiments. Based on the results, it was realized that even though improvements were made in order to reach larger sizes, 200μm or larger, the pinhole and ring gap openings needed to be greatly increased. Stemming from the largest and most successful design in the previous trial, Figure 3.10c, the next designs continue to increase the pinhole size, in 30μm increments, and the first gap, in 3μm increments, as shown in Figure 3.12a. Also, increasing the outside second ring gap is experimented with by following the same design parameters as the previously mentioned design, but in addition increasing the second ring gap in 1μm increments, as shown in Figure 3.12b.

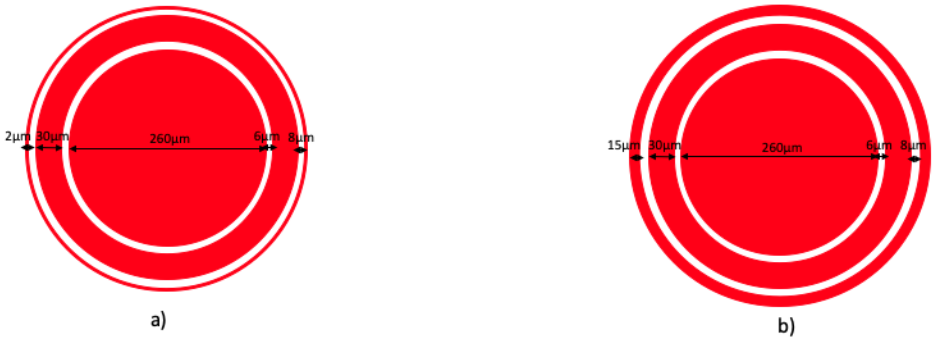

Figure 3.12. a) Largest design of increasing pinhole and first gap with the other gap and rings having "optimal" sizing from the 100μm design in Figure 3.1a b)Largest design of increasing pinhole and gaps with the rings having "optimal" sizing from the 100μm design in Figure 3.1a

From the results of the increasing pinhole and gap trials a noticeable improvement in the final HSR mold depth is observed, seen in Table 3.2. In comparison to the best design results in the previous trial, 130μm in depth, the deepest etch reached is 149μm. This maximum depth is consistent amongst 6 of the designs, 3 from each design category. The issue that goes along with this size increase is that the symmetry dropped to around .6 for the depth to radius ratio. This makes them slightly too close to the .5 mark shown in the COMSOL symmetry model in Figure 1.5. The resulting device would be shallow and perform great for in-plane acceleration, but consequently perform poorly in the out-of-plane acceleration category as shown in the summary Table 3.3. The smaller devices for the most part had

better symmetry, with the best being 117μm deep and having a .95 symmetry ratio. The issue that arises with this is that a better ratio and deeper etch was reached with designs in the previous trial.

Table 3.2. Results from second set of designs in pinhole and gaps trial

Depth(μm)	**Radius(μm)**	**Depth to Radius Ratio**
	Control	
90	88	1.02
	Larger Pinhole and 1st Gap	
128	138	.92
136	150	.91
136	162	.84
137	187	.73
149	225	.66
149	225	.66
149	250	.6
	Larger Pinhole and Gaps	
117	123	.95
123	130	.95
96	138	.7
149	200	.745
120	175	.68
149	237	.63
115	225	.51
149	250	.6

Table 3.3. Summary table of structure shape versus acceleration insensitivity from the OxideMEMS 2018 Acceleration Insensitive HSR paper[4]

	Acceleration Insensitivity		
Structure	**In-plane (ax or ay)**	**Out-of-plane(az)**	**ax x az**
Shallow	Best	Bad	Bad
Hemisphere	Good	Good	Excellent
Deep	Bad	Best	Bad

From the data, a better idea of how the pop-up ring design works was gained for the next round of designs to be made, demonstrated in the plot in Figure 3.13. It is observed that the largest designs reached 149μm before the vertical etch became limited and the lateral etch

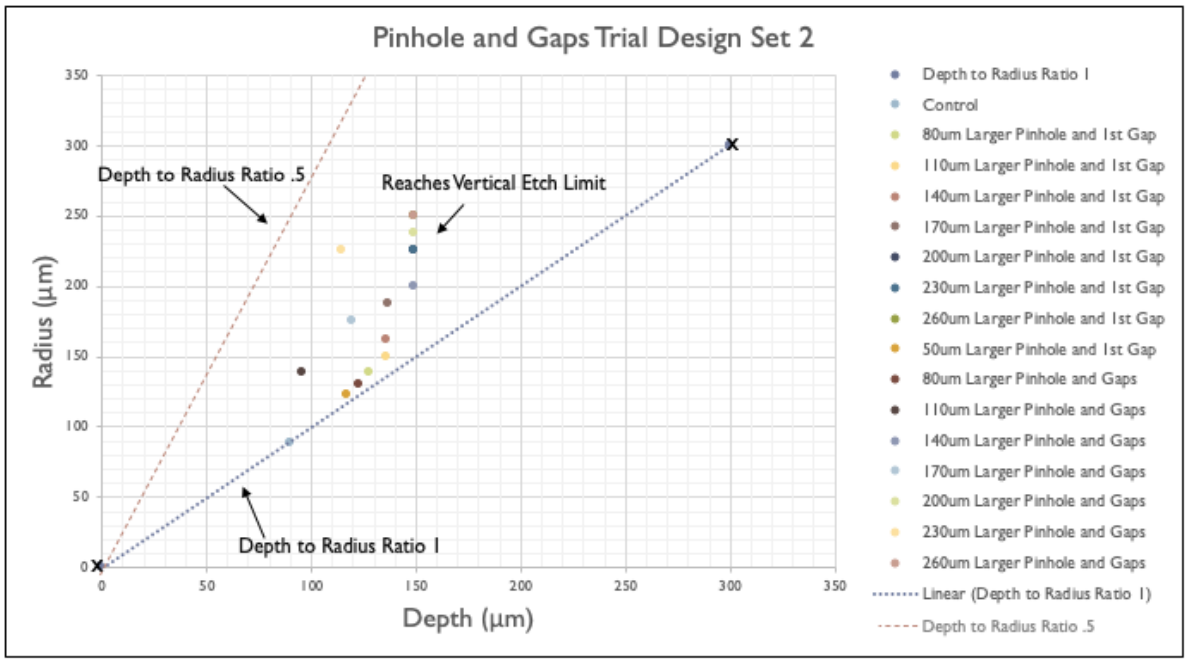

Figure 3.13. Plot of 2nd set of pinhole and gaps trial results where size limit is reached

created the shallow molds seen in the Figure 3.13 and Table 3.2. It was thought that the limited vertical etch was caused due to the pop-up rings being too small in relation to how large the pinhole and ring gaps became. This disproportionality caused the HNA wet etch to pop off the rings too quickly creating a shallow mold. In order to test this theory, the next trial experimented with increasing the nitride rings. It should be noted that adjustments to the process flow were also needed for the larger structures due to substantial increase in the size of the mask design openings. It was found that measuring the amount of silicon nitride left on the mask would be necessary in conjunction with viewing the undercut of the molds on a SEM in order to keep the end point of all the etches fairly similar. Also, it was found that in order to fully etch the larger HSR molds a longer etch would be necessary and therefore a thicker silicon nitride mask would be needed, approximately 600nm. With these process and design changes the properties of the silicon nitride rings could be further researched for design optimization.

3.3 Silicon Nitride Rings

With the improvements in depth found in pinhole and gap trials, the size and number of silicon nitride rings were altered in order to continue improving the depth of the etch as well as the symmetry. The first of the silicon nitride ring trials took four designs that created larger molds from each of the design types: larger pinhole and first gap, and larger pinhole and gaps. The new designs doubled the size of the rings based on the optimal 100μm device design. The size of the rings is based on the maximum ring size that was reached in the first design trials before the rings no longer popped off. In addition to these designs taken from the previous trial, the number of silicon nitride rings was experimented with by reducing it from two to one. It was decided to reduce rather than increase the number of rings because of the need to make the molds less shallow and more symmetric. Experimentation with more rings was also already done within the OxideMEMS 2018 HSR trials. It was found then that too many rings would fly off too quickly and leave a more shallow mold which is not desirable for these trials based on the past data.[4]

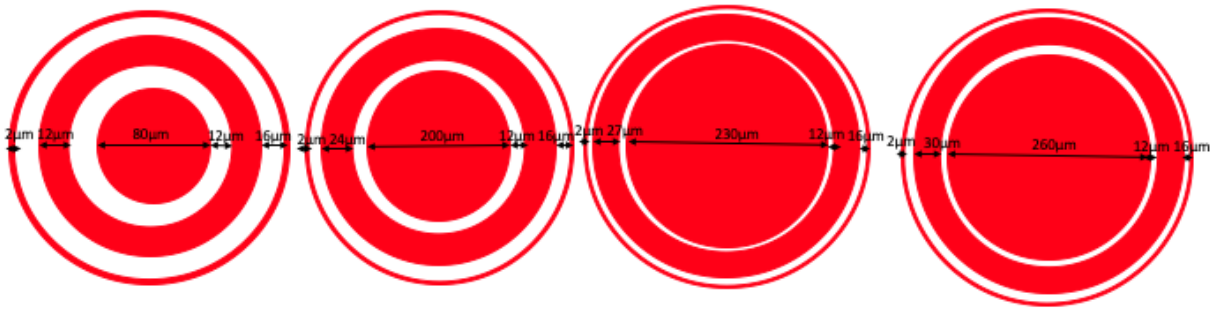

Figure 3.14. Larger nitride ring designs with larger pinhole and first ring gap

The results of the first silicon nitride ring trials showed substantial improvement in the size of the HSR molds for mostly all of the designs as can be seen in Table 3.4 and Figure 3.17. The single pop-up rings showed the most potential with the design molds reaching close to 200μm in depth. Also, the same largest single pop-up ring mold had the best symmetry,

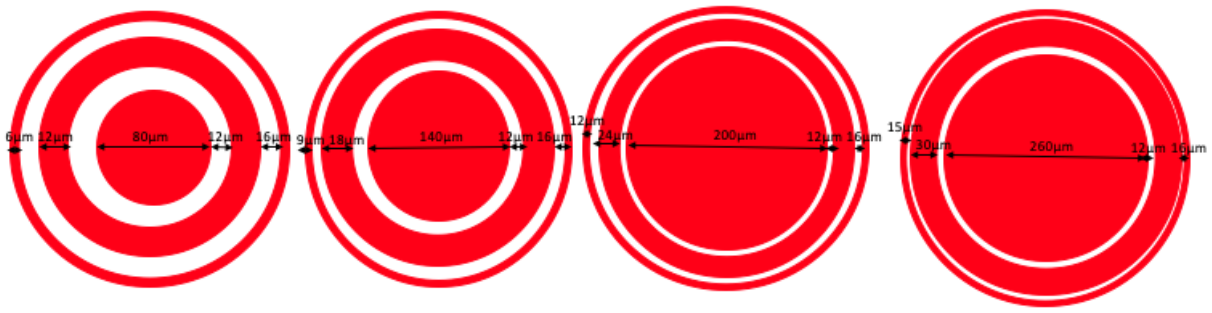

Figure 3.15. Larger silicon nitride ring designs with larger pinhole and gaps

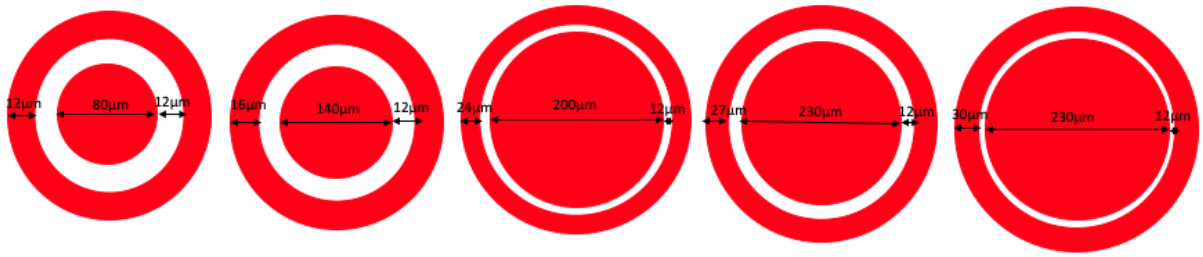

Figure 3.16. Single silicon nitride pop-up ring design

.687 depth to radius ratio, out of the designs that at least reached 190μm. Still the device came out shallow indicating the rings may still need to be larger. The larger pinhole and gaps design also reached the same depth as the single pop-up ring design but had slightly worse symmetry coming out even more shallow. Finally, the larger pinhole and first ring design only etched 183μm and had a depth to radius symmetry ratio of .614. With these improvements to the HSR molds made by only doubling the silicon nitride ring size, the theory that the rings were too thin and flying off too quick was confirmed. With this new information the next trial to continue the silicon nitride ring experiments could be done. The best designs from the single ring and two rings with a larger center ring designs were chosen for their potential to improve on the shallowness issue. The next silicon nitride ring trial then expanded upon this one by incrementally increasing the rings by up to 10 times based on the 100μm optimal ring sizes. From this next trial, the effects of solely increasing pop-up rings are observed.

Table 3.4. Results from first set of designs in silicon nitride rings trial

Depth(μm)	**Radius(μm)**	**Depth to Radius Ratio**
	Control	
109	110	.991
	Larger Pinhole and 1st Gap	
169	197	.858
181	265	.683
183	298	.614
181	298	.607
	Larger Pinhole and Gaps	
164	190	.863
175	250	.7
195	310	.629
190	320	.594
	Single pop-up ring	
155	170	.912
167	211	.791
177	254	.697
193	297	.65
195	284	.687

From the last of the silicon nitride ring trials an improvement in both size and symmetry is observed, as seen in Figure 3.18 and Table 3.5. A comparative analysis was done with each of the chosen designs in order to note the changes that occur with the continued increase of silicon nitride ring sizes. The results gained from these trials were to allow for a general model to be created of the pop-up rings.

The first design analysis is on the 80μm designs, shown in Figure 3.19, that increased from 3 to 6 times the optimal ring size. The designs that are up to 5 times the silicon nitride ring size reach around the same depth of 167μm. An improvement is seen once the rings reach 6 times the 100μm ring size. At this point a significant increase in mold size is seen with the final depth being 191μm. Also, the symmetry is able to be held to .743, allowing for better insensitivity to in-plane and out-of-plane acceleration in comparison to the 190μm devices in the previous trial. These improvements prove to be in line with the theory that the rings needed to be made larger to sufficiently allow for a full etch before flying off in

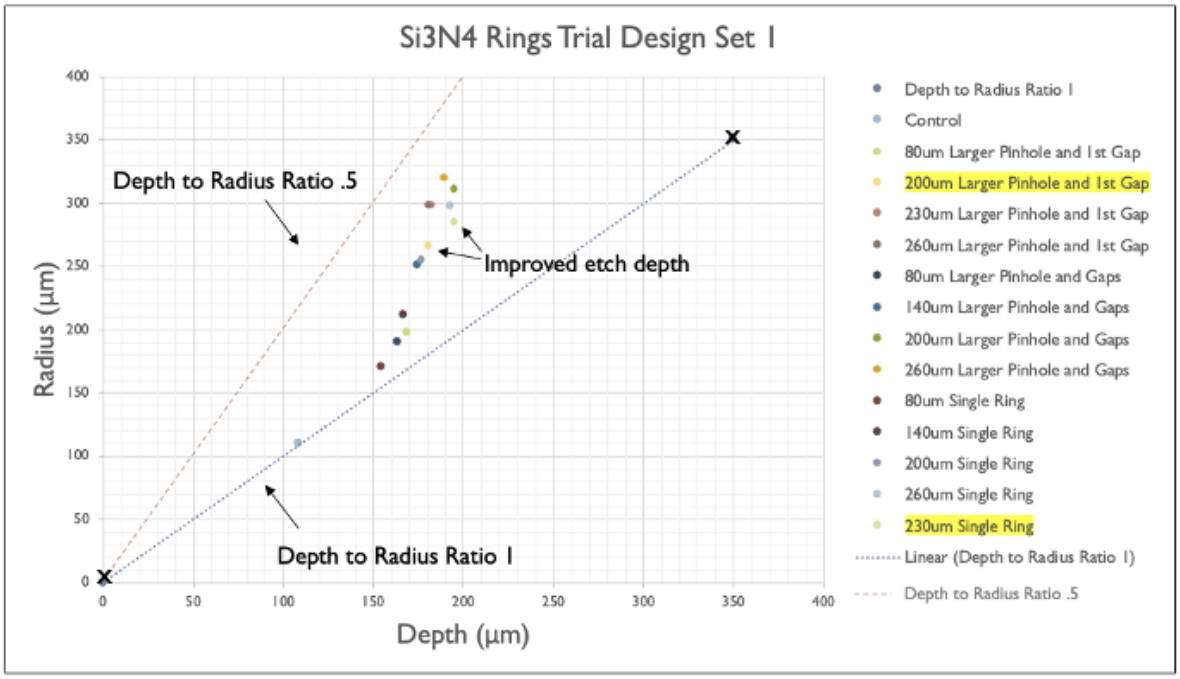

Figure 3.17. Plot of 1st set of silicon nitride trial results with larger less symmetric molds

order to both improve size and symmetry. This best mold showed a size improvement of 22μm and came close to the experimental goals of reaching 200μm devices while bettering the symmetry by around .1 in comparison to other 190μm devices.

Next, the 200μm designs, Figure 3.20, increased the ring size from 4 to 10 times the size of the 100μm design rings. Again, as the ring grew larger it allowed for a continuously deeper etch. The first two designs shown in Figure 3.20 reach around the 200μm depth target and the first one has improved symmetry reaching a .75 depth to radius ratio. The noticeable increase in size occurs once the rings reach 8 times the 100μm size. The first of the two larger designs was finally able to significantly break the 200μm threshold while maintaining .72 symmetry. Then the largest design that is 10 times larger than the 100μm layout reached its greatest depth at 236μm while maintaining a better symmetry of .735.

Table 3.5. Results from second set of designs in silicon nitride rings trial

Depth(μm)	**Radius(μm)**	**Depth to Radius Ratio**
	Control	
110	110	1
	80μm pinhole two ring	
167	200	.835
168	211	.796
167	230	.726
191	257	.743
	200μm pinhole one ring	
201	268	.75
196	278	.705
216	300	.72
236	321	.735
	230μm pinhole one ring	
208	294	.707
227	319	.711
249	344	.724
	230μm pinhole two ring	
236	332	.711
247	361	.684
267	394	.678
235	405	.58

The 230μm designs, Figure 3.21, proved to create the deepest isotropic etches while maintaining symmetry ratios of .7 or above as shown in Figure 3.18. Again, the trend continued where as the silicon nitride ring size increases, the size and symmetry of the resulting molds improved. With the first design, the etch depth reached 208μm while holding a .707 depth to radius ratio. Then the next design had a deeper etch and reached 227μm while improving the symmetry ratio to .711. Finally, the third design was able to reach the deepest etch at 249μm. The symmetry was also the best of the three reaching .724.

The final design type, the 230μm two ring design, had the deepest etches of all the design types, but also the worst symmetry as well, shown in Figure 3.22. The etch did continue the trend of improving size as the nitride rings grew larger but failed to do so in the symmetry area. The smallest mold reached 235μm and the largest made it to 267μm. The

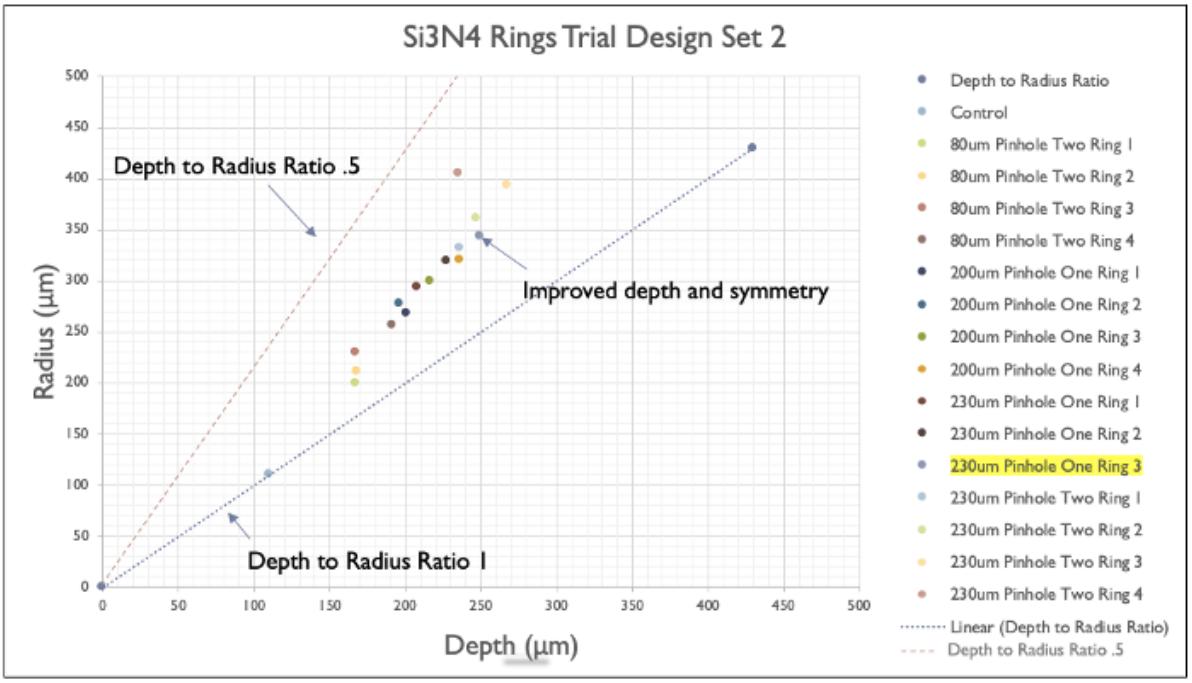

Figure 3.18. Plot of 2nd set of silicon nitride trial results with balanced larger and symmetric single ring design mold

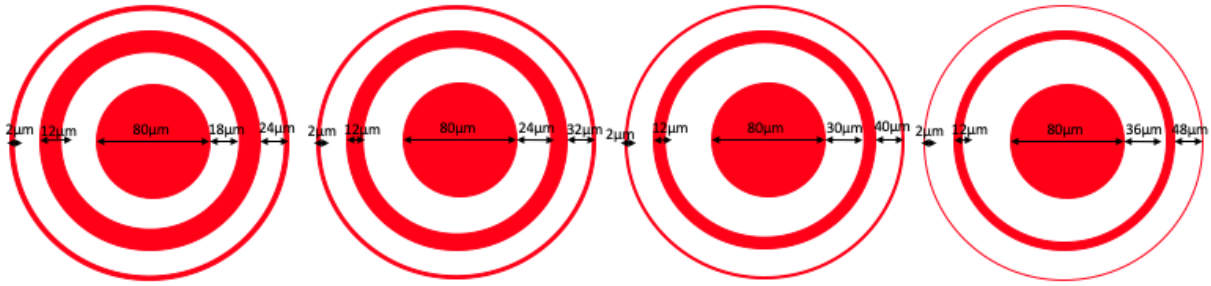

Figure 3.19. 80um pinhole two ring designs with increasing silicon nitride rings

largest design had poor symmetry in comparison to the other ones and reached a symmetry ratio of .678. Also, the most symmetric mold of these designs only reached .711, and it did not have a significantly deep etch only reaching 236μm.

The results from the silicon nitride ring trials resulted in the confirmation of the theory that by increasing ring size, the pop-up rings fly off time could be slowed down allowing for a deeper etch. Within these trials the etch depth goal of 200μm is met by multiple designs.

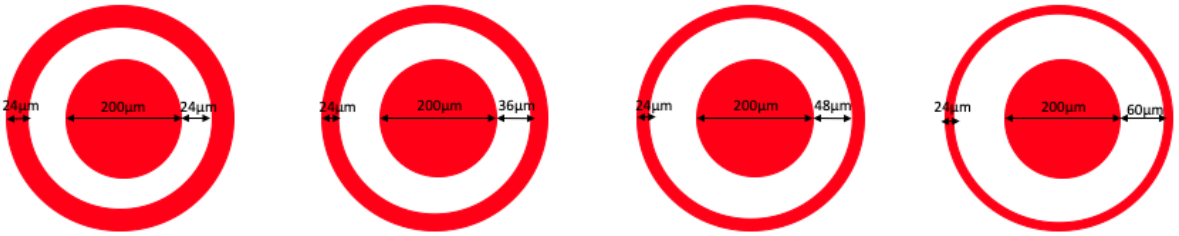

Figure 3.20. 200um pinhole one ring designs with an increasing nitride ring

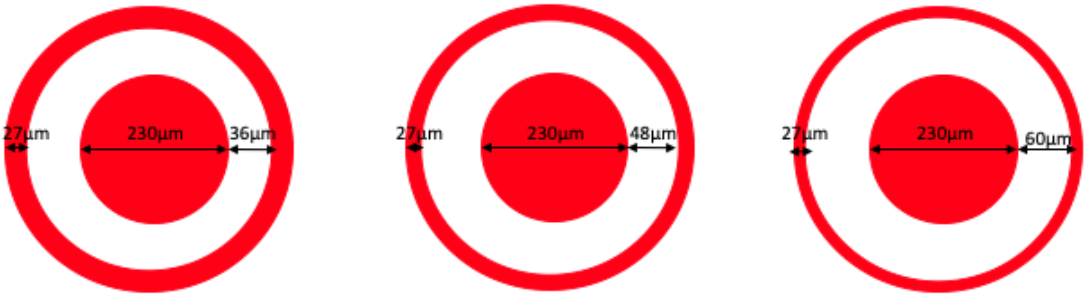

Figure 3.21. 230um pinhole one ring designs with an increasing nitride ring

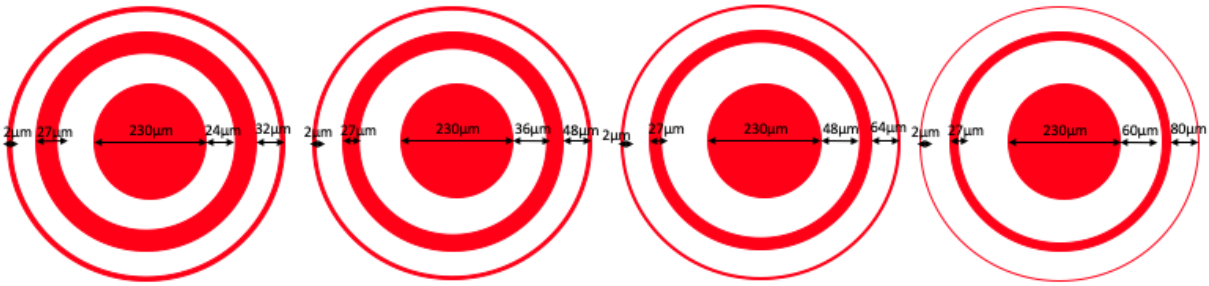

Figure 3.22. 230um pinhole two ring design with increasing silicon nitride

Although the symmetry is not in the .9 depth to radius range as the optimum 100μm design, it is shown that symmetry can still be held with the best mold of all the designs in the trial reaching 249μm with a symmetry ratio of .724. With the conclusion of the silicon nitride rings tests along with the analysis done with the pinhole and gap trials, a more accurate model is able to be created for future optimization of these larger HSR molds based on the pop-up ring design.

4. CONCLUSION

This research set out to fabricate larger symmetric HSR molds while gaining a deeper understanding of the pop-up rings design. From the series of design tests and fabrication experiments it can be concluded that larger HSR molds can be made using the pop-up ring design method while maintaining symmetry. Comparative analysis of the results shows that the pop-up ring design performed the best at creating molds that balanced symmetry and size. The information gained from various types of pop-up ring designs tested allowed for a new cross section model to be made, shown in Figure 4.1. With this model a better representation of the properties of the pop-up rings is created.

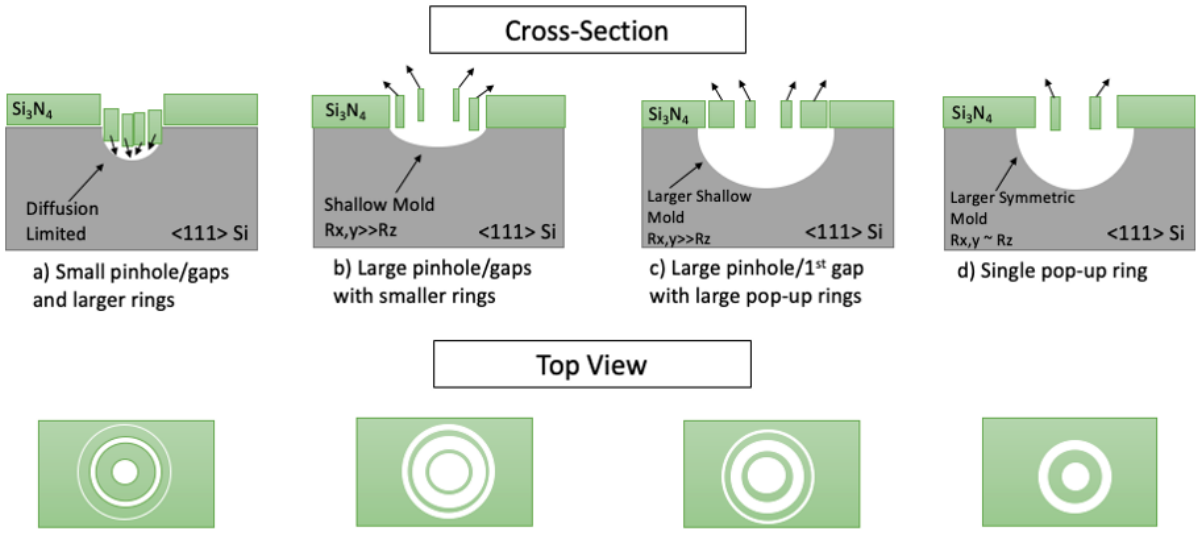

Figure 4.1. Cross section from results of larger HSR mold trials

A continuation of the work done for MEMS HSR gyroscope sensing structures was successfully completed by creating a systematic series of design and fabrication tests to learn about the promising pop-up rings design method. The comparison of the pop-up rings design to the past pinhole designs helps to indicate what path should be followed for future HSR fabrication. In addition to the improvements made to the design methodology, improvements to the fabrication process allows for better control and a higher yield. The silicon nitride

mask was made thicker allowing for longer etches without worry of prematurely stripping the masks leading to an inadequate mold. Then the metrology tools were better utilized to more accurately track etch rates and depth. Past wet etch analysis used only a SEM to track the undercut of the molds in order to estimate etch diameter and depth. This method starts to fail as you experiment with drastically increasing the size of the pop-up ring and pinhole designs leading to early stoppage of the wet etch. In order to more accurately track the wet etch, in addition to monitoring the undercut, the amount of silicon nitride left after each etch period is measured to make sure that the etching is consistent across all trials. Also, a high-quality SEM is used to view the pop-up ring design openings and make sure that the rings were able to fly off and didn't sink into the mold. These improvements to the fabrication methods allowed for more accurate and beneficial trials throughout the research.

With the data from the results, the characteristics of the pop-up rings were able to be used to optimize the size and symmetry of the HSR. The initial trials show that increasing the pop-up ring designs in small increments does not increase the size of the mold in comparison to the previously known 100μm designs. Eventually using this design methodology causes the rings to become large enough where they sink into mold instead of popping off causing the wet etch to be limited. To solve the issues, the next trials experimented with creating large pinhole and ring gap opening to make sure that the rings would fly off and a deeper etch could be reached. The pinhole and gap tests demonstrated that a deeper etch could start to be reached while maintaining some symmetry using the pop-up ring method. The issues that arose at the end of these trials were that depth became limited to around a 50% increase from the 100μm design and the final designs became less symmetric and shallow. Based on the data from the best of the pinhole and ring gaps designs, Figure 4.2, the final set of trials were set up. With these tests the rings were increased in size in hopes of creating a deeper and more symmetric etch.

During the initial silicon nitride ring increase trials, an improvement is seen in the size of the molds with the largest design reaching close to 200μm. This is a 100% increase from the original optimal pop-up ring design for 100μm devices. The trial consisted of

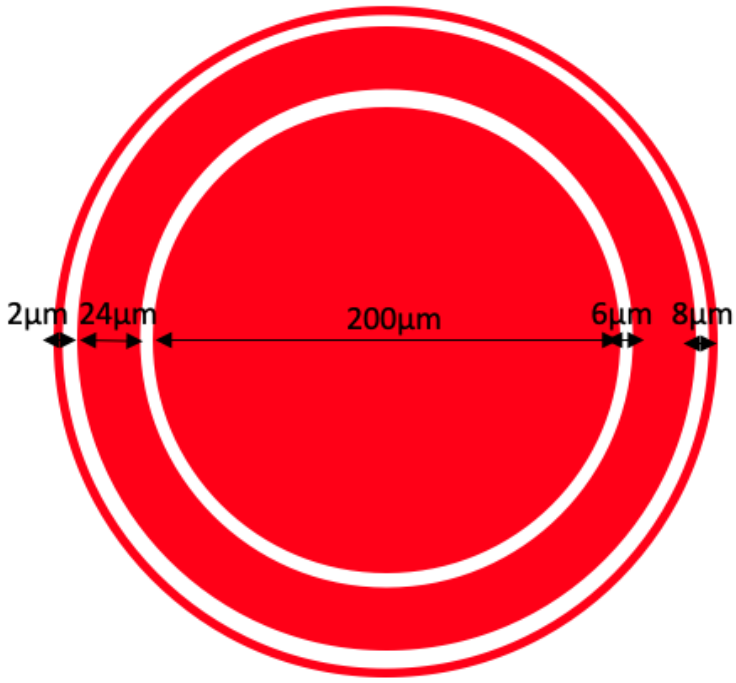

Figure 4.2. Cross section of larger HSR mold results

two ring designs that increased the ring sizes based on best results of the previous trials. Then because of the shallowness issue, a single pop-up ring design is tested to focus the etch more towards the center of the mold. The success from these changes proved that the desired size increases could be reached by using an alteration of the pop-up ring method. Also, an improvement in the symmetry occurred with the molds becoming less shallow. Because of these improvements, the ring sizes continued to be increased in hopes of continued improvement of the symmetry. The final silicon nitride ring experiments continued to follow the trend seen in the first trial. A deeper etch is achieved overall and the best design, Figure 4.3, from the research maintained a significant amount of symmetry. The single ring designs have a better balance of size and symmetry with the best single ring design reaching 249μm in depth and having a depth to radius symmetry ratio of .724 as seen in the SEM and depth profile shown in Figure 4.4. The deepest single ring design reached 267μm, but had a poorer symmetry ratio of .678 so therefore the previously mentioned design proved to be the most optimal. In comparison, the two ring designs had better symmetry with the best design reaching a depth to radius ratio of .835. Even though the symmetry is better, the mold

size is still limited with it reaching only 167μm. Since the main goal of the research is to be able to create larger HSR structures, the single ring designs prove to be more effective in reaching this goal while maintaining a significant amount of symmetry. Therefore, at the conclusion of the investigation it is seen that the single ring design shown in figure 4.3 created the most optimal results from the trials reaching a depth of 249μm and a symmetry ratio of .724. These final results were a significant improvement with the final mold more than doubling the size of the original 100μm devices. Also, the symmetry of the larger molds was noticeably improved with the initial large structures having a poor depth to radius ratio closer to .5 that was eventually optimized to allow some of the best devices to reach close to .8. With the data collected from these experiments and an optimal design to work with, future fabrication of larger symmetric HSR structures can be done more effectively.

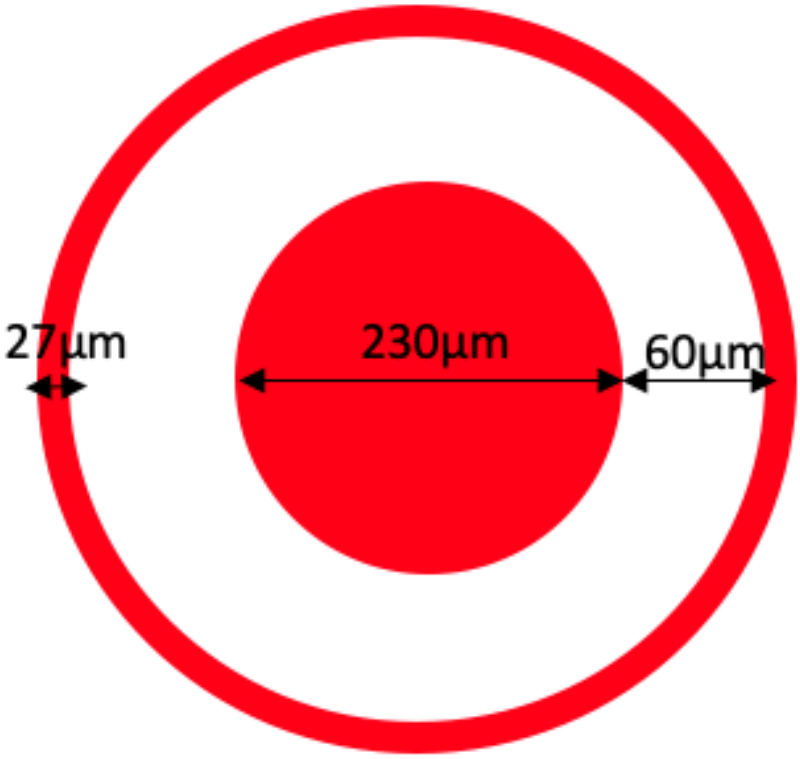

Figure 4.3. Best overall design from final nitride ring experiments

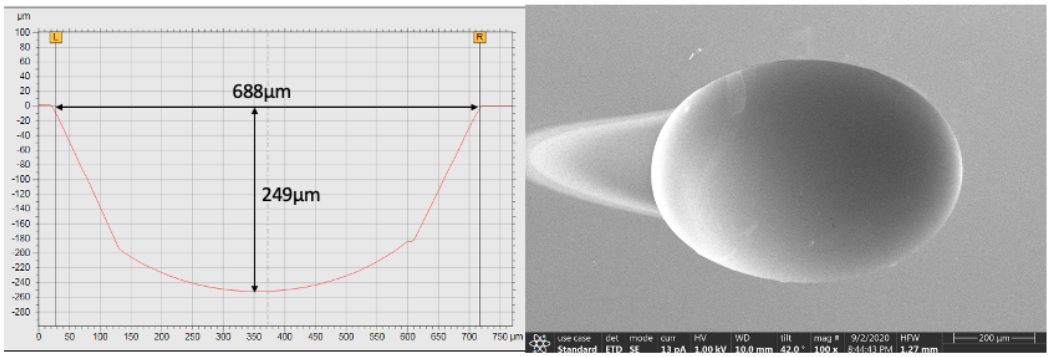

a) Depth graph of largest and most symmetric HSR mold

b) SEM of largest and most symmetric HSR mold

Figure 4.4. a) Depth chart of largest and most optimal HSR mold b) SEM image of most optimal mold

Based on the conclusions found in the research, future work can be done to make larger and more symmetric HSR devices. From these results it would be recommended to work on a predictive model using the collected data to observe any patterns that occur between the 100μm devices and the final most optimal 249μm device. With a predictive model, time and materials can be saved from the fabrication process as well as more insight to the specifics of the etch depths in relation to pinhole and gap openings. In addition to a computer modeling program, further improvement can be made by continuing the design process done in this research of first increasing the size of the openings and right after increasing the size of the silicon nitride rings to bring the HSR devices closer to the mm scale. Also, the larger molds currently made can be optimized by experimenting with the ratio of the outside ring gap to the single ring of the 230μm pinhole design. It is believed that better symmetry can be achieved by increasing the outside gap size while maintaining the other parameters. These larger molds can then be released using a XeF_2 as done in the trials shown in the 2018 OxideMEMS paper. After the release of the largest devices from these trials they should be tested, and the frequency response can be recorded and compared to previous 100μm results. Finally, once a series of optimized devices from 250μm to 500um are fabricated and released, a series of acceleration induced noise insensitivity tests can be done to understand

the different sized devices as it continues to get closer to mm size. With this information a greater spectrum of applications for variously sized MEMS gyroscopes can be made.

BIBLIOGRAPHY

[1] Rozelle, David. (2009). The Hemispherical Resonator Gyro: From Wineglass to the Planets. Advances in the Astronautical Sciences. 134. 1157-1178.

[2] Torunbalci, Mert. Purdue University, 2018, pp. 1–17, Design of Experiments: Experiments for Silicon Mold.

[3] Joubert, Stephan Shatalov, Michael Fay, Temple. (2009). Rotating structures and Bryan's effect. American Journal of Physics. 77. 520-525. 10.1119/1.3088877.

[4] M. M. Torunbalci, S. Dai, A. Bhat and S. A. Bhave, "Acceleration insensitive hemispherical shell resonators using pop-up rings," 2018 IEEE Micro Electro Mechanical Systems (MEMS), Belfast, 2018, pp. 956-959, doi: 10.1109/MEMSYS.2018.8346716.

[5] Rahman, Mahbubur Xie, Yan Mastrangelo, C.H. Kim, Hanseup. (2014). 3-D hemispherical micro glass-shell resonator with integrated electrostatic excitation and capacitive detection transducers. Proceedings of the IEEE International Conference on Micro Electro Mechanical Systems (MEMS). 672-675. 10.1109/MEMSYS.2014.6765730.

[6] Wang, Renxin et al. "Design and Fabrication of Micro Hemispheric Shell Resonator with Annular Electrodes." Sensors (Basel, Switzerland) vol. 16,12 1991. 25 Nov. 2016, doi:10.3390/s16121991

[7] L. C. Fegely, D. N. Hutchison and S. A. Bhave, "Isotropic etching of 111 SCS for wafer-scale manufacturing of perfectly hemispherical silicon molds," 2011 16th International Solid-State Sensors, Actuators and Microsystems Conference, Beijing, 2011, pp. 2295-2298, doi: 10.1109/TRANSDUCERS.2011.5969536.

[8] J. Cho, J. -. Woo, J. Yan, R. L. Peterson and K. Najafi, "A high-Q birdbath resonator gyroscope (BRG)," 2013 Transducers Eurosensors XXVII: The 17th International Conference on Solid-State Sensors, Actuators and Microsystems (TRANSDUCERS EUROSENSORS XXVII), Barcelona, 2013, pp. 1847-1850, doi: 10.1109/Transducers.2013.6627150.

[9] Zhang, Yongmeng; Wu, Yulie; Wu, Xuezhong; Xi, Xiang; Wang, Jianqiu. 2015. "A Novel Vibration Mode Testing Method for Cylindrical Resonators Based on Microphones." Sensors 15, no. 1: 1954-1963

A. POP-UP RING DESIGNS FROM 2ND PINHOLE AND GAPS TRIAL

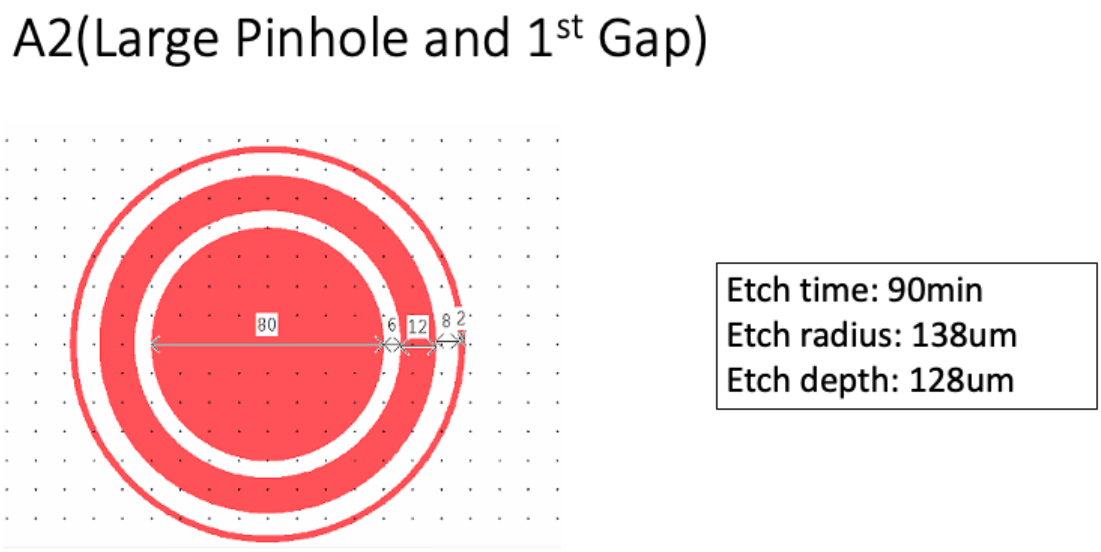

Figure A.1. 80μm Large pinhole and 1st gap design

B1(Large Pinhole and 1st Gap)

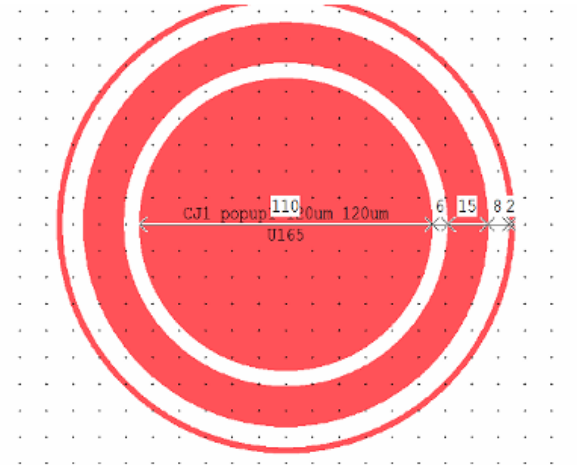

Etch Time: 90min
Etch Radius: 150um
Etch Depth: 136um

Figure A.2. 110μm Large pinhole and 1st gap design

B2(Large Pinhole and 1st Gap)

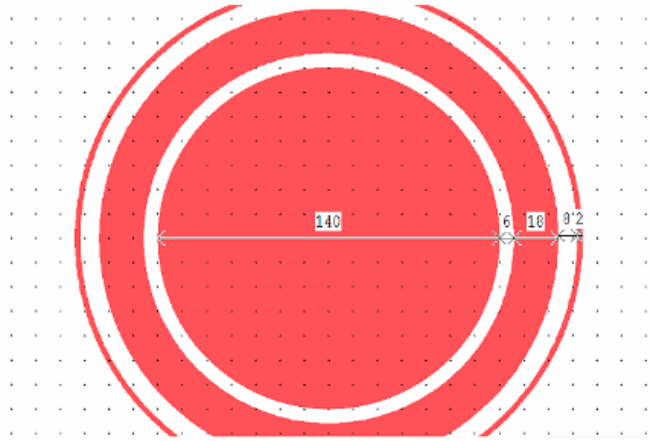

Etch time: 90min
Etch radius: 162um
Etch depth: 136um

Figure A.3. 140μm Large pinhole and 1st gap design

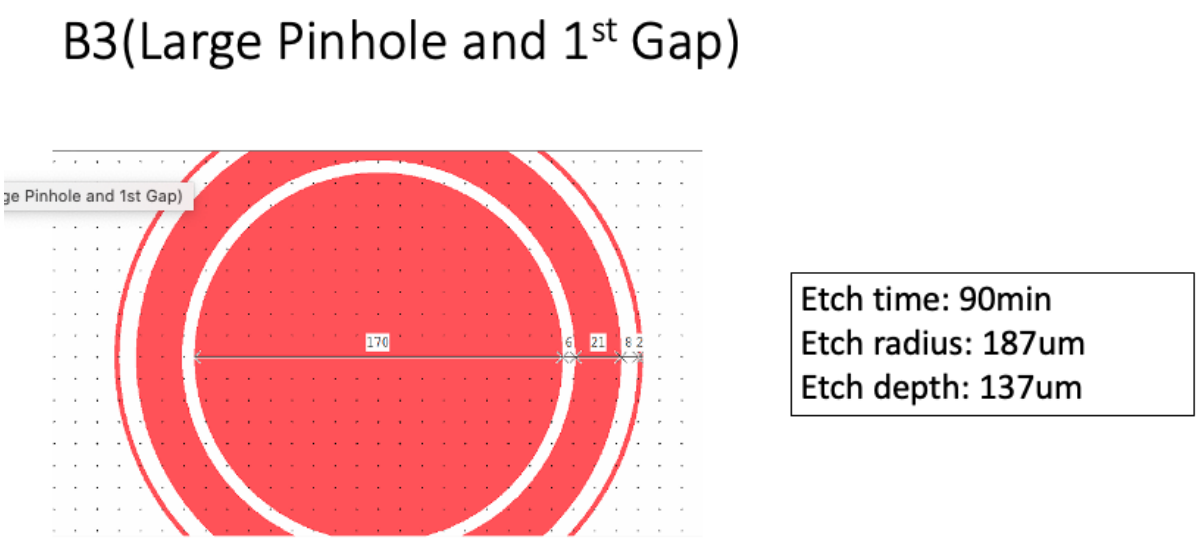

Figure A.4. 170μm Large pinhole and 1st gap design

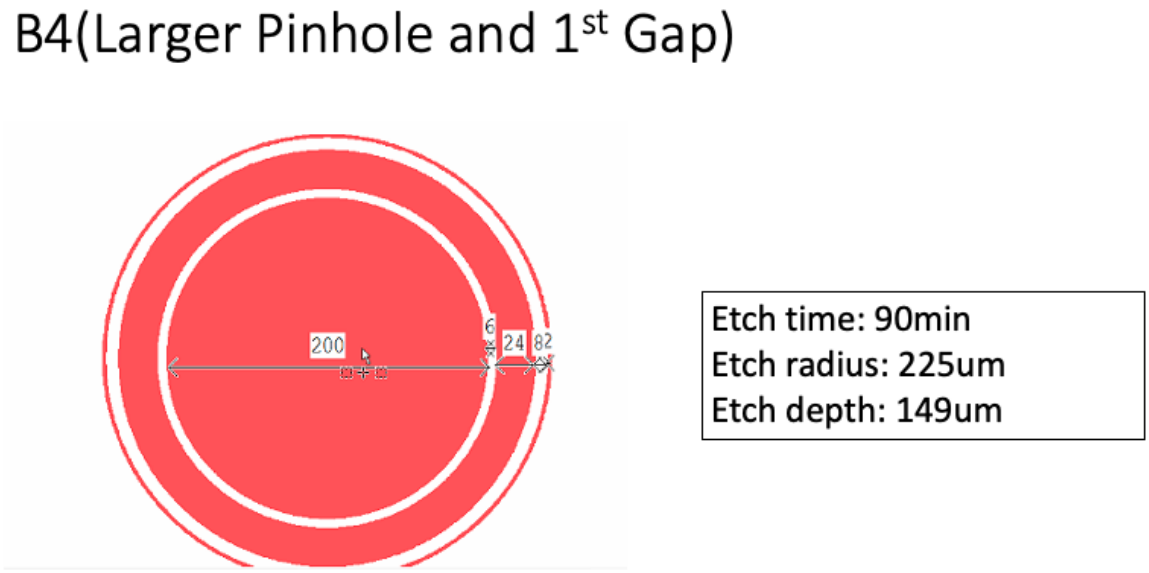

Figure A.5. 200μm Large pinhole and 1st gap design

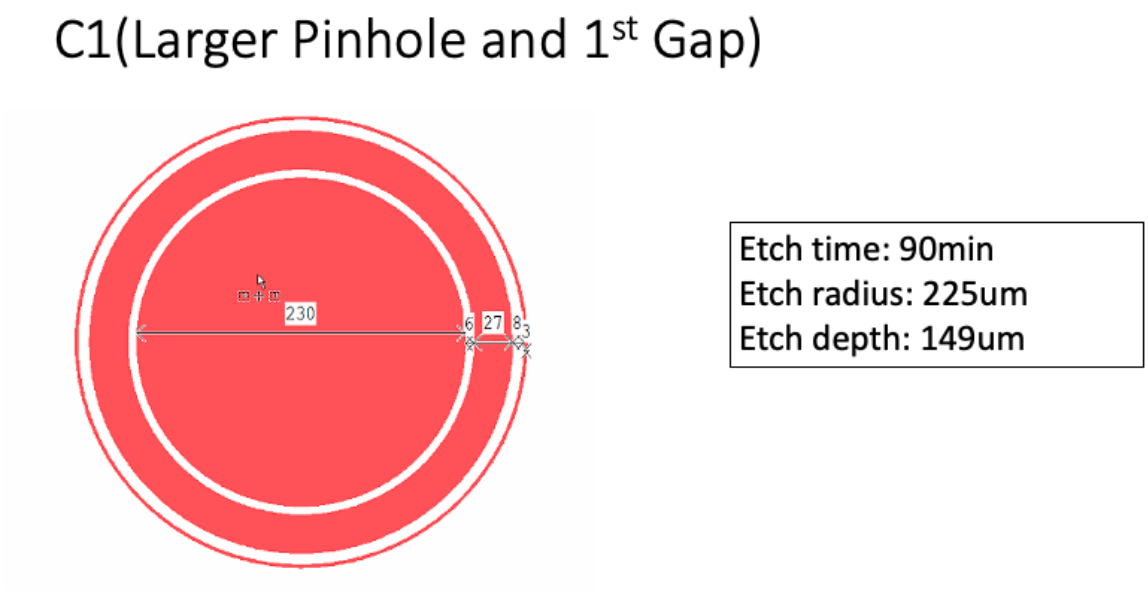

Figure A.6. 230μm Large pinhole and 1st gap design

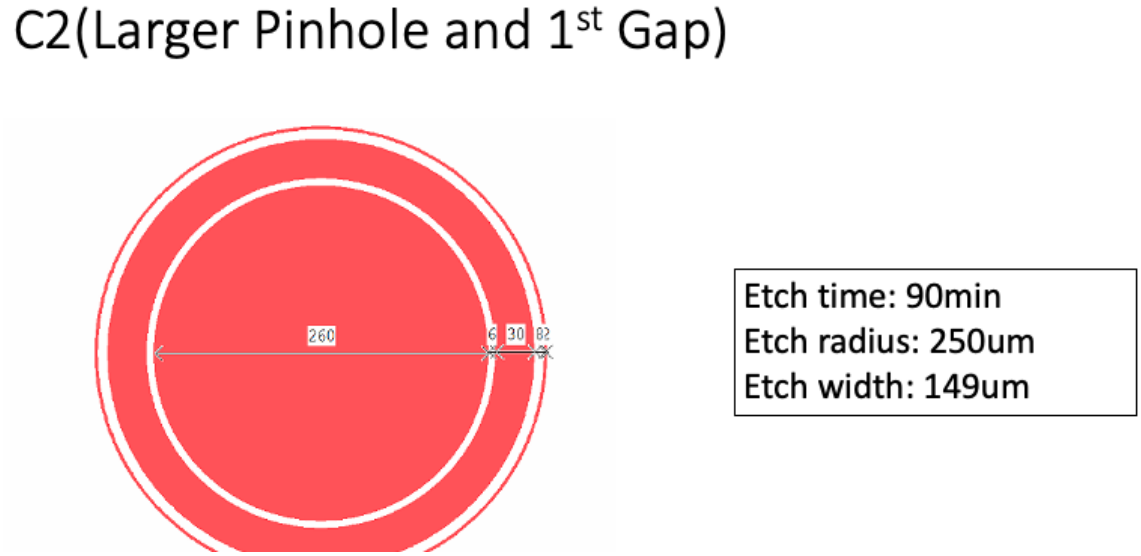

Figure A.7. 260μm Large pinhole and 1st gap design

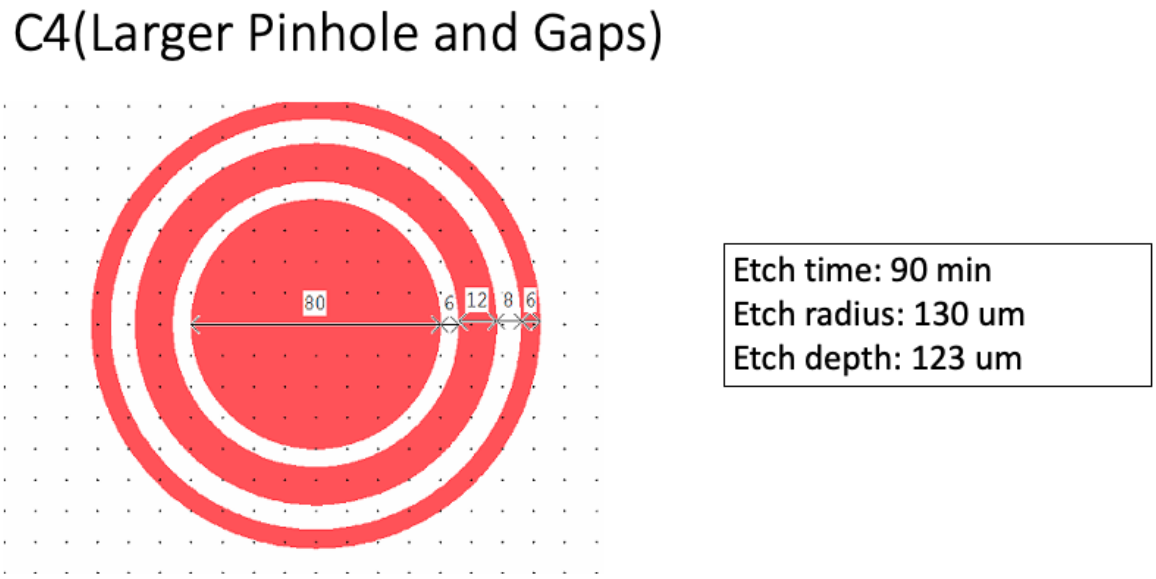

Figure A.8. 80μm Large pinhole and gaps design

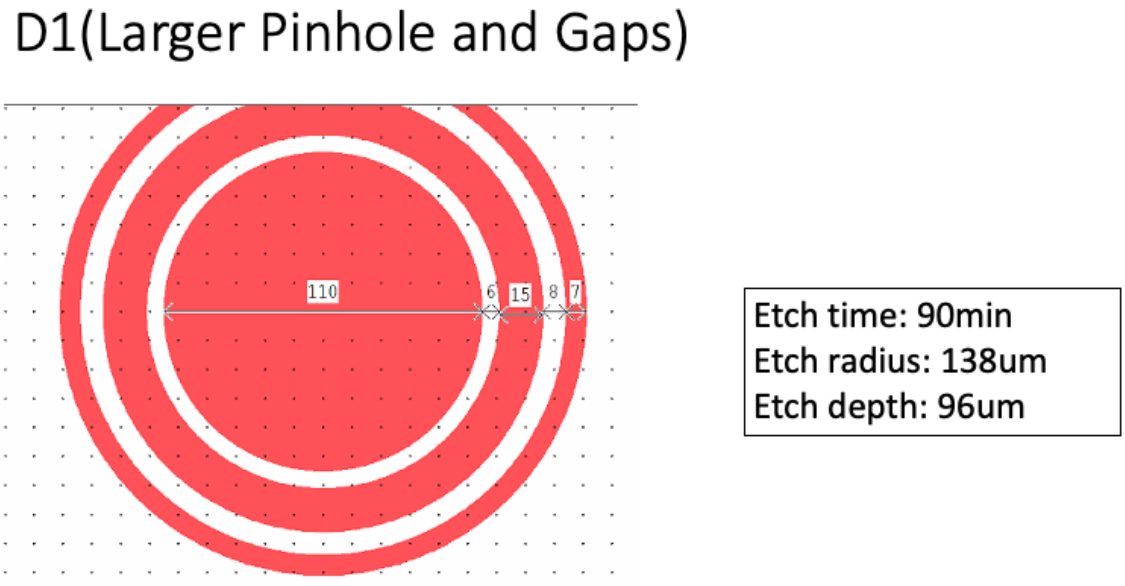

Figure A.9. 110μm Large pinhole and gaps design

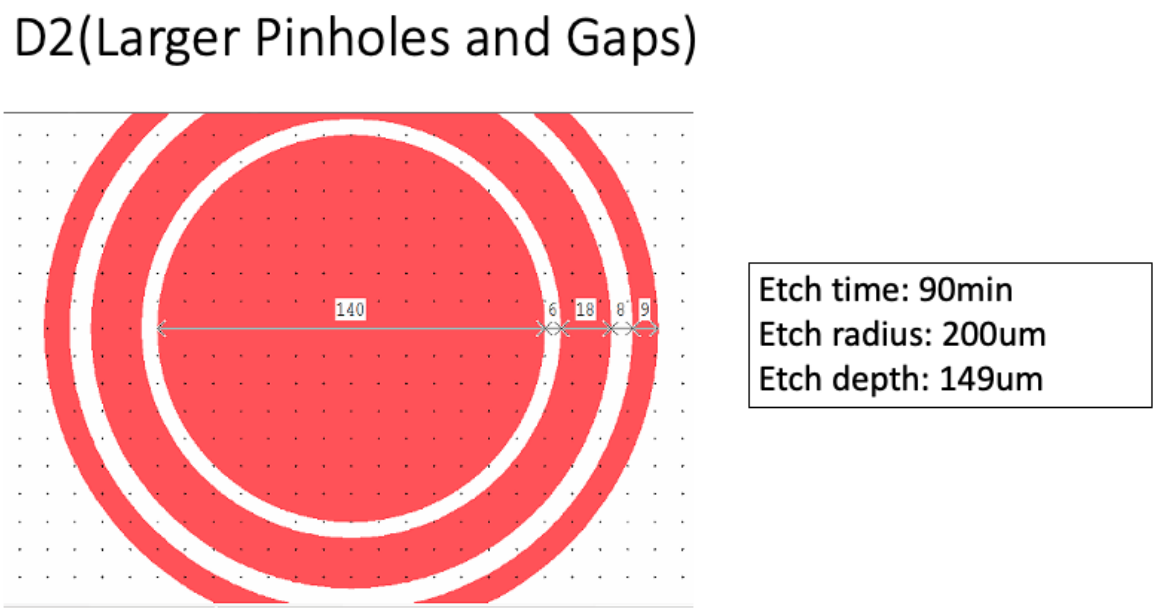

Figure A.10. 140μm Large pinhole and gaps design

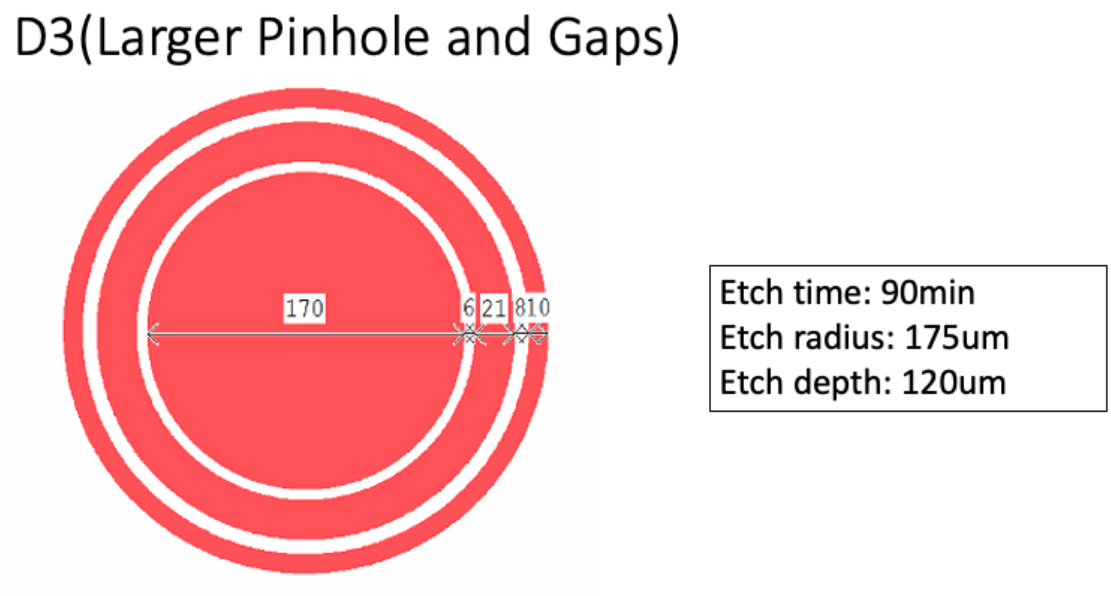

Figure A.11. 170μm Large pinhole and gaps design

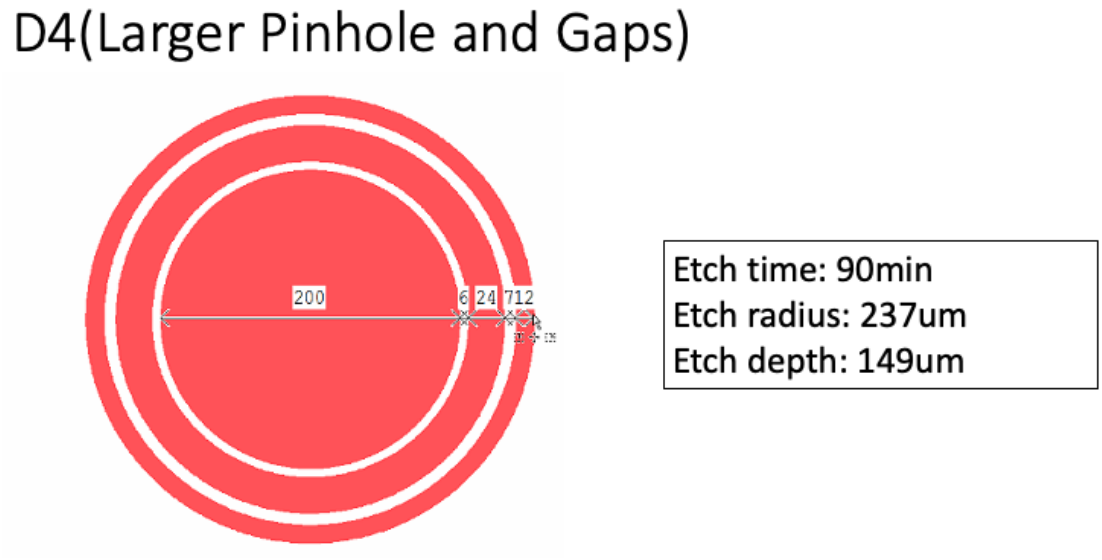

Figure A.12. 200μm Large pinhole and gaps design

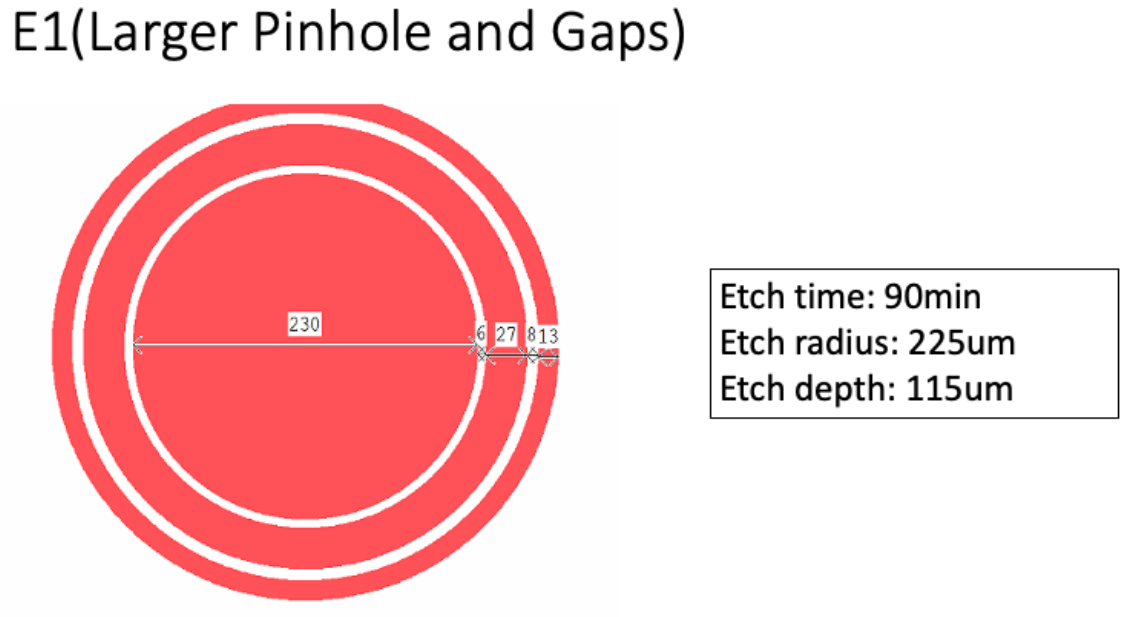

Figure A.13. 230μm Large pinhole and gaps design

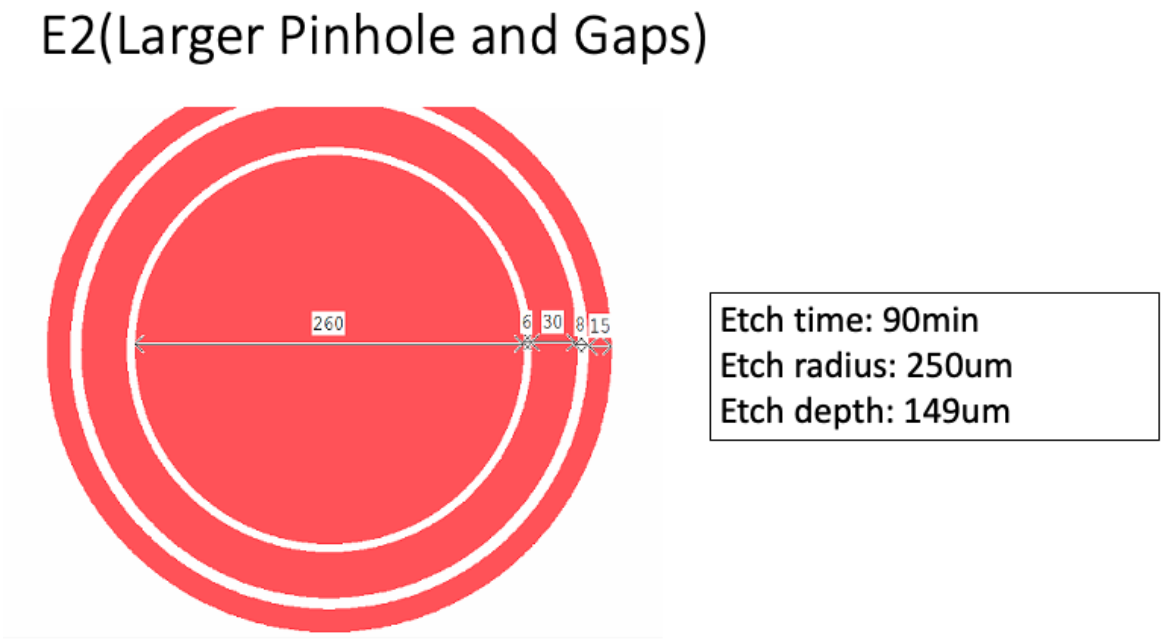

Figure A.14. 260μm Large pinhole and gaps design

B. DEPTH PROFILES

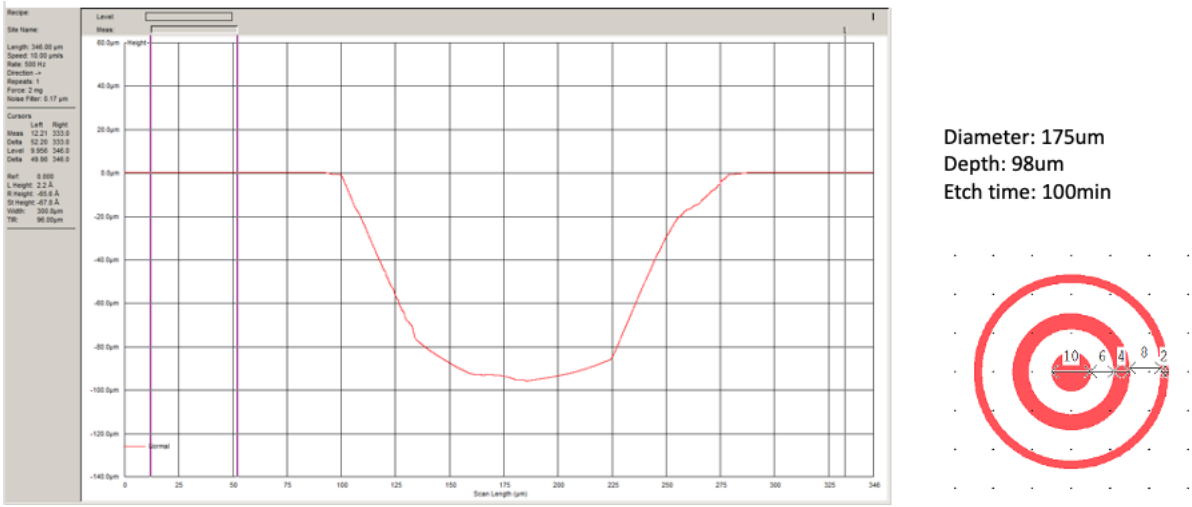

Figure B.1. Depth Profile of control design from 1st pinhole and gaps trial

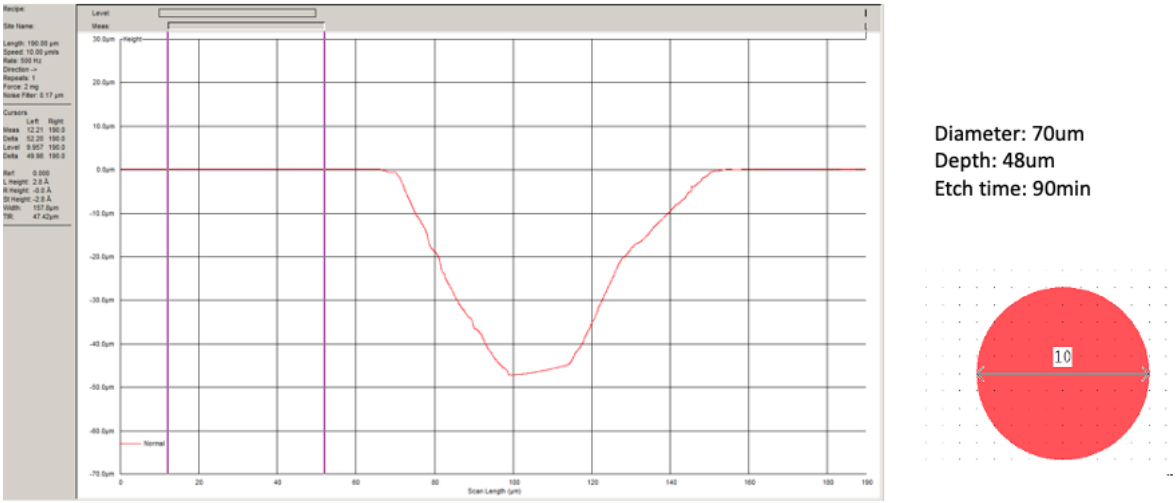

Figure B.2. Depth Profile of 10μm pinhole only design from 1st pinhole and gaps trial

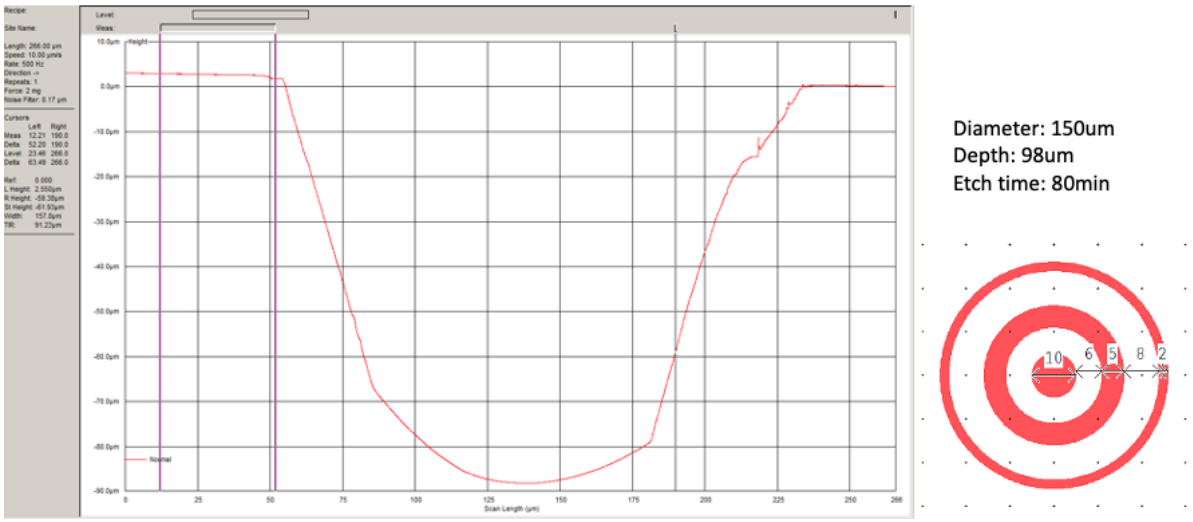

Figure B.3. Depth Profile of 10μm pinhole and larger first gap design from 1st pinhole and gaps trial

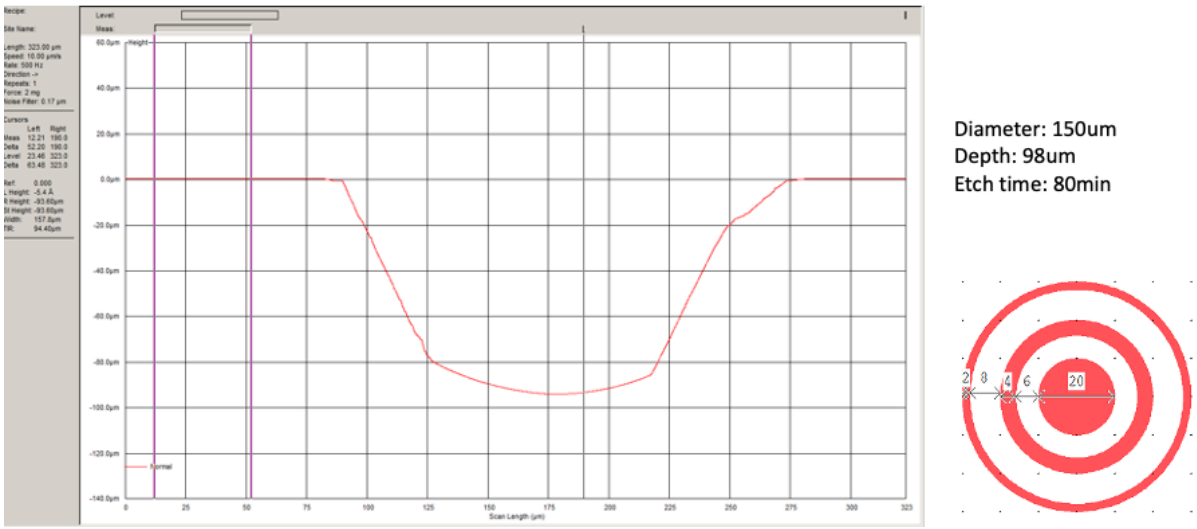

Figure B.4. Depth Profile of 20um pinhole with ideal ring gap design from 1st pinhole and gaps trial

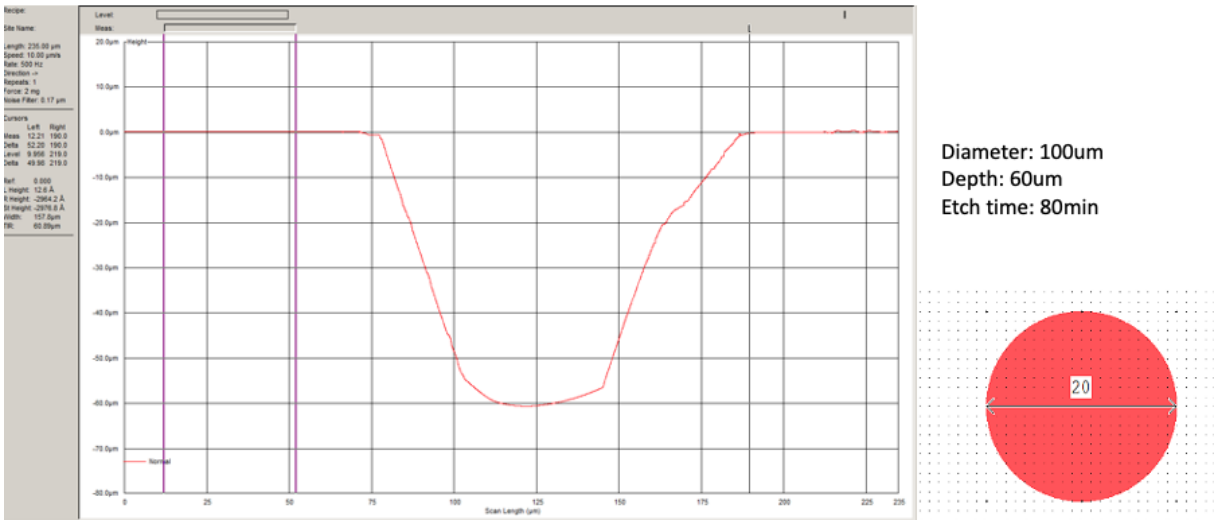

Figure B.5. Depth Profile of 20μm pinhole only design from 1st pinhole and gaps trial

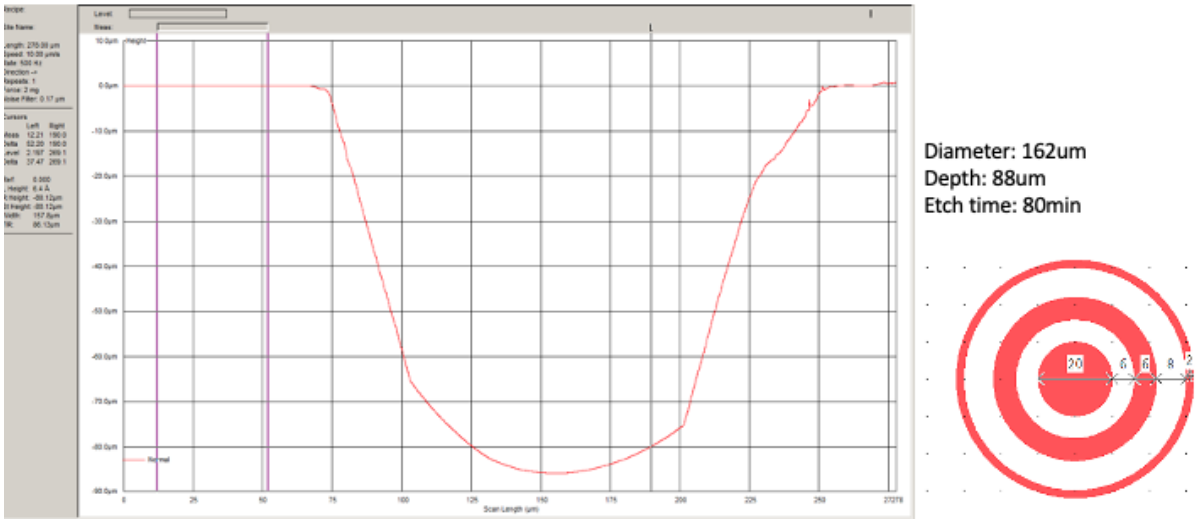

Figure B.6. Depth Profile of 20μm pinhole and larger first gap design from 1st pinhole and gaps trial

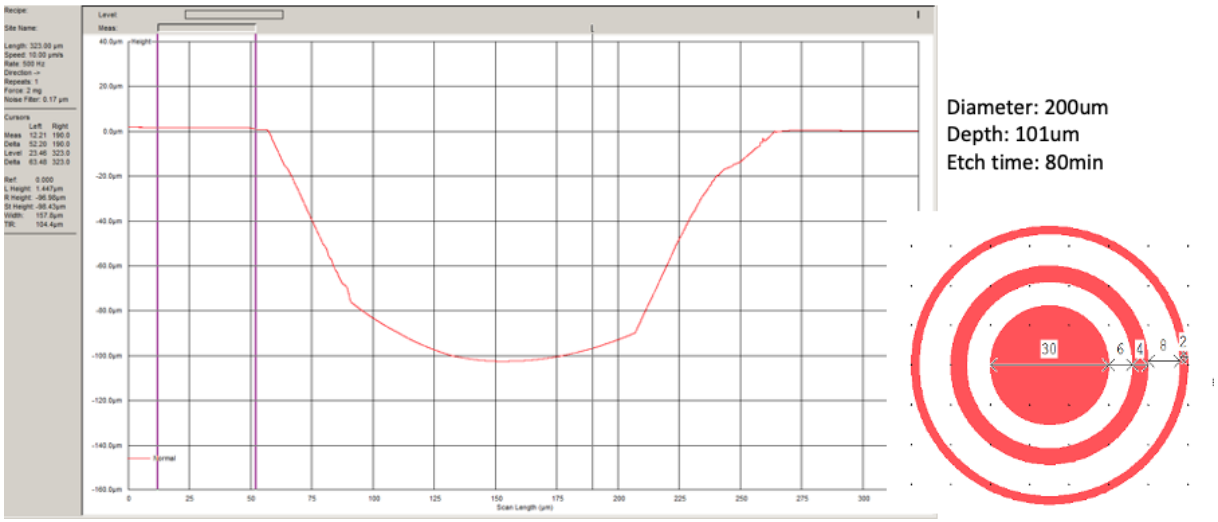

Figure B.7. Depth Profile of 30um pinhole with ideal ring gap design from 1st pinhole and gaps trial

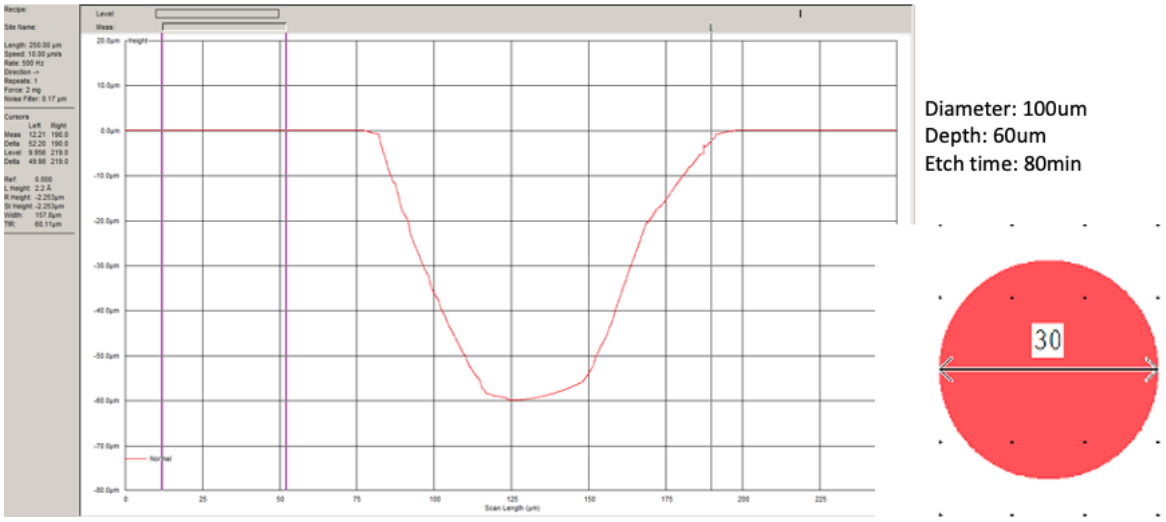

Figure B.8. Depth Profile of 30μm pinhole only design from 1st pinhole and gaps trial

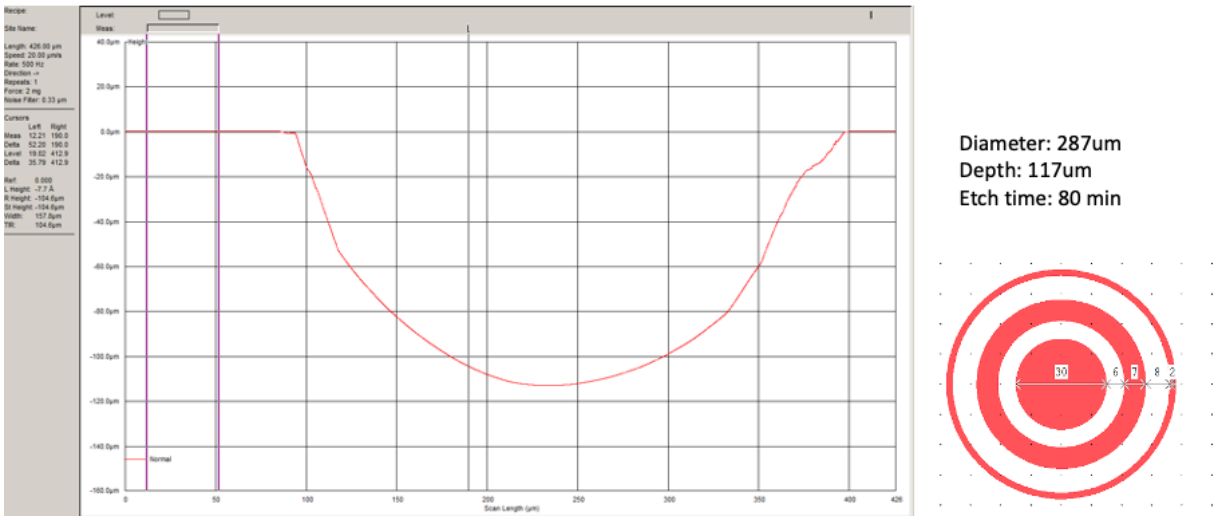

Figure B.9. Depth Profile of 30μm pinhole and larger first gap design from 1st pinhole and gaps trial

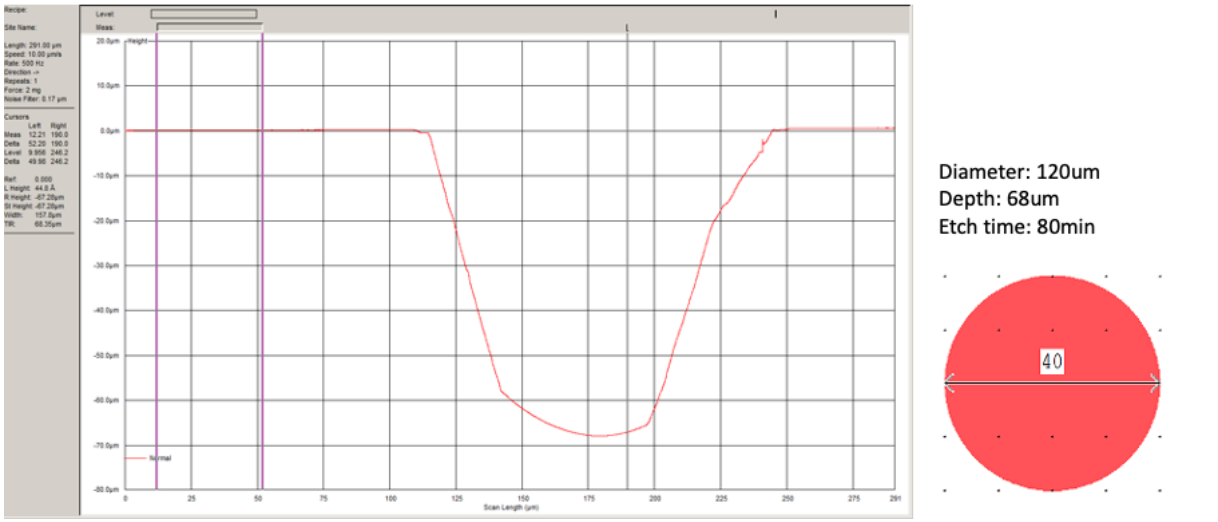

Figure B.10. Depth Profile of 40μm pinhole only design from 1st pinhole and gaps trial

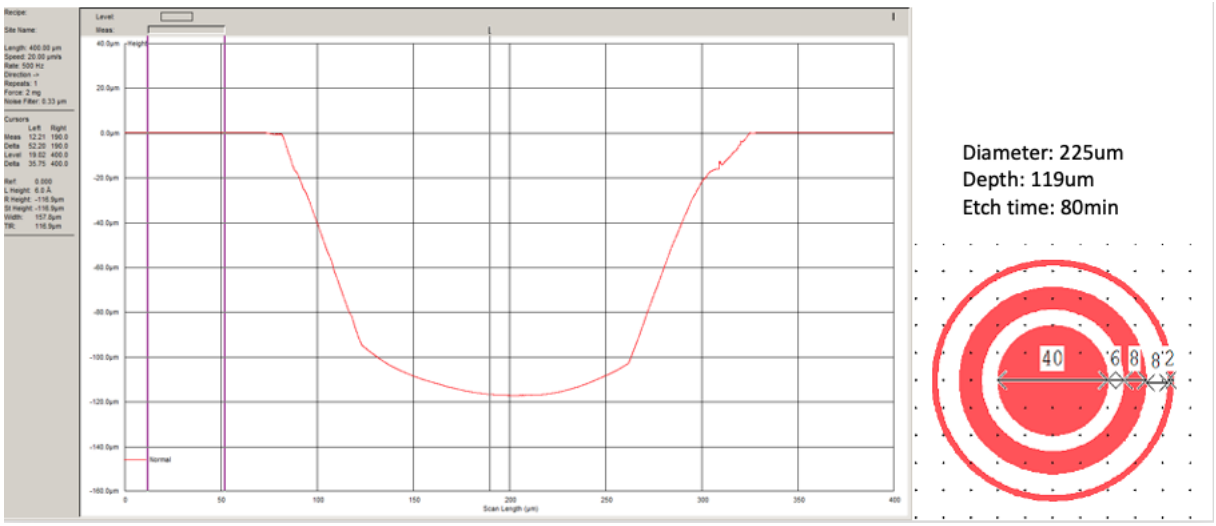

Figure B.11. Depth Profile of 40μm pinhole and larger first gap design from 1st pinhole and gaps trial

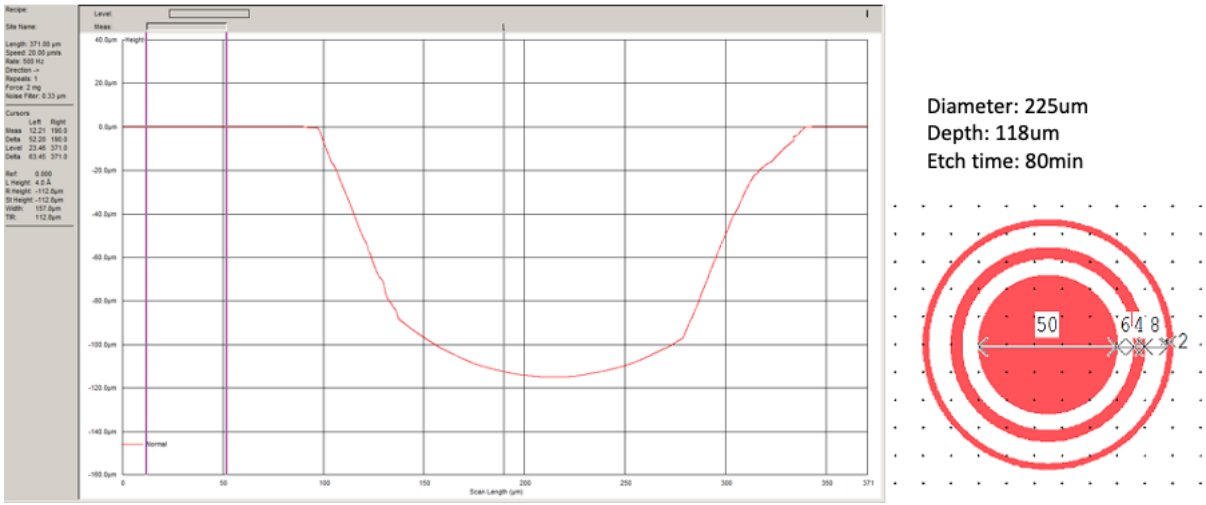

Figure B.12. Depth Profile of 50um pinhole with ideal ring gap design from 1st pinhole and gaps trial

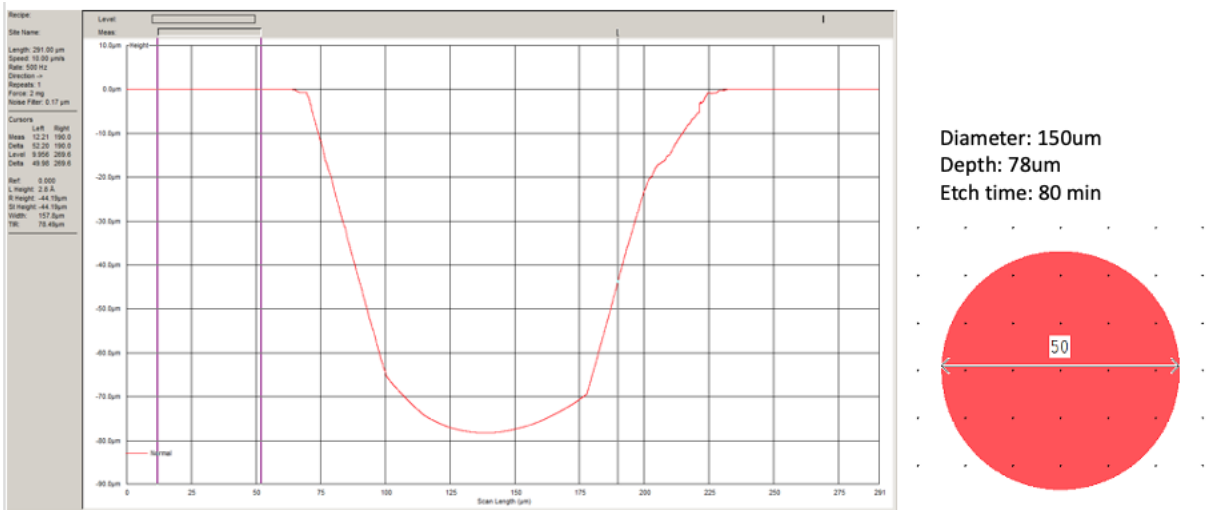

Figure B.13. Depth Profile of 50μm pinhole only design from 1st pinhole and gaps trial

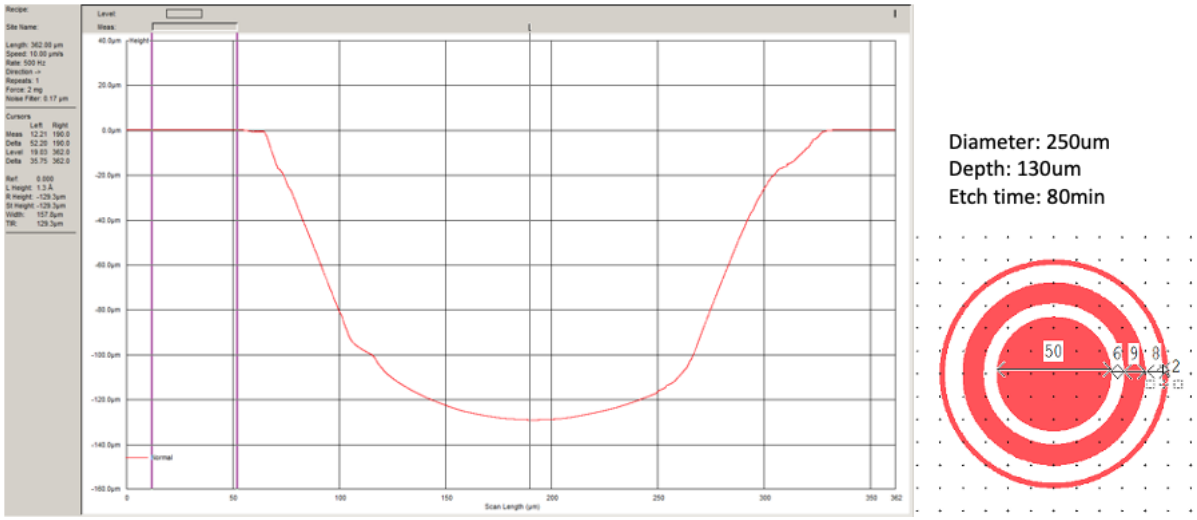

Figure B.14. Depth Profile of 50μm pinhole and larger first gap design from 1st pinhole and gaps trial

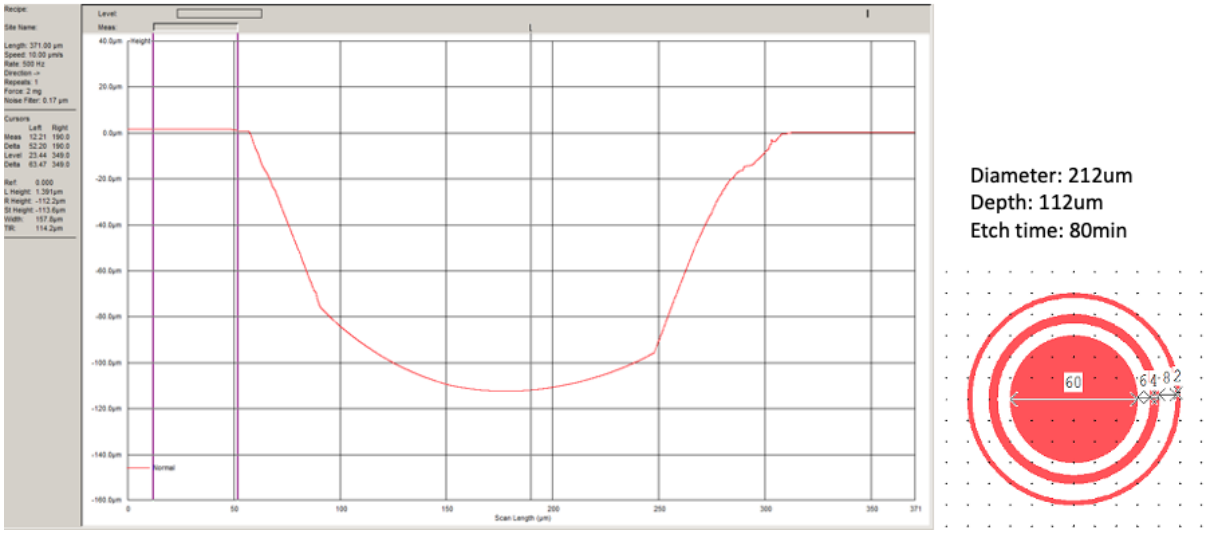

Figure B.15. Depth Profile of 60μm pinhole and larger first gap design from 1st pinhole and gaps trial

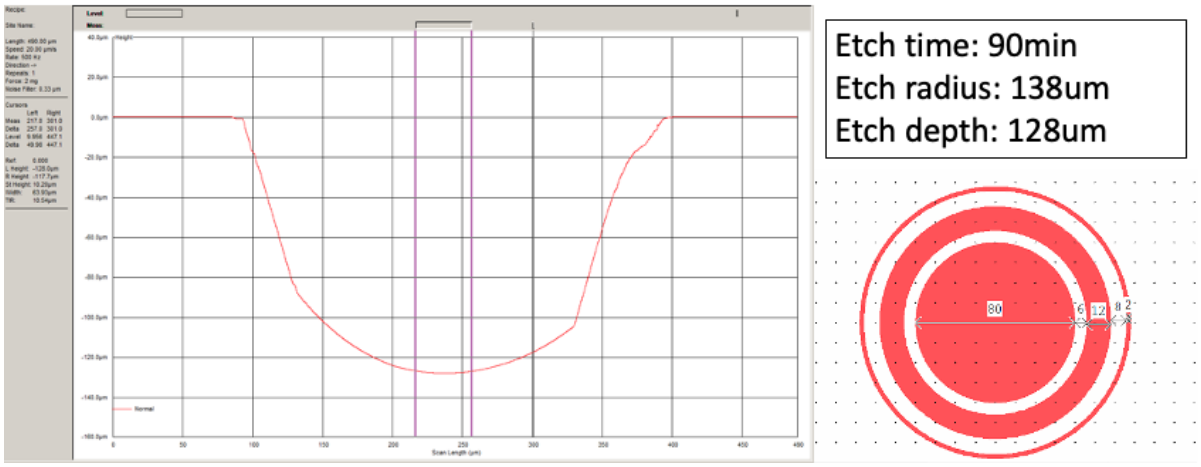

Figure B.16. Depth Profile of 80μm pinhole and larger first gap design from 2nd pinhole and gaps trial

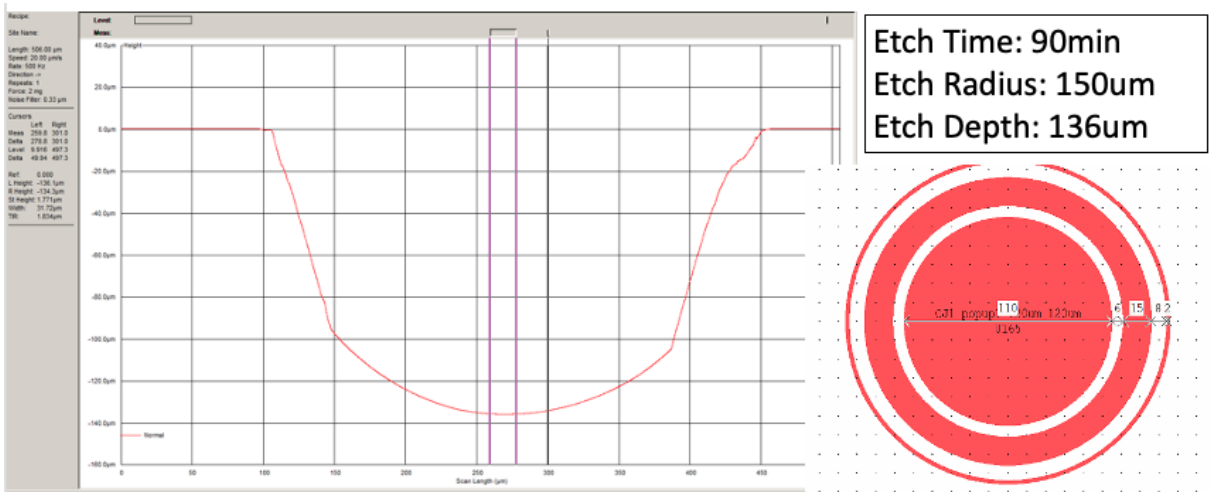

Figure B.17. Depth Profile of 110μm pinhole and larger first gap design from 2nd pinhole and gaps trial

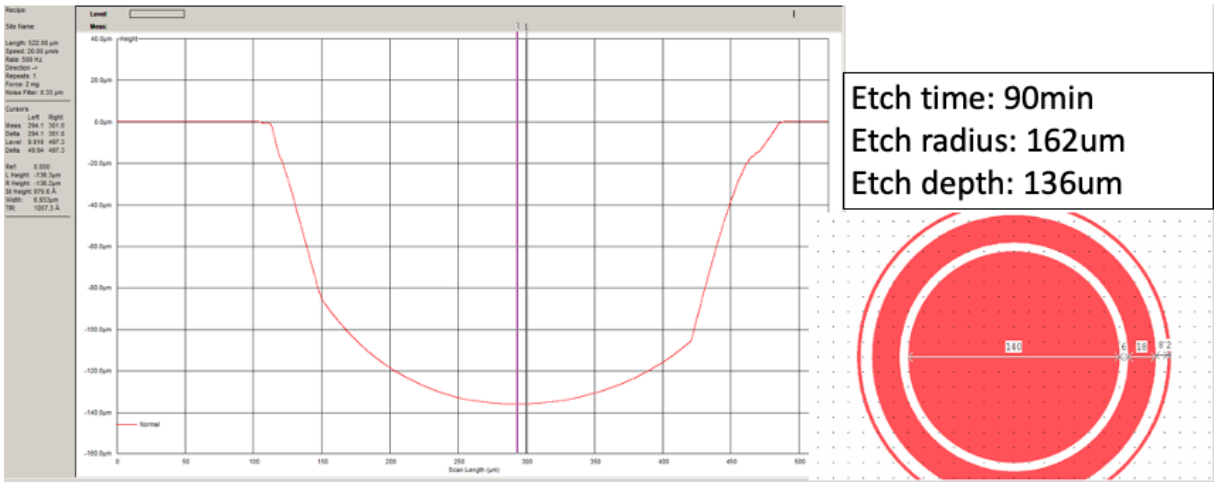

Figure B.18. Depth Profile of 140μm pinhole and larger first gap design from 2nd pinhole and gaps trial

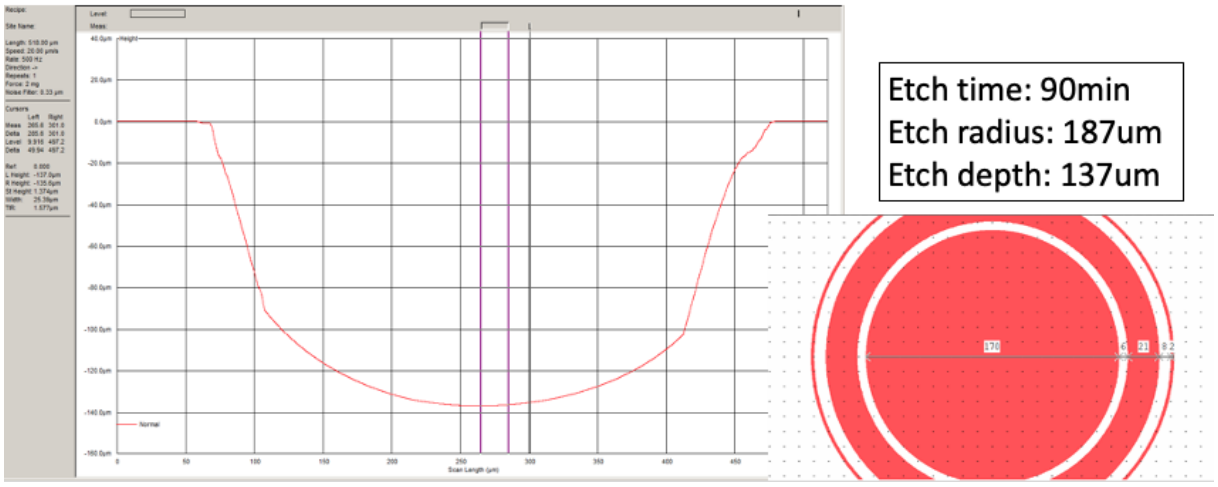

Figure B.19. Depth Profile of 170μm pinhole and larger first gap design from 2nd pinhole and gaps trial

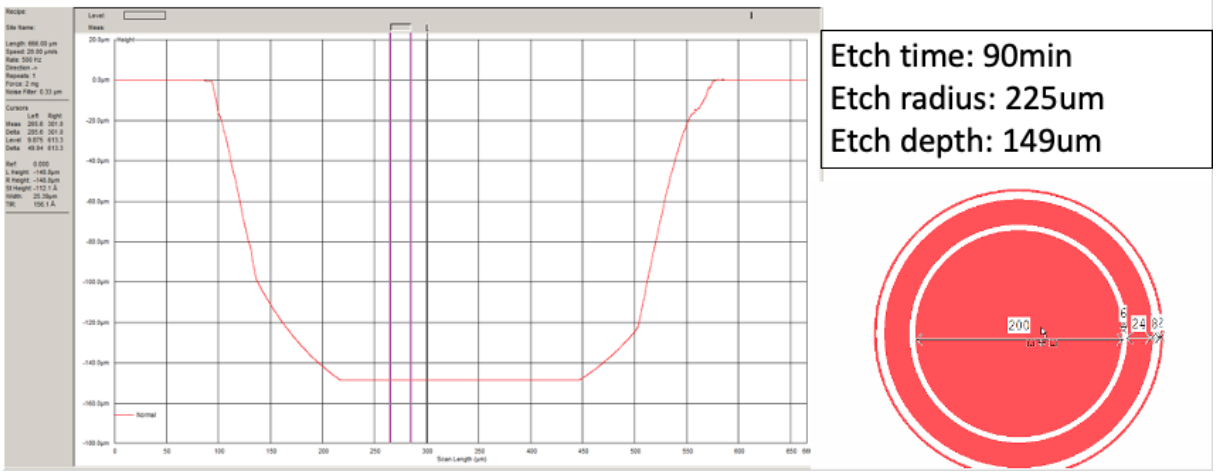

Figure B.20. Depth Profile of 200μm pinhole and larger first gap design from 2nd pinhole and gaps trial

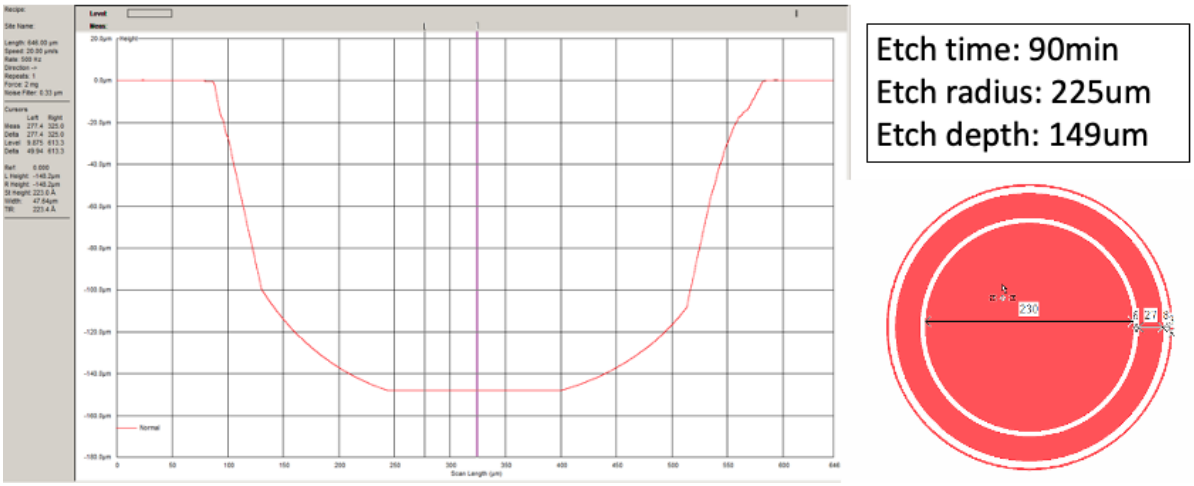

Figure B.21. Depth Profile of 230μm pinhole and larger first gap design from 2nd pinhole and gaps trial

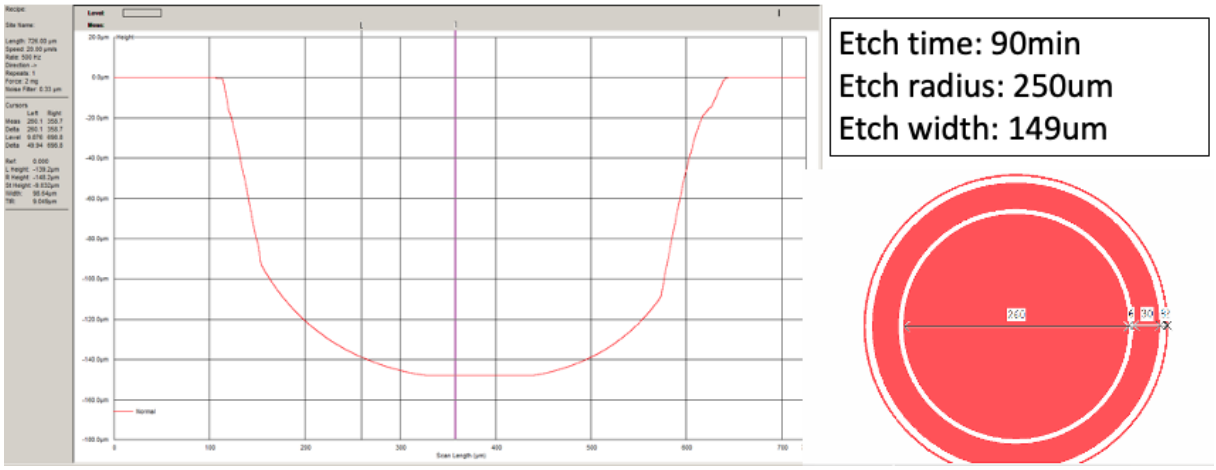

Figure B.22. Depth Profile of 260μm pinhole and larger first gap design from 2nd pinhole and gaps trial

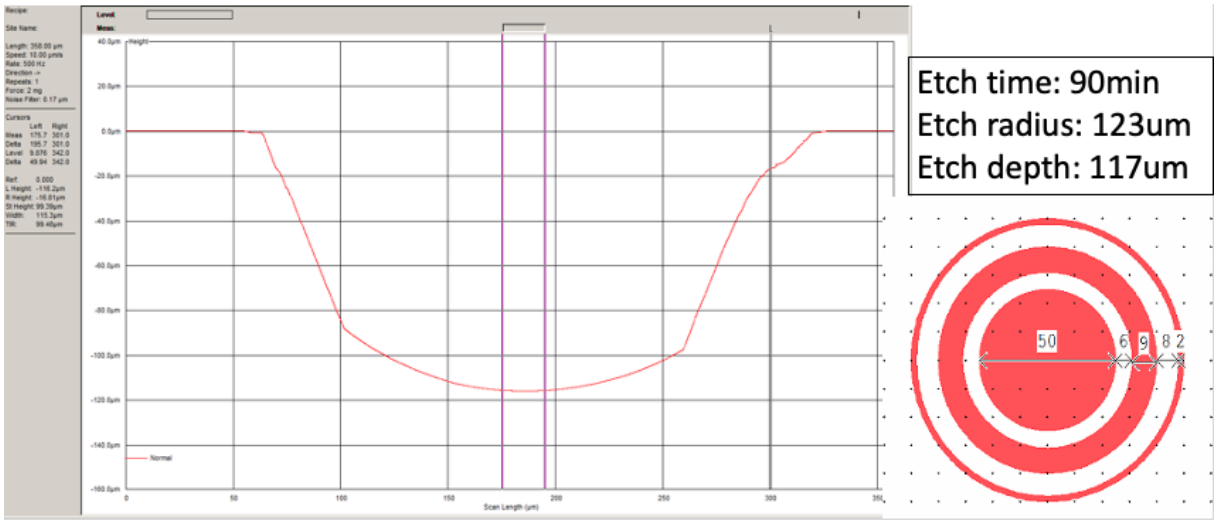

Figure B.23. Depth Profile of 50μm pinhole and larger first gap design from 2nd pinhole and gaps trial

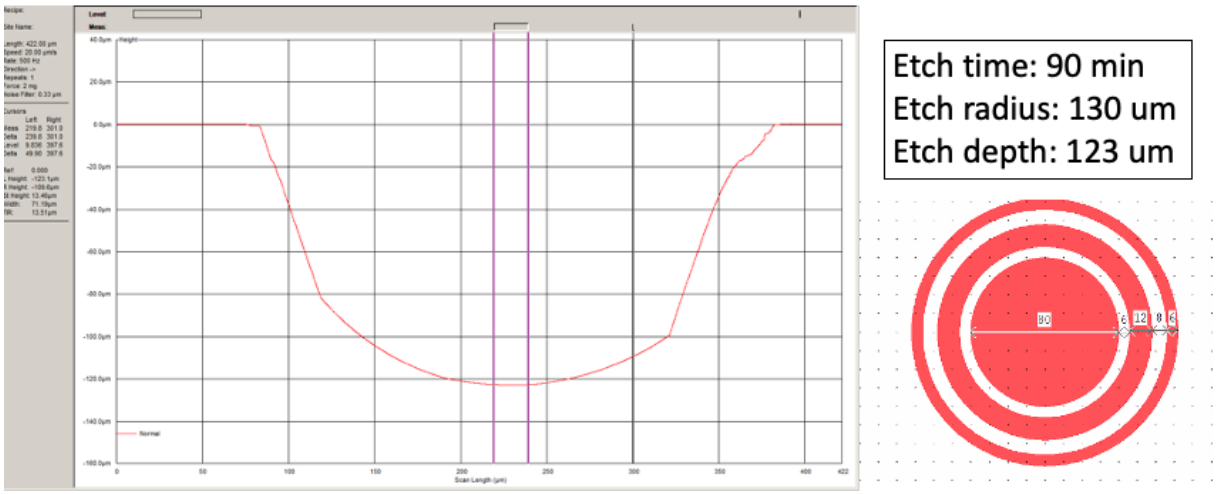

Figure B.24. Depth Profile of 80μm pinhole and larger ring gaps design from 2nd pinhole and gaps trial

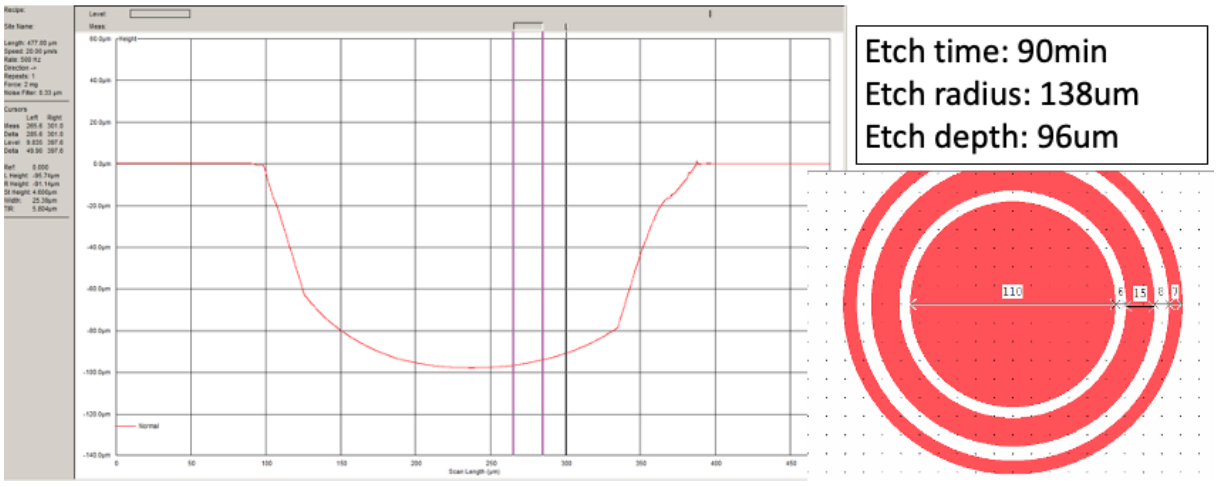

Figure B.25. Depth Profile of 110μm pinhole and larger ring gaps design from 2nd pinhole and gaps trial

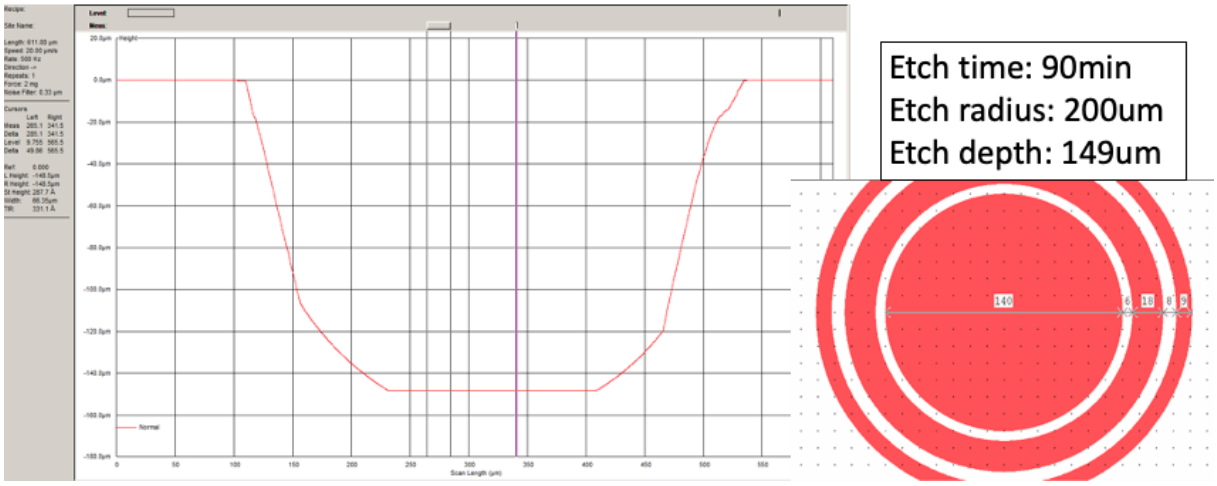

Figure B.26. Depth Profile of 140μm pinhole and larger ring gaps design from 2nd pinhole and gaps trial

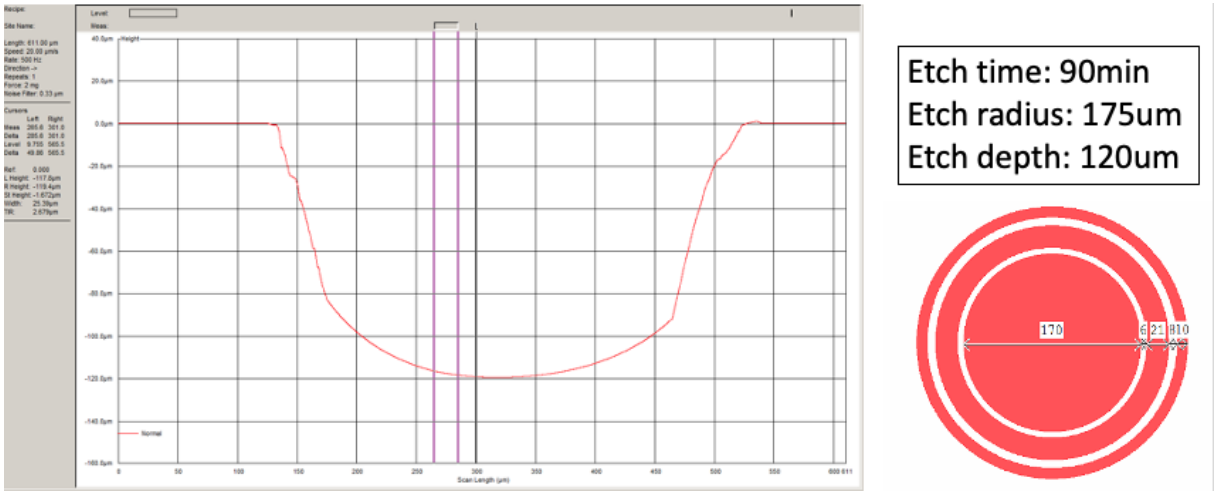

Figure B.27. Depth Profile of 170μm pinhole and larger ring gaps design from 2nd pinhole and gaps trial

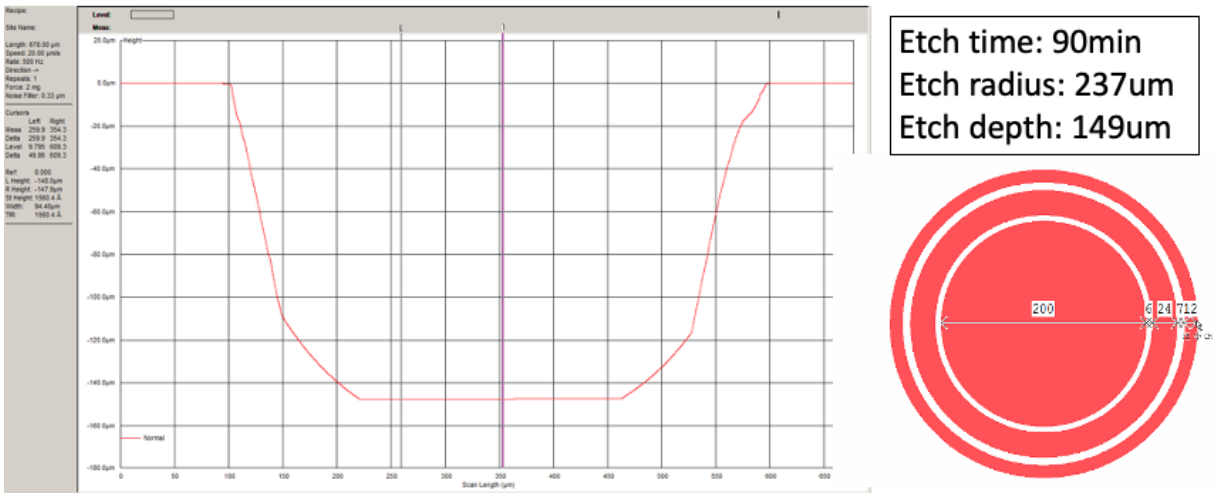

Figure B.28. Depth Profile of 200μm pinhole and larger ring gaps design from 2nd pinhole and gaps trial

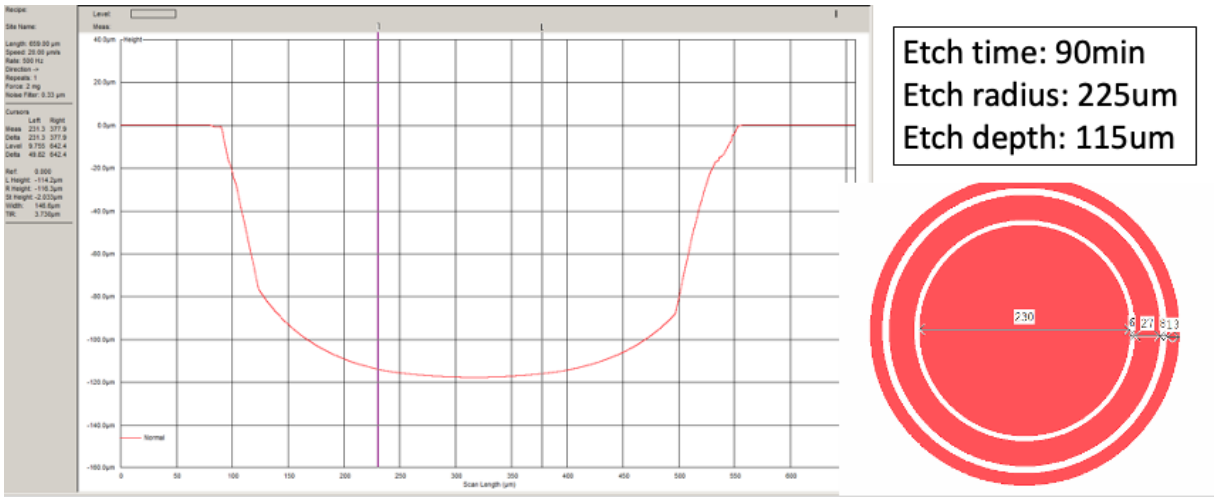

Figure B.29. Depth Profile of 230μm pinhole and larger ring gaps design from 2nd pinhole and gaps trial

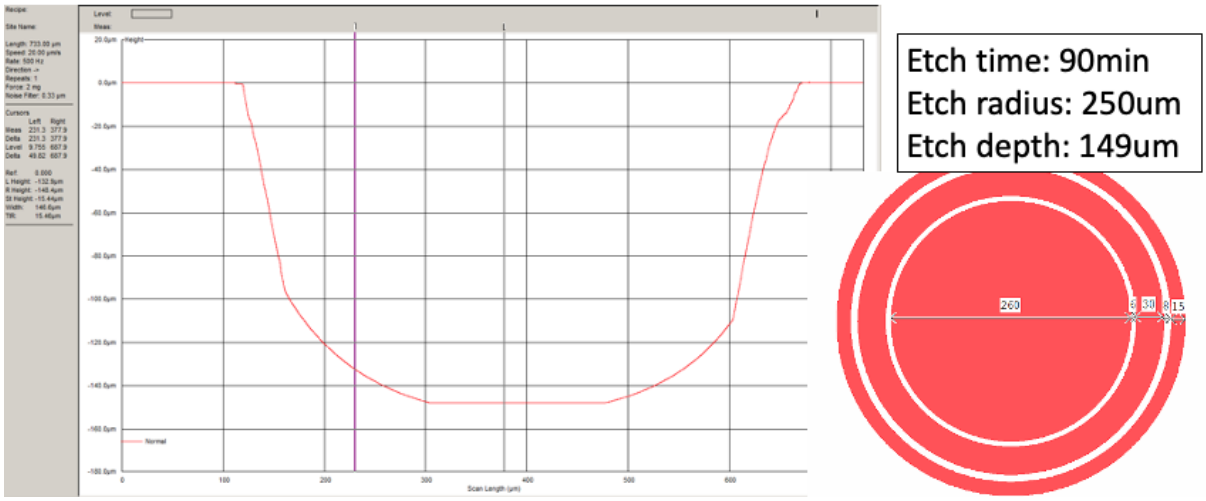

Figure B.30. Depth Profile of 260μm pinhole and larger ring gaps design from 2nd pinhole and gaps trial

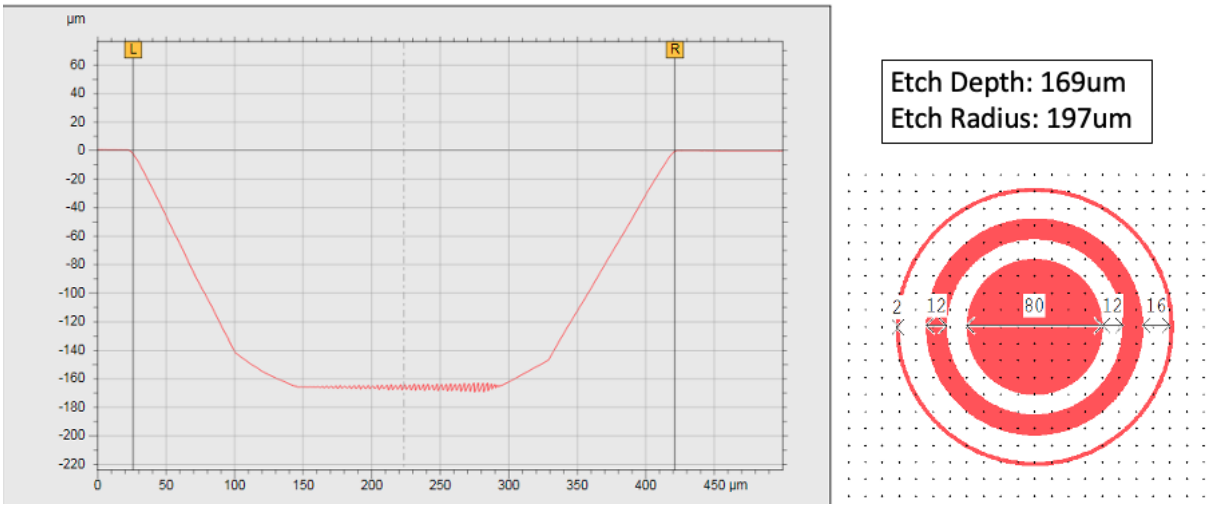

Figure B.31. Depth Profile of 80μm pinhole, larger nitride rings and 1st gap design from 1st nitride rings trial

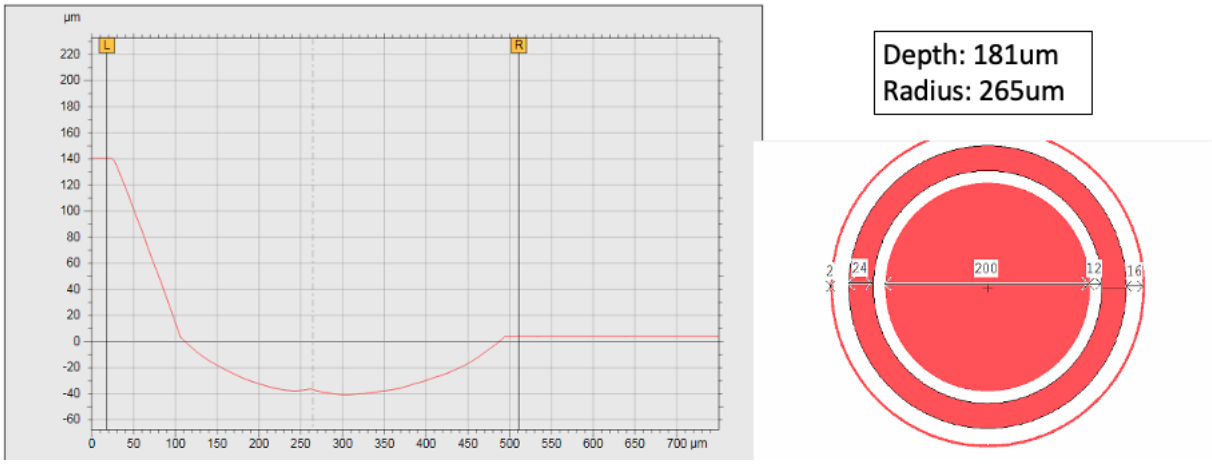

Figure B.32. Depth Profile of 200μm pinhole, larger nitride rings and 1st gap design from 1st nitride rings trial

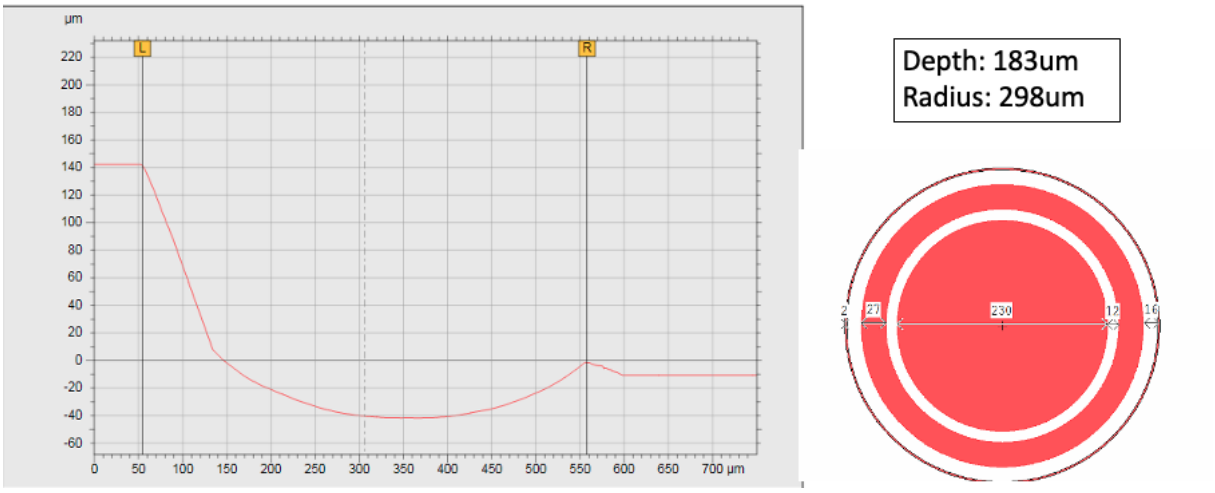

Figure B.33. Depth Profile of 230μm pinhole, larger nitride rings and 1st gap design from 1st nitride rings trial

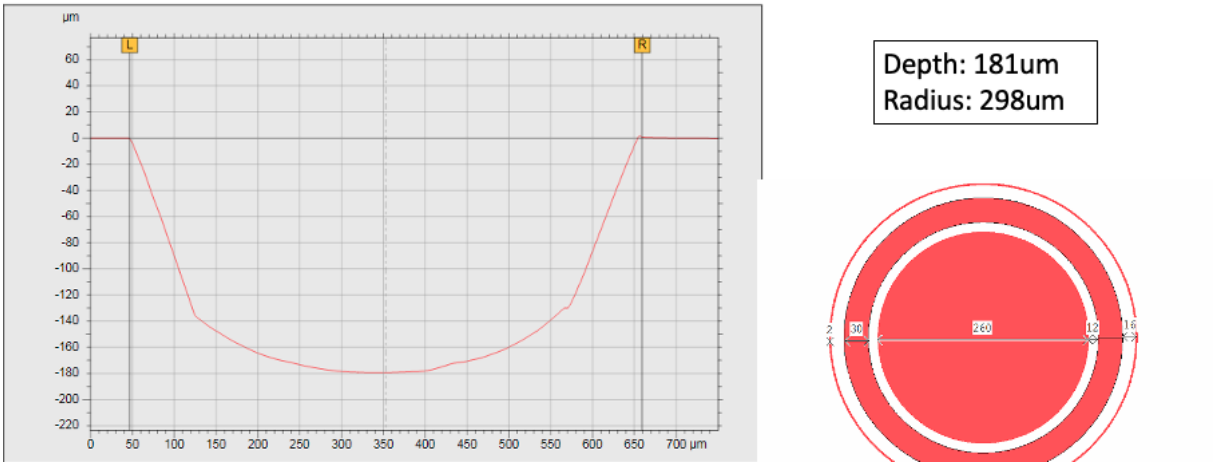

Figure B.34. Depth Profile of 260μm pinhole, larger nitride rings and 1st gap design from 1st nitride rings trial

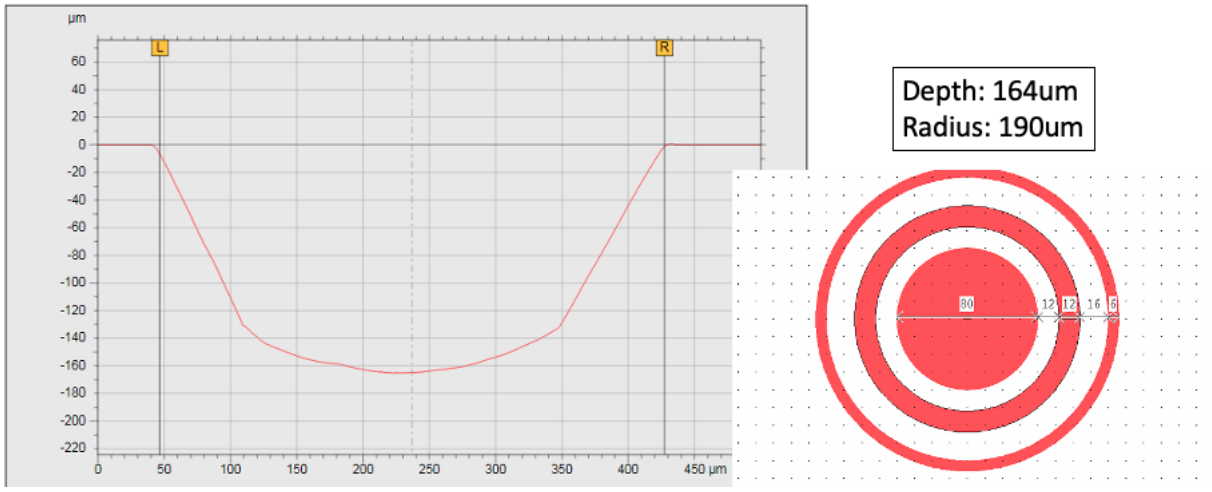

Figure B.35. Depth Profile of 80μm pinhole, larger nitride rings and gaps design from 1st nitride rings trial

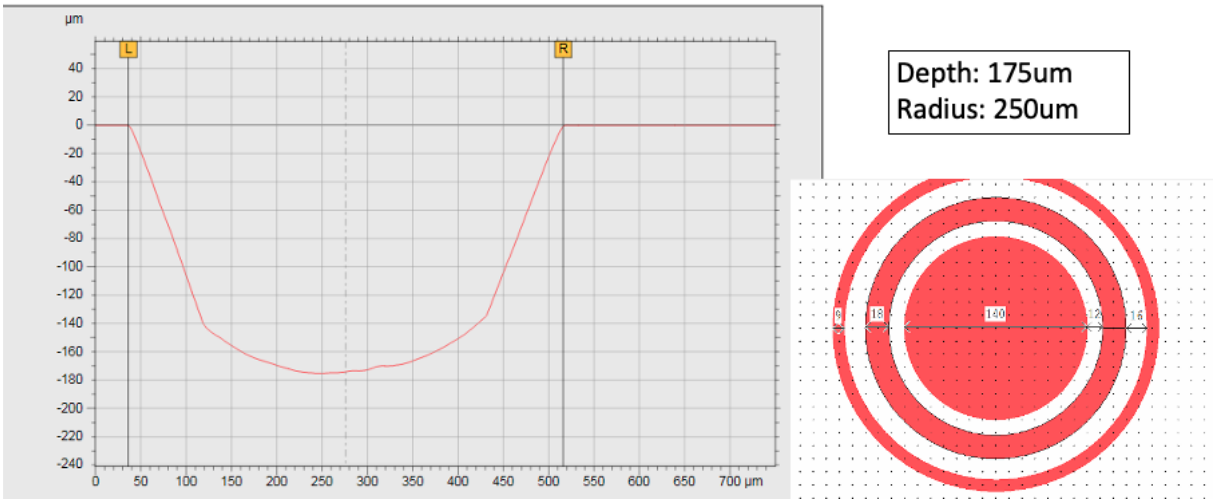

Figure B.36. Depth Profile of 140μm pinhole, larger nitride rings and gaps design from 1st nitride rings trial

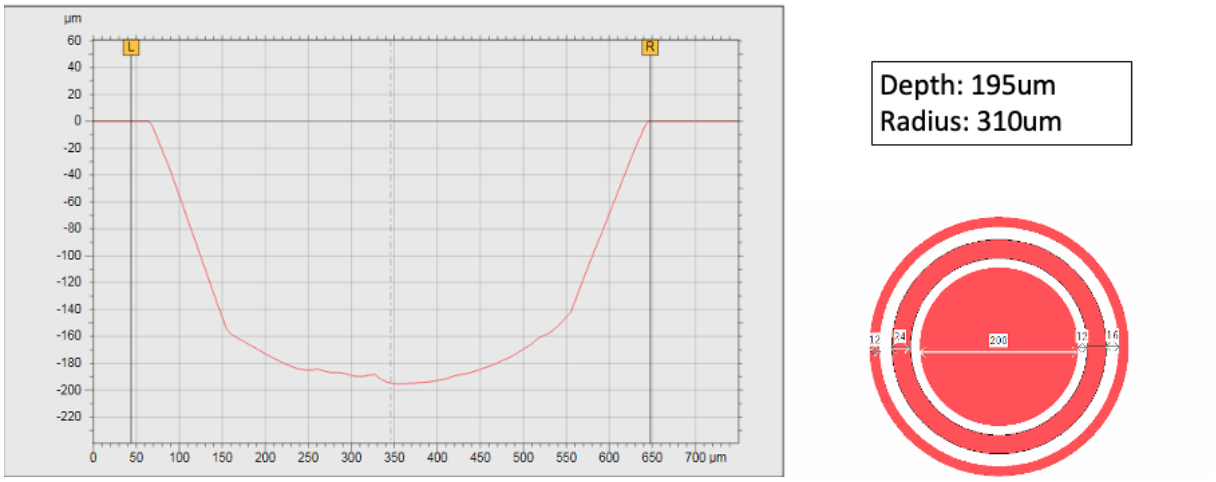

Figure B.37. Depth Profile of 200μm pinhole, larger nitride rings and gaps design from 1st nitride rings trial

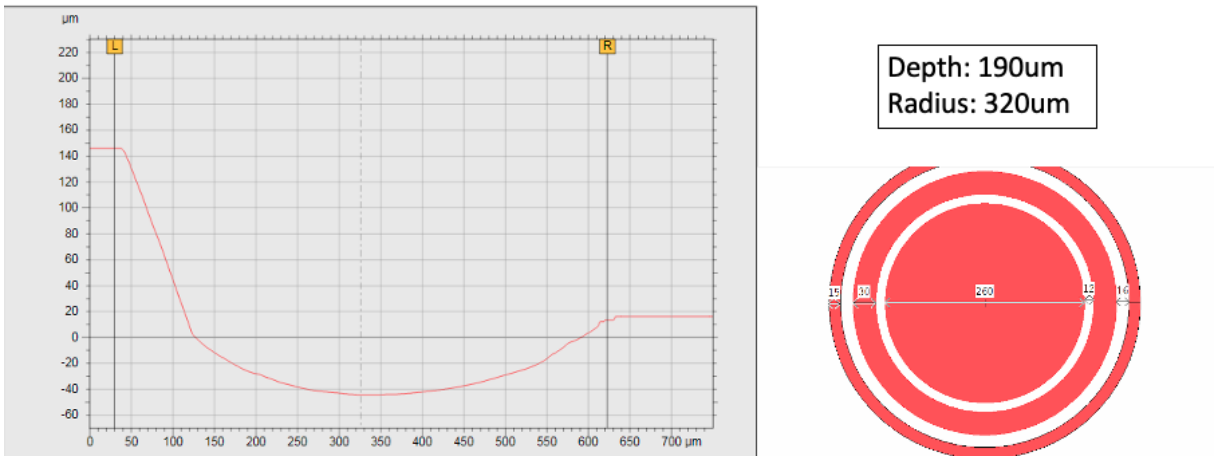

Figure B.38. Depth Profile of 260μm pinhole, larger nitride rings and gaps design from 1st nitride rings trial

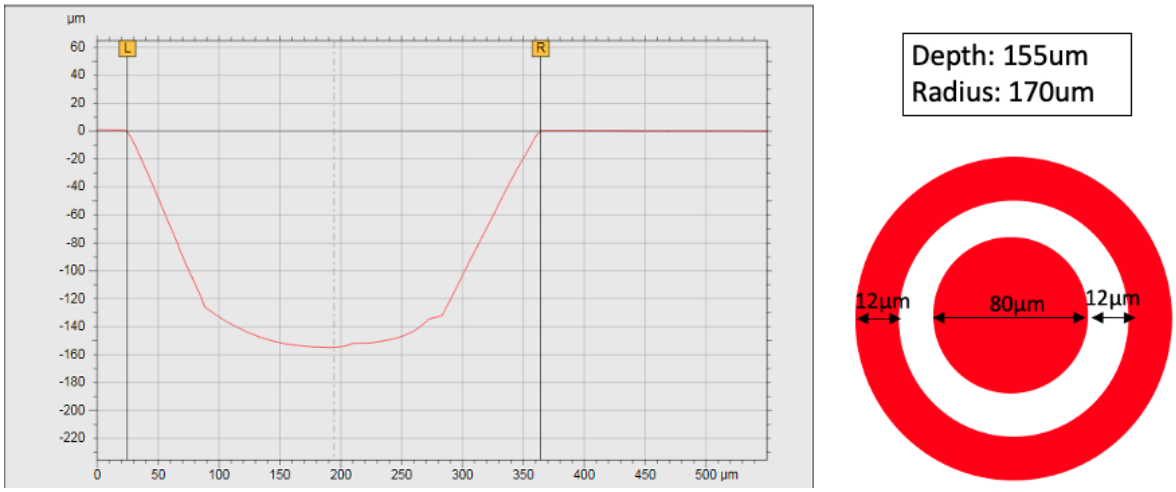

Figure B.39. Depth Profile of 80μm pinhole and single nitride ring design from 1st nitride rings trial

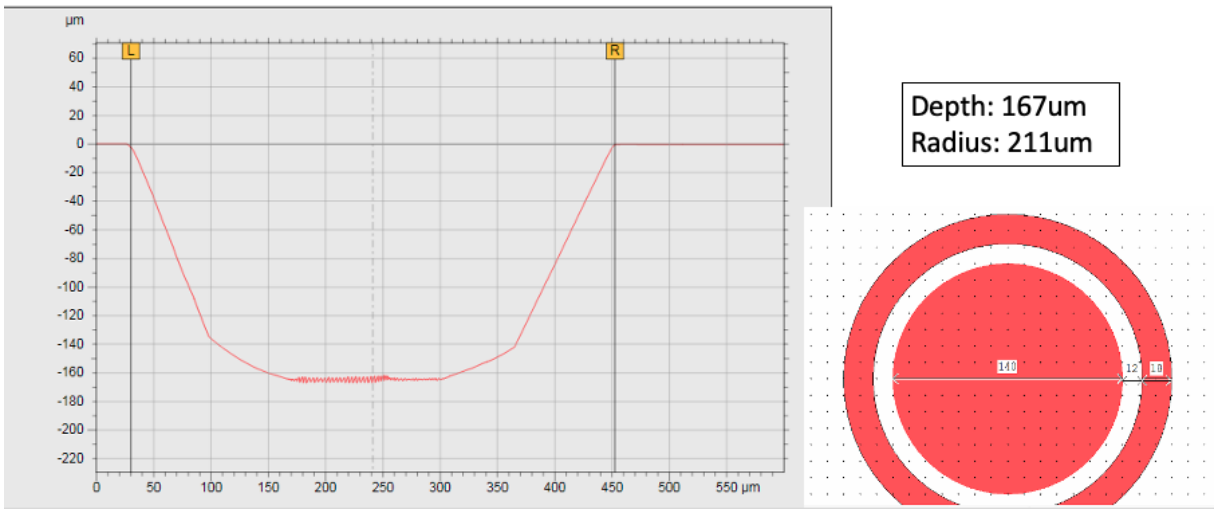

Figure B.40. Depth Profile of 140μm pinhole and single nitride ring design from 1st nitride rings trial

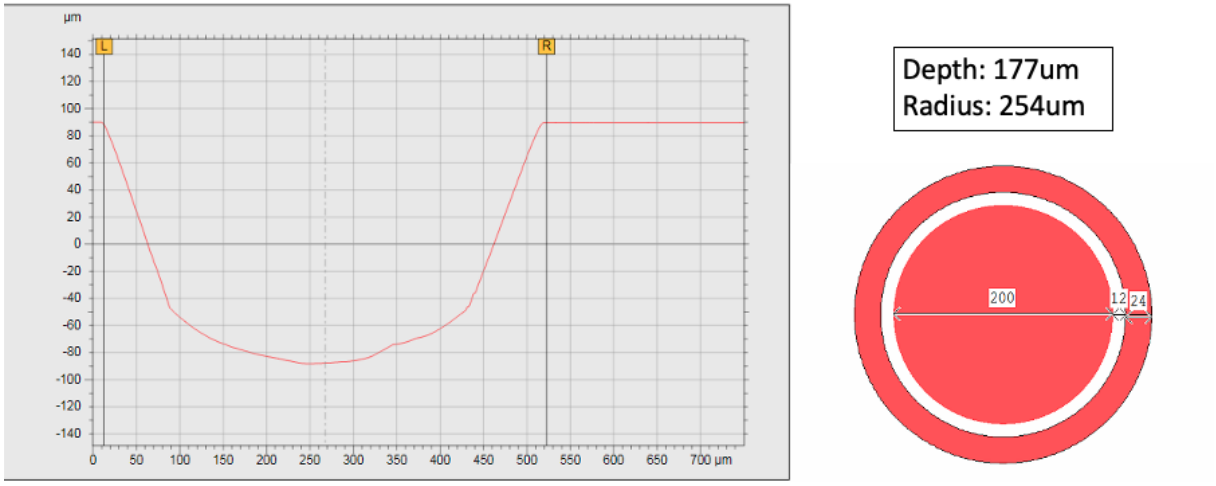

Figure B.41. Depth Profile of 200μm pinhole and single nitride ring design from 1st nitride rings trial

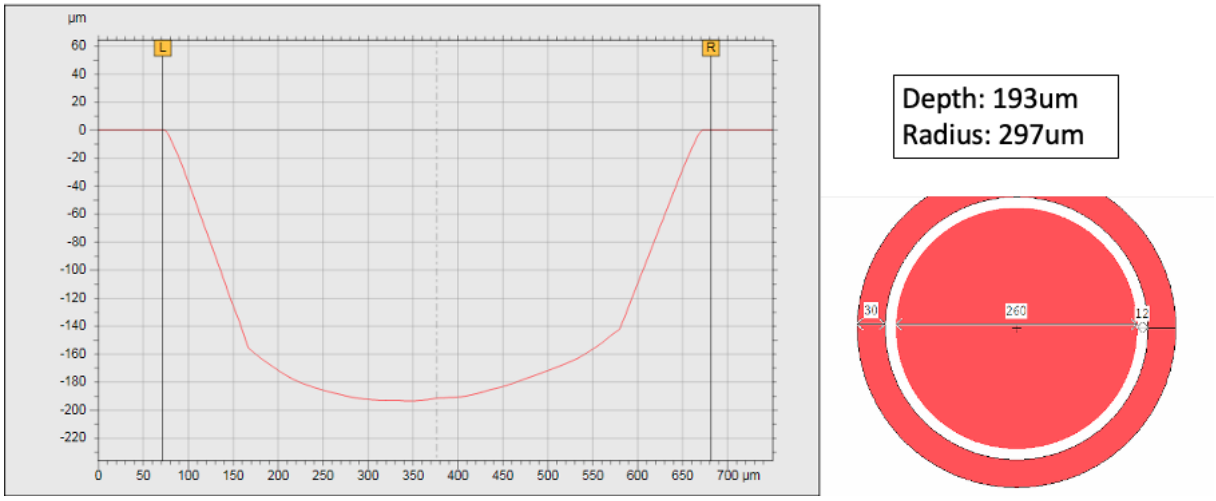

Figure B.42. Depth Profile of 260μm pinhole and single nitride ring design from 1st nitride rings trial

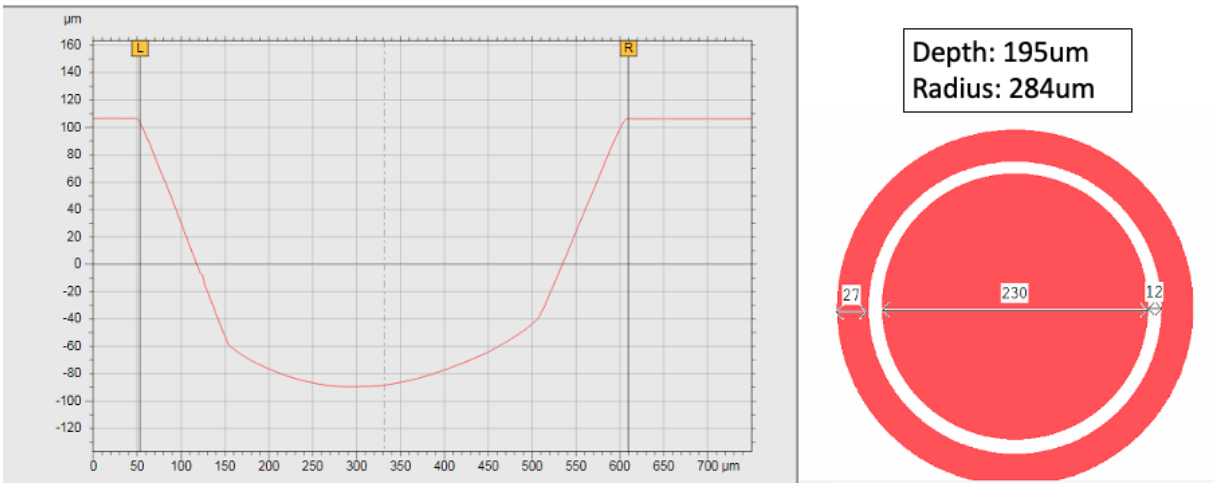

Figure B.43. Depth Profile of 230μm pinhole and single nitride ring design from 1st nitride rings trial

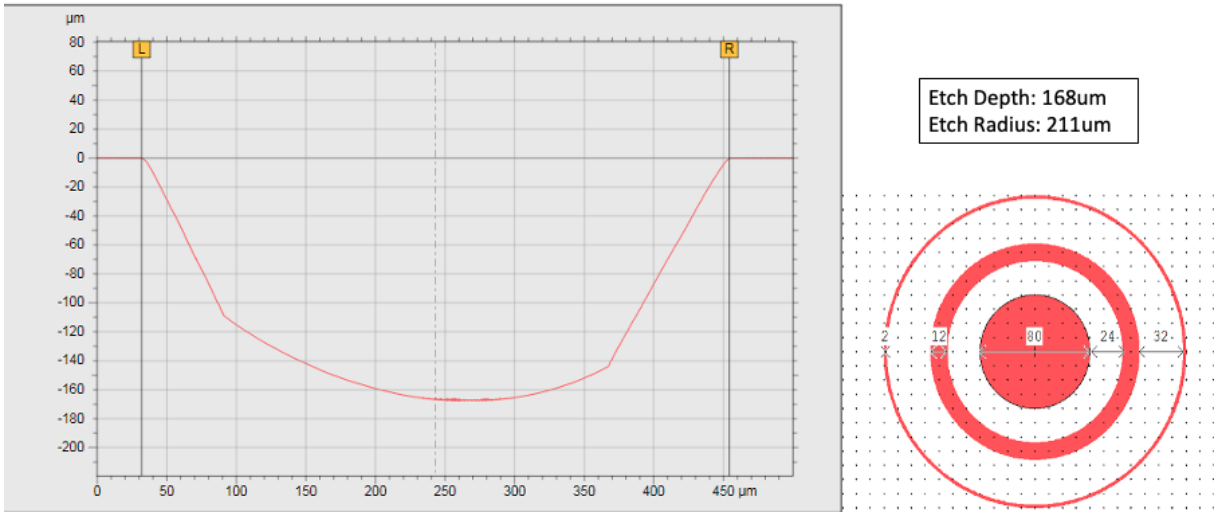

Figure B.44. Depth Profile of 80μm pinhole, larger first gap and larger nitride rings design from 2nd nitride rings trial

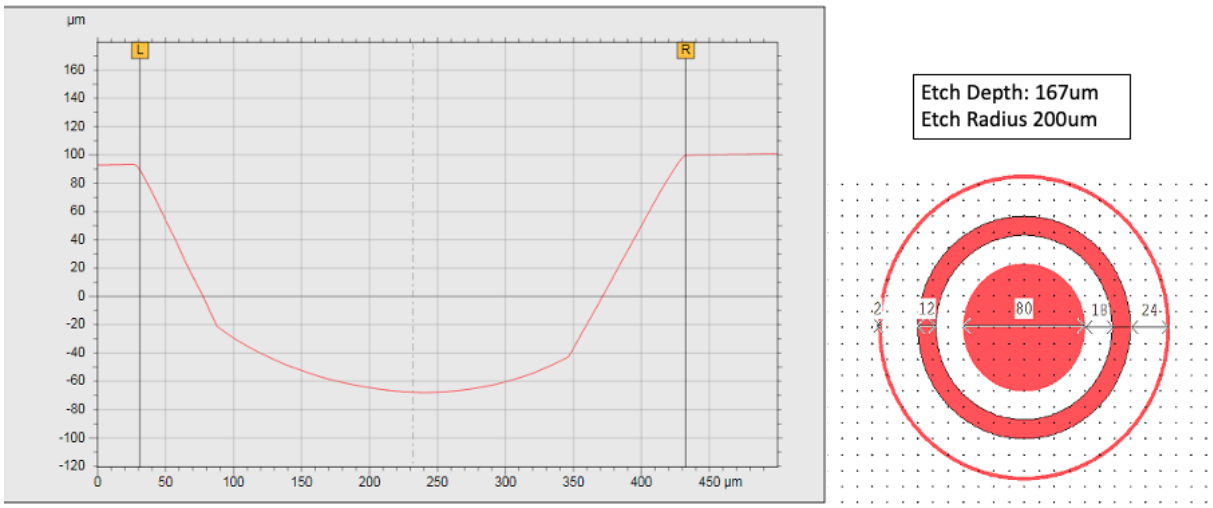

Figure B.45. Depth Profile of 80μm pinhole, larger first gap and larger nitride rings design from 2nd nitride rings trial

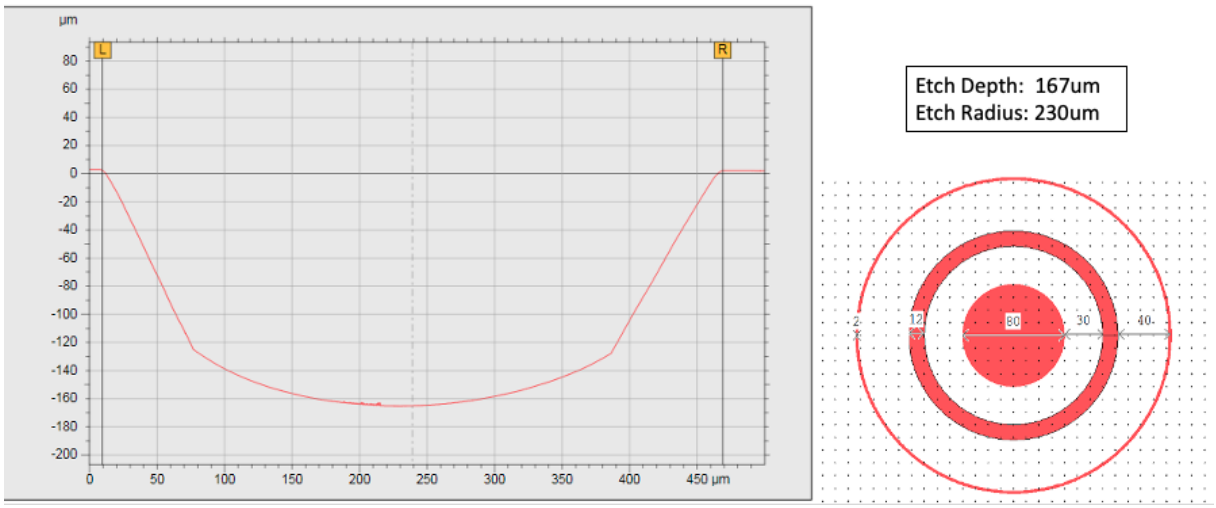

Figure B.46. Depth Profile of 80μm pinhole, larger first gap and larger nitride rings design from 2nd nitride rings trial

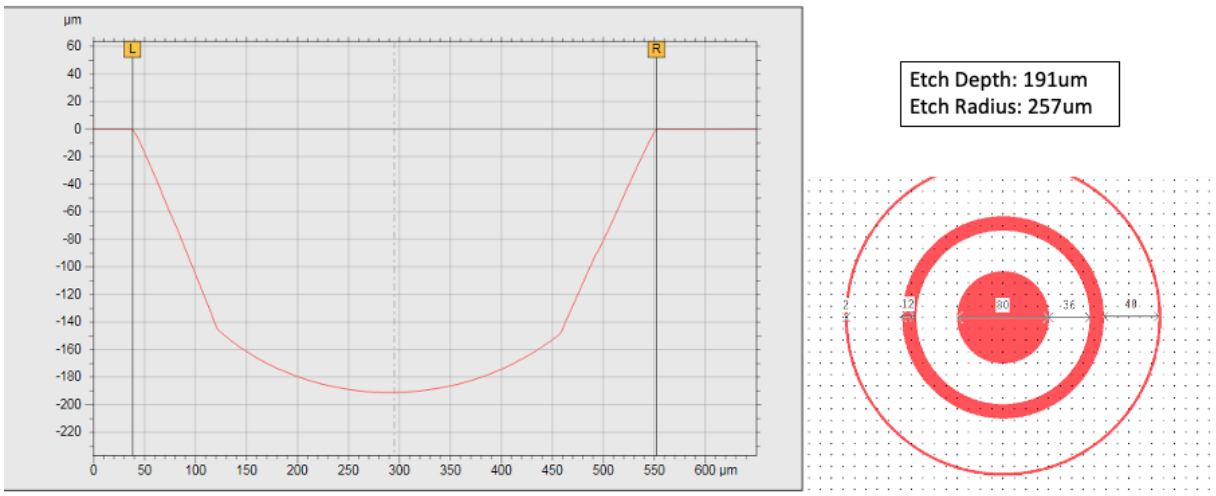

Figure B.47. Depth Profile of 80μm pinhole, larger first gap and larger nitride rings design from 2nd nitride rings trial

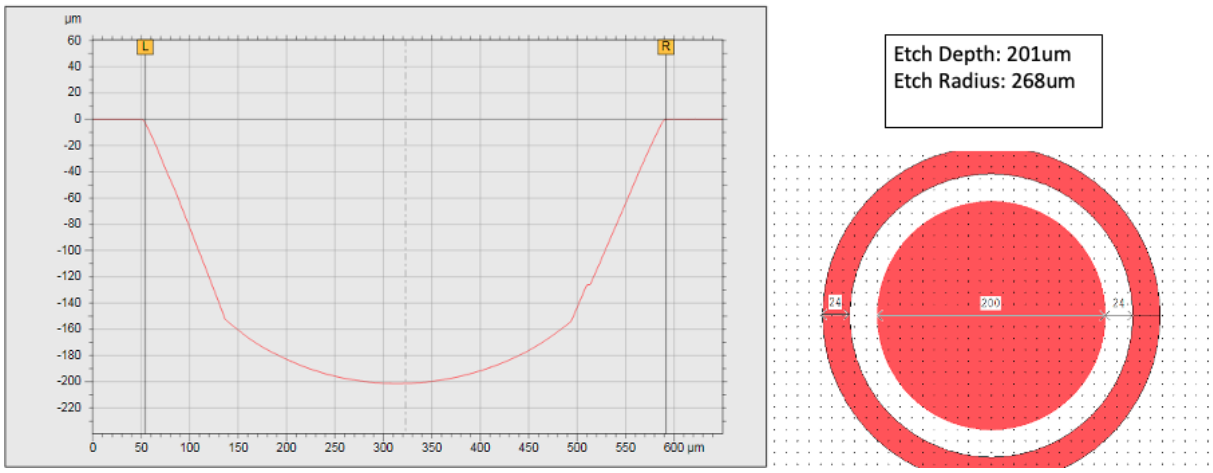

Figure B.48. Depth Profile of 200μm pinhole, and larger single nitride ring design from 2nd nitride rings trial

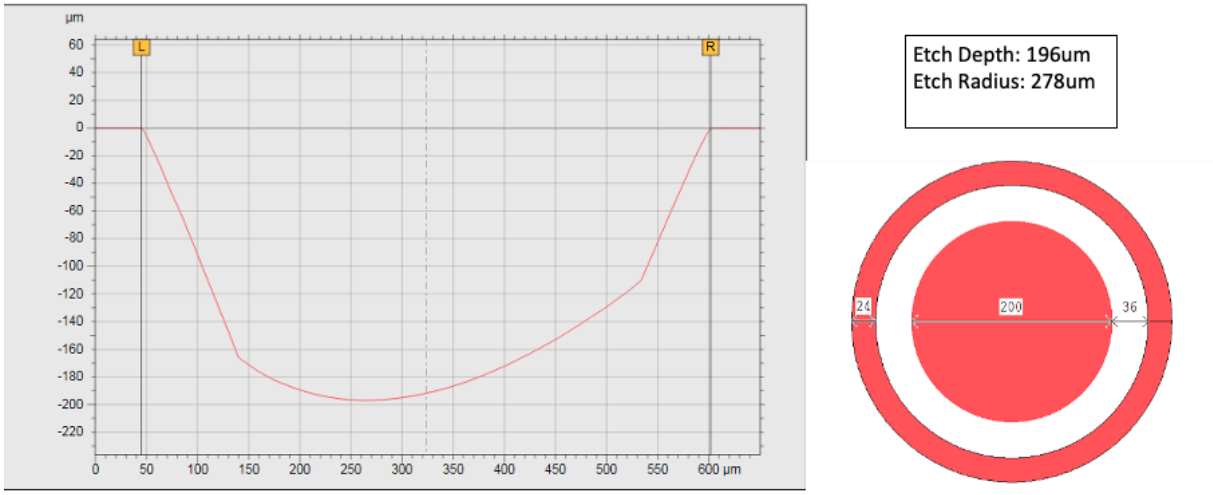

Figure B.49. Depth Profile of 200μm pinhole, and larger single nitride ring design from 2nd nitride rings trial

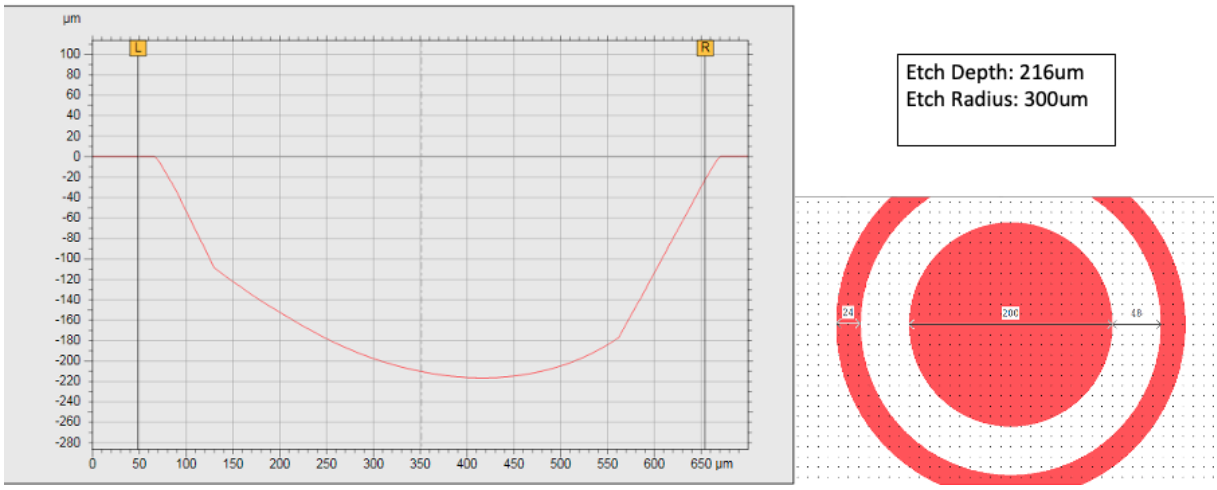

Figure B.50. Depth Profile of 200μm pinhole,and larger single nitride ring design from 2nd nitride rings trial

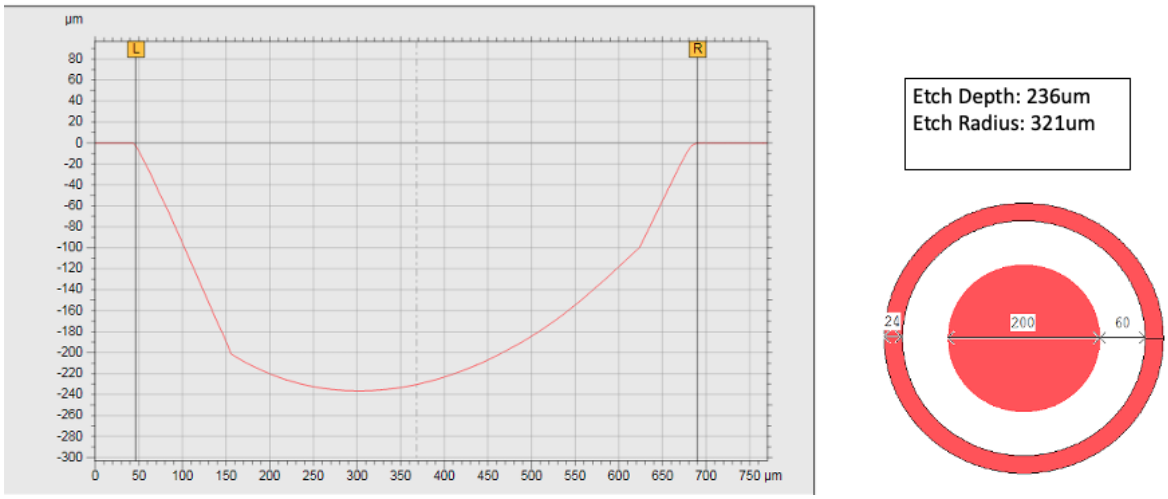

Figure B.51. Depth Profile of 200μm pinhole, and larger single nitride ring design from 2nd nitride rings trial

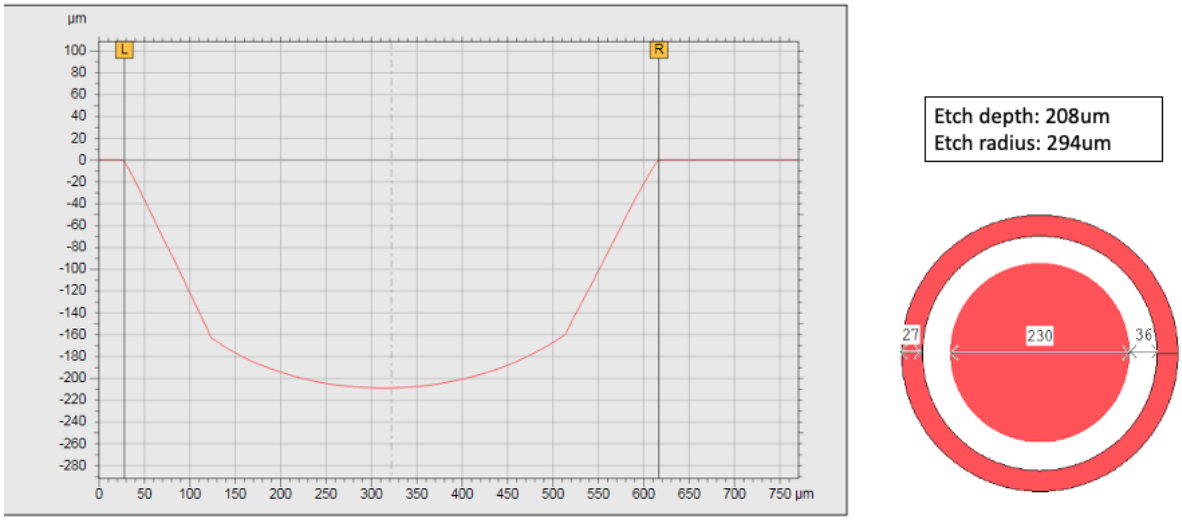

Figure B.52. Depth Profile of 230μm pinhole, larger single nitride ring design from 2nd nitride rings trial

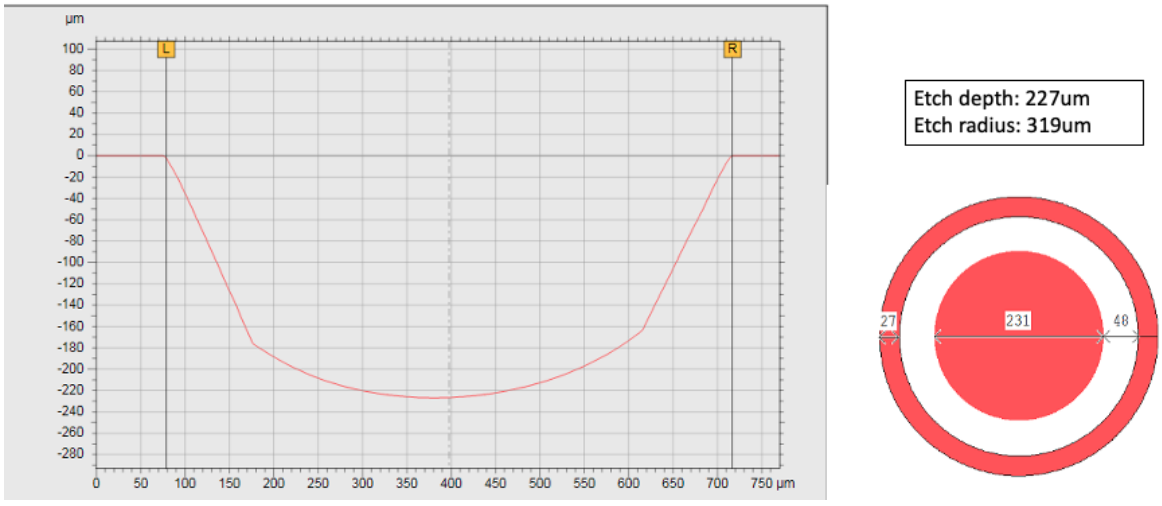

Figure B.53. Depth Profile of 230μm pinhole, larger single nitride ring design from 2nd nitride rings trial

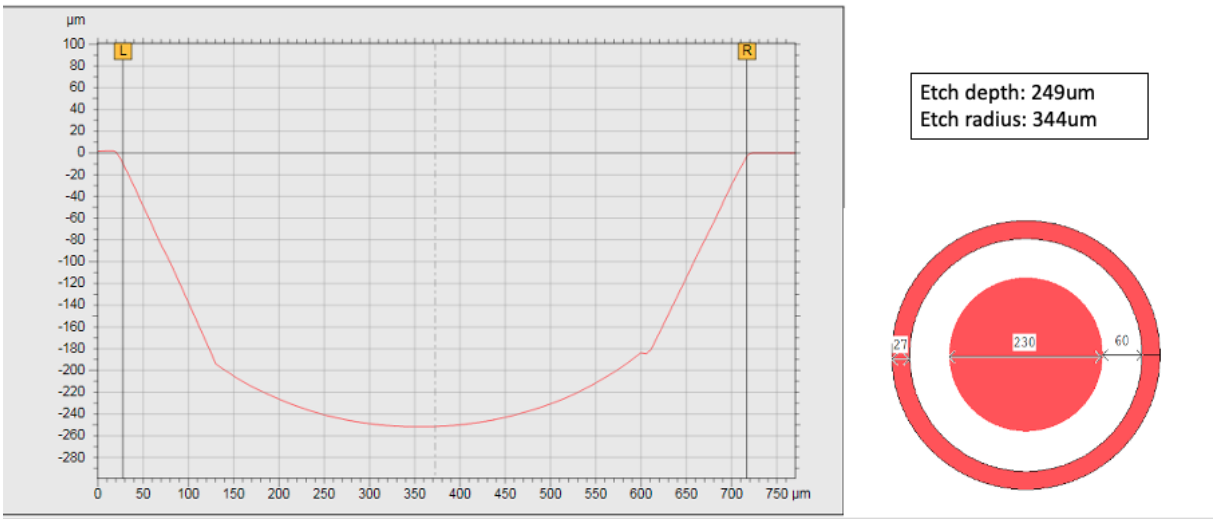

Figure B.54. Depth Profile of 230μm pinhole, larger single nitride ring design from 2nd nitride rings trial

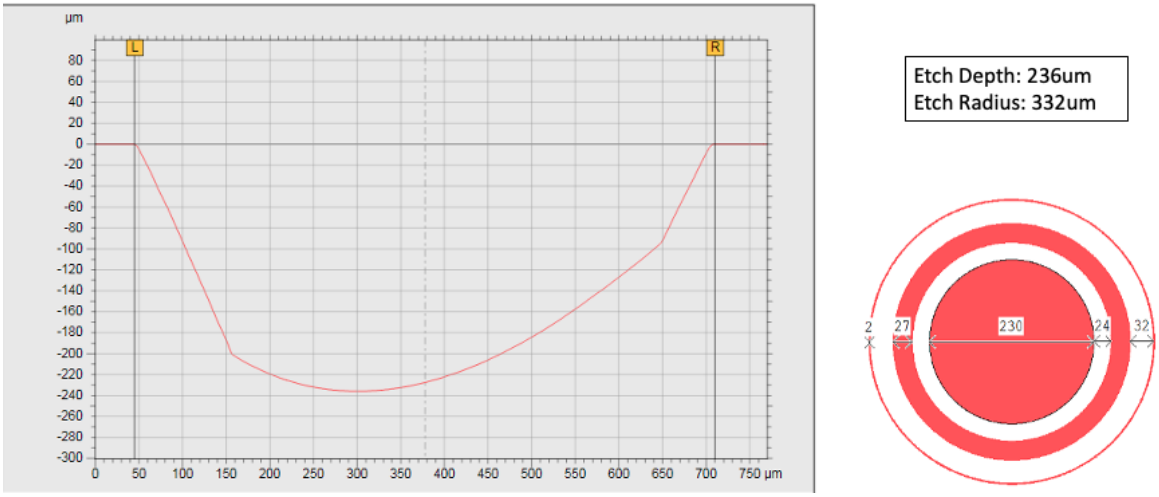

Figure B.55. Depth Profile of 230μm pinhole, larger first gap, and larger nitride rings design from 2nd nitride rings trial

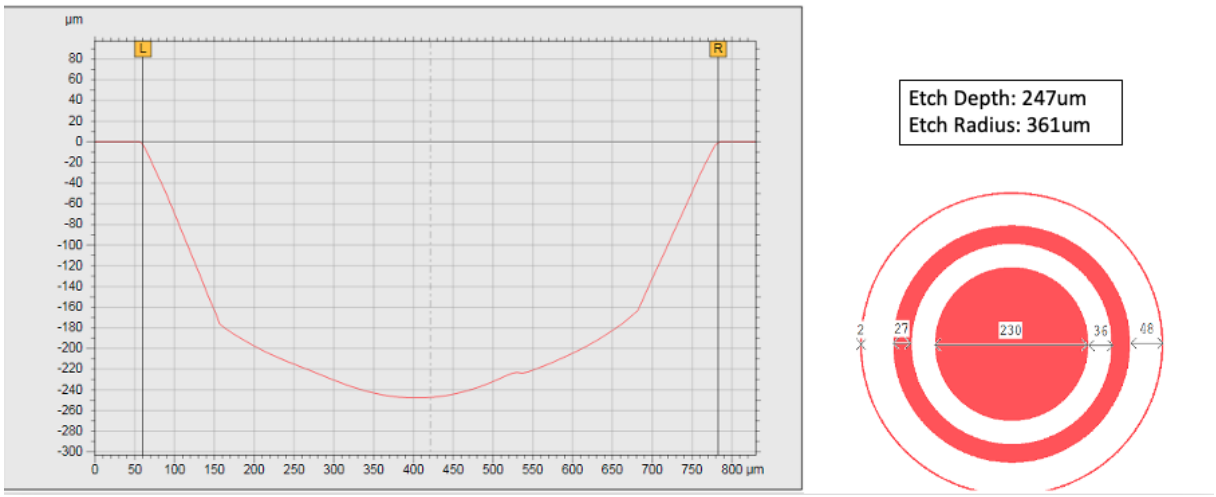

Figure B.56. Depth Profile of 230μm pinhole, larger first gap, and larger nitride rings design from 2nd nitride rings trial

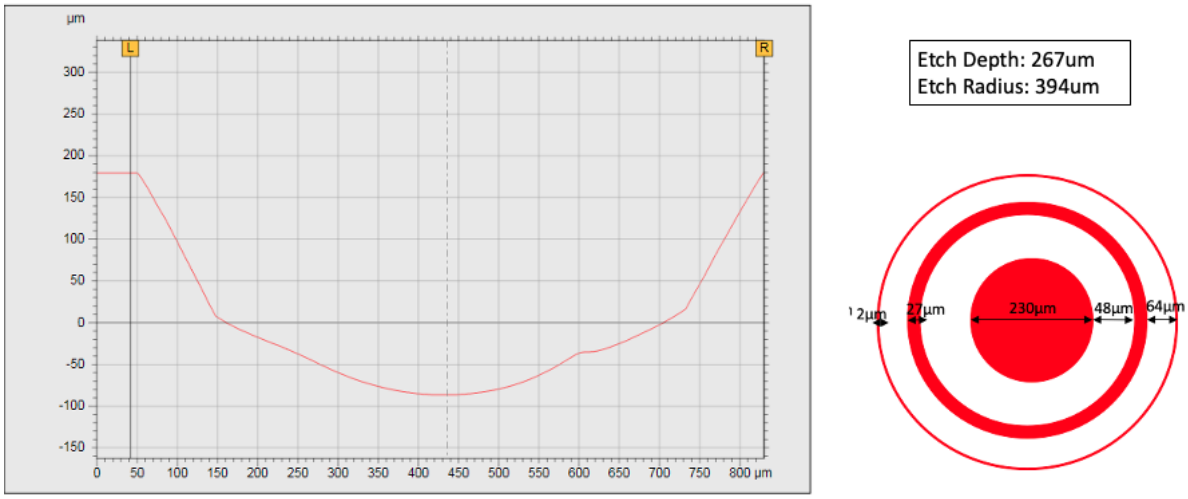

Figure B.57. Depth Profile of 230μm pinhole, larger first gap, and larger nitride rings design from 2nd nitride rings trial

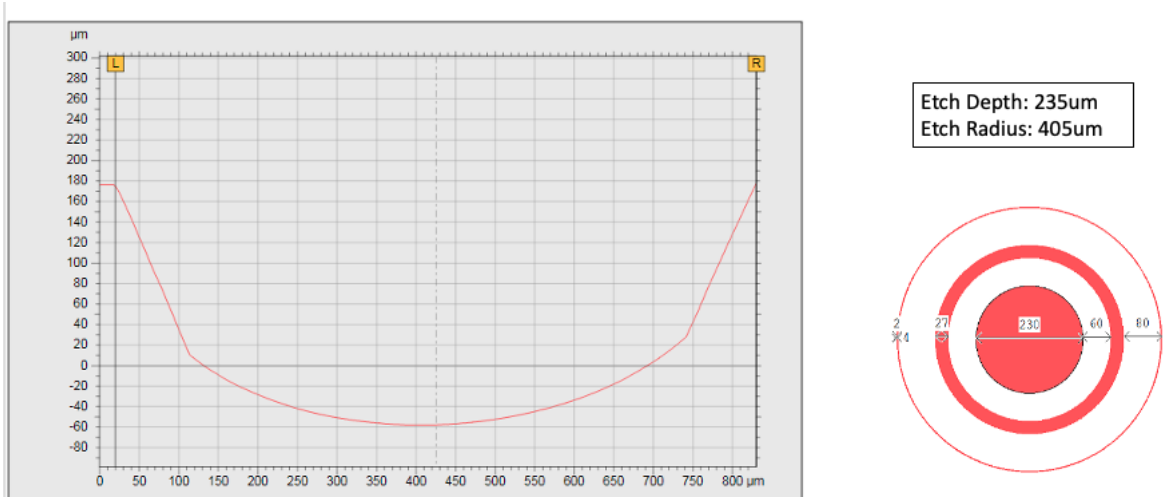

Figure B.58. Depth Profile of 230μm pinhole, larger first gap, and larger nitride rings design from 2nd nitride rings trial